Modelling of Slotted Bolted Friction Connections as Seismic Energy Dissipaters in Braced Steel Frames

by

Jacques Le Febre Terblanche

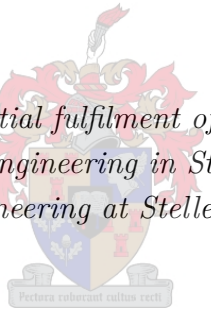

Thesis presented in partial fulfilment of the requirements for the degree of Master of Engineering in Structural Engineering in the Faculty of Engineering at Stellenbosch University

Department of Structural Engineering,
University of Stellenbosch,
Private Bag X1, Matieland 7602, South Africa.

Supervisor: Dr Trevor Neville Haas
Co-supervisor: Mr Etienne van der Klashorst

December 2015

The financial assistance of the National Research Foundation (NRF) towards this research is hereby acknowledged. Opinions expressed and conclusions arrived at, are those of the author and are not necessarily to be attributed to the NRF.

Declaration

By submitting this thesis electronically, I declare that the entirety of the work contained therein is my own, original work, that I am the sole author thereof (save to the extent explicitly otherwise stated), that reproduction and publication thereof by Stellenbosch University will not infringe any third party rights and that I have not previously in its entirety or in part submitted it for obtaining any qualification.

Signature: .....

Date: .....

Summary

The Slotted Bolted Connection provides additional energy dissipation during seismic loading, which leads to a reduction in structural damage. The effects of past earthquakes have shown that braced steel frames are susceptible to structural damage, particularly in the braces and connections. Although steel structures did not collapse during previous earthquakes, such as the 1994 Northridge earthquake, the numerous brittle failures motivated the development of seismic provisions for enhanced ductility. The improved provisions however still result in significant damage following an earthquake, which was seen after the 2011 Christchurch earthquake. One approach to minimise earthquake damage is by using energy dissipation devices. In contrast to other devices, the Slotted Bolted Connection is simple and economic while energy dissipation is provided by the relative sliding between plates in a friction connection. Slotted Bolted Connections were proposed as brace connections in Concentrically Braced Frames, but the lack of a published design procedure has restricted their use.

The absence of a design procedure for Slotted Bolted Connection-braces is attributed to insufficient research conducted on the subject. Previous research concentrated mainly on testing of friction materials for the connection. Literature indicated that there is insufficient understanding of the effect that the configuration of the Slotted Bolted Connection has on its performance. To address this, a Finite Element Analysis study was undertaken. Firstly, a Finite Element model of the Slotted Bolted Connection was calibrated using existing experimental results. The Finite Element model was used to investigate; the effect of bolt-impact with the slot-ends, the differences between Symmetric and Asymmetric Slotted Bolted Connections and the influence of the connection on a braced bay. In addition, a modelling technique was developed to perform a non-linear dynamic analysis of a multi-storey building with Slotted Bolted Connection-braces. The bolt-impact investigation demonstrated that the connection requires suitable detailing to ensure ductility. The analyses indicated that the performance of the Symmetric connection was preferable to that of the Asymmetric connection. Contact between the bolt-shanks and the slot-sides during sliding of the connection in a braced bay affected the hysteresis behaviour, but not detrimentally. Dynamic analysis indicated that the Slotted Bolted Connections successfully decreased brace-damage by providing enhanced lateral drift capacity. The findings have clarified important aspects with regard to the configuration of the connections and have demonstrated the benefits of their introduction to Concentrically Braced Frames. The enhanced understanding contributes to the development of a design procedure for Slotted Bolted Connection-braces.

Opsomming

Die Geboute Gleufverbinding lei tot verminderde strukturele skade deur addisionele energie dissipering tydens seismiese belasting te verskaf. Die nagevolge van vorige aardbewings het die vatbaarheid van verspande staalrame vir strukturele skade bewys, veral in die verspanning en verbindings. Al het staalstrukture tydens vorige aardbewings, soos die 1994 Northridge-aardbewing, nie ineengestort nie, het die talle bros falings tot die ontwikkeling van seismiese voorskrifte vir verbeterde duktiliteit gelei. Die verbeterde voorskrifte lei egter steeds tot beduidende skade, soos gesien ná die aardbewing in Christchurch in 2011. 'n Benadering om aardbewing-skade te verminder, is om van energie dissiperings toestelle gebruik te maak. In teenstelling met ander toestelle, is die Geboute Gleufverbinding eenvoudig en ekonomies. Deur die gly van plate relatief tot mekaar word energie gedissipeer in die verbinding. Die voorstel is om Geboute Gleufverbindings as verspannings-verbindings in Konsentries Verspande Rame te gebruik, maar die gebrek aan 'n gepubliseerde ontwerp-prosedure het die gebruik tot dusver beperk.

Die gebrek aan 'n gepubliseerde ontwerp-prosedure vir Geboute Gleufverbinding-verspanning kan aan 'n navorsingstekort op die gebied toegeskryf word. Vorige navorsing het meestal op die toets van wrywing-materiale vir die verbinding, gefokus. Literatuur het 'n onvoldoende begrip oor die uitwerking, wat die opset van die Geboute Gleufverbinding op die gedrag van die verbinding het, aangedui. Om hierdie aan te spreek, is 'n Eindige Element Analise-studie onderneem. Eerstens is 'n Eindige Element-model van die Geboute Gleufverbinding met bestaande eksperimentele resultate gekalibreer. Die Eindige Element-model is gebruik om die volgende te bestudeer: die uitwerking wat bout-impak met die gleuf-ente het; die verskille tussen die Simmetries en Asimmetriese Geboute Gleufverbindings en ook die invloed van die verbinding op 'n verspande vak. 'n Modelleringstegniek om 'n nie-lineêre dinamiese analise van 'n multi-verdieping gebou met Geboute Gleufverbinding-verspanning uit te voer, is ontwikkel. Die bout-impak-ondersoek het gewys dat die verbinding geskikte detaillering verlang om duktiliteit te verseker. Die analises het aangedui dat die gedrag van die Simmetriese verbinding, bó die van die Asimmetriese verbinding, verkies word. Kontak tussen die boutskagte en die gleufkante tydens gly in 'n verspande vak, het 'n verandering in die histerese-gedrag veroorsaak, maar dit was nie nadelig nie. Die dinamiese analise het aangedui dat die Geboute Gleufverbindings tot 'n vermindering in verspanning-skade gelei het deur die sywaartse verplasing-kapasiteit te vermeerder. Die bevindinge het die belangrike aspekte van die opset van die verbindings verklaar en het ook die voordele van die gebruik van die verbindings in Konsentries Verspande Rame aangetoon. Die verbeterde begrip dra by tot die ontwikkeling van 'n ontwerp-prosedure vir Geboute Gleufverbinding-verspanning.

Acknowledgements

I would like to thank the following people:

- My supervisors; Trevor and Etienne, for their guidance.
- My colleagues and friends from the office; Danielle, Herman, Michael, Petri and Willem, for their advice and memorable times inside and outside of the office over the past two years.
- My parents, for their support throughout my studies.
- Nelia, for all the motivation and her patience over the past months.
- The CDSS, for the financial support.
- The financial support of the National Research Foundation (NRF) towards this research is hereby acknowledged. Opinions expressed and conclusions arrived at, are those of the author and are not necessarily to be attributed to the NRF.

Contents

List of Figures

List of Tables

Abbreviations

AMD - *Active Mass Damper*

ARS - *Abrasion Resistant Steel*

ASBC - *Asymmetric Slotted Bolted Connection*

CBF - *Concentrically-Braced Frame*

CHS - *Circular Hollow Section*

EBF - *Eccentrically-Braced Frame*

FE - *Finite Element*

FEA - *Finite Element Analysis*

FEM - *Finite Element Method*

KBF - *Knee-Braced Frame*

LCF - *Low-Cycle Fatigue*

LVDT - *Linear Variable Displacement Transducer*

MRF - *Moment Resisting Frame*

OCBF - *Ordinary Concentrically-Braced Frame*

PED - *Passive Energy Dissipation*

PGA - *Peak Ground Acceleration*

SBC - *Slotted Bolted Connection*

SCBF - *Special Concentrically Braced Frames*

SHJ - *Sliding Hinge Joint*

SMA - *Shape Memory Alloy*

SSBC - *Symmetric Slotted Bolted Connection*

TSA - *Thermally Sprayed Aluminium*

Nomenclature

Latin upper case letters

A_a - Apparent Contact Area

A_r - Real Contact Area

E - Modulus of Elasticity

E_I - Absolute Earthquake Input Energy

E_K - Absolute Kinetic Energy

E_μ - Energy Dissipation Through Hysteretic/Inelastic Action

E_ξ - Energy Dissipation Through Viscous Damping

E_S - Elastic Strain Energy

F - Force

F_{slip} - Slip-Force of the SBC

P_{flat} - Load Required to Achieve Flat Deflection of a Spring Washer

R_a - Ratio of the maximum Retrofitted to the Maximum Reference Acceleration

R_d - Ratio of the Maximum Retrofitted to the Maximum Reference Inter-Storey Drift

T_b - Bolt Tension

Latin lower case letters

c_v - Coefficient of Variation

f_d - Friction Force of Damper

f_s - Force in Entire Configuration

f_u - Ultimate Strength

f_y - Yield Strength

f_{yk} - 5th Percentile Yield Strength

g - Gravitational Acceleration

k_b - Stiffness of Bracing Member

n_b - Number of Bolts

n_p - Number of Spring Washers in Parallel Stack

n_s - Number of Spring Washers in Series Stack

p - Contact Pressure

u - Displacement

Greek lower case letters

δ - Spring Washer Group Deflection

$\delta_{Belleville}$ - Flat Deflection of a Particular Belleville Spring Washer

δ_{flat} - Flat Deflection of Spring Washers

ε_u - Ultimate Strain

ε_y - Yield Strain

μ - Coefficient of Friction

μ_k - Coefficient of Kinetic Friction

μ_s - Coefficient of Static Friction

μ_x - Mean Value

ν - Poisson ratio

σ_x - Standard deviation

τ_{crit} - Critical Shear Stress

Chapter 1

Introduction

The *Slotted Bolted Connection* (SBC) is an innovative approach for application in steel framed structures. It could lead to enhanced seismic performance as well as reduced structural damage following an earthquake. By dissipating energy through friction, the SBC reduces the demand on the surrounding structural and non-structural elements.

During past earthquakes, seismic design code provisions have succeeded in averting structural collapse of steel buildings. The 1994 Northridge earthquake is a typical example thereof. Although no collapse of steel buildings were reported, extensive damage occurred (Tremblay et al., 1995). Brittle failure modes such as weld fracture in *Moment Resisting Frames* (MRFs), shown in Figure 1.1 (a), and brace fracture in *Concentrically-Braced Frames* (CBFs), shown in Figure 1.1 (b), were widespread. This prompted research aimed at developing design provisions for more ductile steel structures. Ductility in this case refers to a structure's inelastic deformation capacity (Engelhardt, 2009).

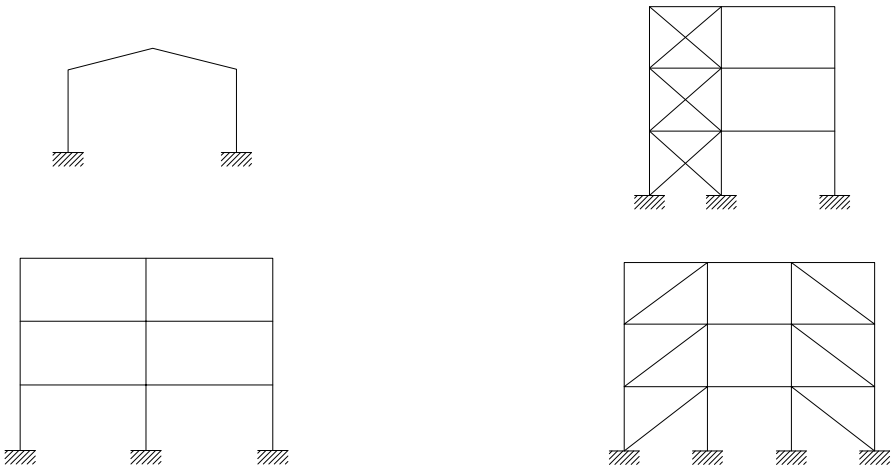

(a) Moment Resisting Frames (MRFs): resist lateral loading using moment-fixed beam-column connections

(b) Concentrically-Braced Frames (CBFs): resist lateral loading by transferring force to brace members

Figure 1.1: Two typical frame systems for steel buildings

The subsequent improvements in seismic design provisions have resulted in more ductile structures. These provisions generally require that structures in high seismic regions are 'capacity designed'. Capacity design can be explained by presenting the chain shown in Figure 1.2. The chain is governed by the strength of the weakest link. If the weakest link possesses adequate ductility, the brittle links can remain free from damage. As a consequence of material variability, structural elements are often significantly stronger than their design resistances. This is called overstrength. It is essential that the design resistance of each brittle link is greater than the overstrength of the ductile link (Paulay et al., 1992). Designers must therefore decide where the 'ductile links' are situated in the structure and ensure that the rest of the structural elements are designed and detailed accordingly.

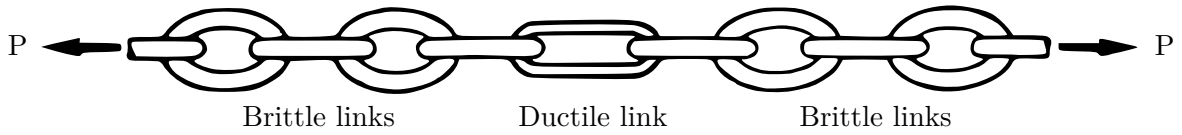

Figure 1.2: Chain with ductile and brittle links (adapted from Paulay et al. (1992))

In contrast to capacity design, the *Ordinary Concentrically-Braced Frame* (OCBF) system does not require specific detailing for ductility. The OCBF is common in regions of low to moderate seismicity and has been adopted by SANS 10160-4 in: *Annex D - Design and detailing of steel structures*. Since it does not require ductile detailing, the OCBF relies on the "inherent ductility of steel structures". This "inherent ductility" necessarily means permanent deformations in the connections and braces following an earthquake.

It is therefore clear that irrespective of the seismicity of the region, current design provisions still result in significant structural damage after an earthquake. An example of this is the unacceptable level of damage from the 2011 Christchurch earthquake (MacRae, 2015a). Low-damage design can mitigate the economic effects of structural damage following an earthquake. One way in which this is achieved is by providing added means for earthquake input energy dissipation. Many supplemental dissipation devices have been developed. The high cost, unconventional installation and novel materials associated with most of these devices have been detrimental to their use in general applications (Grigorian et al., 1993). This study focuses on a simple and economic energy dissipation device, namely; the SBC.

Figure 1.3 shows that the SBC consists of a number of plates. The outer-plates and shims have conventional bolt-holes while the slotted-plate has a slotted hole. Shim plates are normally included in the SBC between the outer- and slotted-plates. Shims are made of materials that exhibit beneficial friction behaviour when in contact with steel. The plates are clamped together by a pre-loaded bolt. The direction in which loading is applied is shown in Figure 1.3. The slotted-plate slips relative to the outer-plates when the friction, or slip-force, is exceeded. Energy is dissipated through friction in this manner.

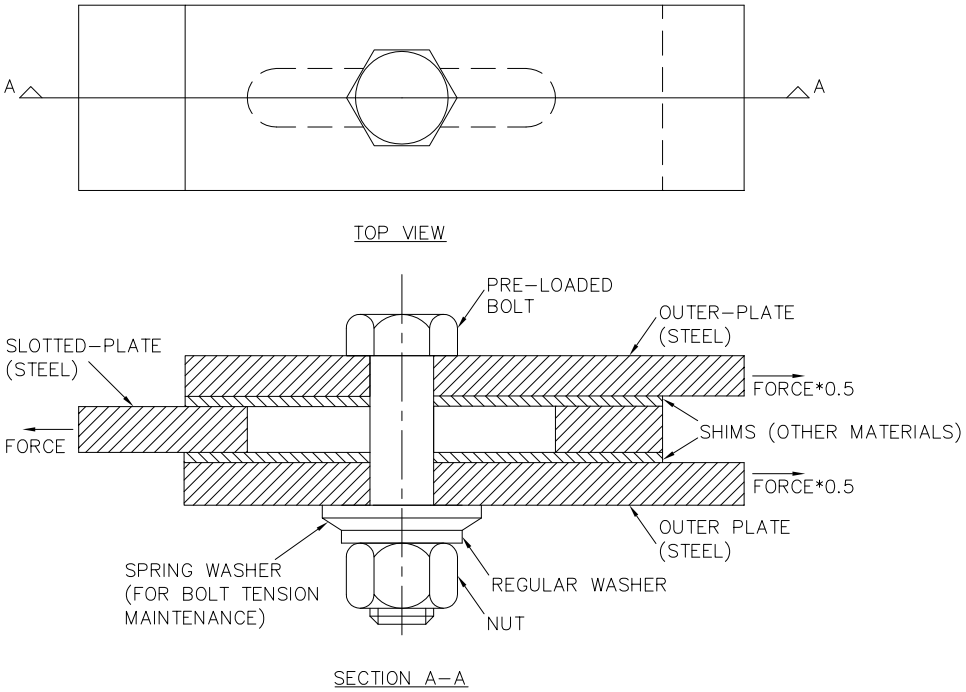

Figure 1.3: A general layout for the Slotted Bolted Connection

Due to their high stiffness, CBFs were shown to be seismically vulnerable (Di Sarno et al., 2002). One of their major deficiencies have been their inability to achieve large inelastic drifts without disproportionate damage to the braces. This can be remedied by introducing the SBC. In CBFs the proposal is to incorporate the SBC in bracing members to offer seismic protection. SBCs alter the structural response and are able to preserve braces during earthquakes. The lack of a published design procedure for SBC-braces has made their application problematic.

A limited number of studies have been conducted on SBCs. The significant advances can be summarised as:

- The implementation of spring washers to maintain bolt tension.
- Finding appropriate materials for stable friction during sliding.
- Understanding the effect of material hardness on friction and wear.
- The subsequent use of *Abrasion Resistant Steel* (ARS) in conjunction with structural steel.
- The simplification of the SBC to a shim-less format incorporating ARS.

Loo et al. (2014) confirmed that the performance of the shim-less SBC incorporating ARS was suitable. This key finding enables construction to be greatly simplified which was not possible as long as shims were required in the SBC. The simplification meant that outer- or slotted-plates could be shop-welded to columns and column-bases. Brace members such as equal leg angles or channel-sections could be used as outer-plates on either side of the gusset plate with slotted holes as shown in Figure 1.4 (a) and (b). Alternatively, I-sections or *circular hollow sections* (CHS) and hollow square sections with extended spade plates could function as the slotted-plates

between two gussets as shown in Figure 1.4 (c). Only bolts and washers then need to be secured on site.

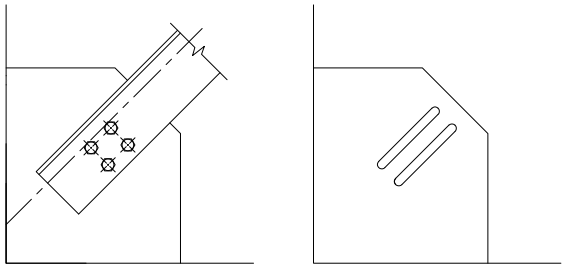

(a) 100x100x10 equal leg angles with 4 M20 bolts and slotted-holes in the gusset with 55 mm slip-length in both directions.

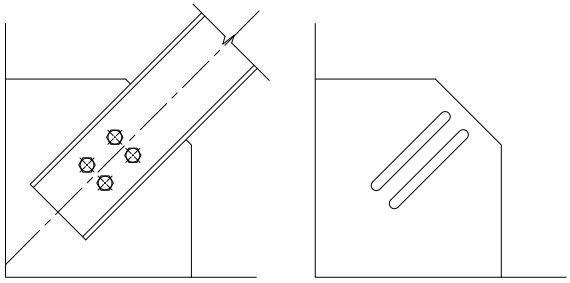

(b) PC200x75 parallel flange channels with 4 M24 bolts and slotted-holes in the gusset with 70 mm slip-length in both directions.

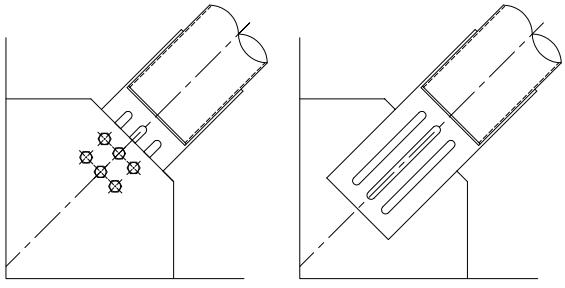

(c) 219.1 mm × 4.5 mm CHS with 6 M20 bolts and slotted-holes in extended spade-plate between two gussets and 85 mm slip-length in both directions.

Figure 1.4: Concepts for the use of different braces with SBCs

Even though SBCs became practical for CBF construction, its use is limited without a published design procedure, therefore requiring more investigation. From the reviewed literature, there is a clear necessity to assess how different arrangements with regards to SBC layout affect its performance. A lack of research into the effect of bolt-impact, which occurs when the bolt reaches the end of the slot-length, motivated this investigation. In addition, the difference between the

Symmetric Slotted Bolted Connection (SSBC) and the *Asymmetric Slotted Bolted Connection* (ASBC) is examined. Further, clarification of how the SBC in the brace-gusset-column connection influences the behaviour of the brace, and vice-versa, is needed. Lastly, a method of global analysis is required that not only accurately captures the behaviour and energy dissipation characteristics of the SBC, but also offers computational efficiency and relatively simple implementation.

Due to the size of a CBF with SBC-braces, experimental testing becomes problematic. Full-scale testing is expensive, time-consuming and few facilities possess the equipment necessary to test such large structural arrangements. In order to address the aforementioned research questions, *Finite Element Method* (FEM) modelling and analysis were used to study the behaviour of the SBC. A model was validated with published test data and expanded to perform further investigations.

1.1 Problem statement

A published design procedure for SBC-braces in CBFs does not currently exist. There is a clear need for more understanding into the behaviour of SBCs, as well as the effect that the SBC has on a global structural level.

1.2 Objectives

The main objective of the study is:

- To model the sliding behaviour of the SBC and calibrate the *Finite Element* (FE) model using existing experimental results.

The calibrated numerical model is used to perform further investigations on how SBC configuration affects its performance. These include:

- The effect of bolt-impact on the SBC.
- The differences between the behaviour of SSBCs and ASBCs.
- The influence of the SBC on a braced bay.

The understanding gained from these investigations is used to:

- Achieve a computationally efficient modelling technique that accurately represents the SBC energy dissipation characteristics.

This is used for non-linear dynamic analysis of a structure subjected to earthquake ground accelerations.

By meeting these objectives, more understanding of the effect of SBC-braces can be obtained. In collaboration with future research, this study will aid progress towards the ultimate objective of developing a design procedure for the application of SBCs into CBFs.

1.3 Scope of the Investigation

Background to seismic design codes and detailing procedures, especially those related to high-ductility structures, will not be discussed in this text.

Experimental testing of the SBC was considered beyond the scope of this study.

General principles and information on advanced FE modelling such as contact will be discussed. However, for discussion of algorithms, mathematical theory and advanced modelling features, the reader is referred to the Abaqus user's manual.

1.4 Exposition

The way in which previous SBC studies affected and motivated this study is examined in the Literature Review that follows in Chapter 2. In Chapter 3, the FE model of the SBC is explained with the verification conducted using test results from published work. Chapter 4 contains the advanced investigations into the SBC's performance. Firstly, the problems related to bolt-impact are investigated which is followed by a section examining the performance differences between the ASBC and SSBC. The final section of Chapter 4 considers a SBC in a braced bay. This was conducted to determine whether sliding that is not collinear with the slot could negatively affect the performance. In Chapter 5 emphasis is placed on the effect of the SBC-braces on the seismic response of the structure. Firstly, the simplified analysis method that accurately captures SBC behaviour is discussed. Then the beneficial effect of the SBCs on the seismic response is presented through the analysis of a multi-storey CBF with SBC-braces. Chapter 6 contains the Conclusion and Recommendations for future studies.

Chapter 2

Literature Review

The Literature Review provides the context and concepts that motivated SBCs as a means to provide structural protection during an earthquake. The chapter commences with a short discussion of earthquakes which is followed by background information on the history of earthquakes in South Africa. The severe financial impacts of past international earthquakes are also reviewed. These earthquakes resulted in damage to steel structures and in particular the braced bays of CBFs. Although structural collapse was averted, the resulting damage motivated the introduction of structural control systems in some cases. These systems allow for added energy dissipation during earthquakes. After a discussion of structural control systems, the SBC is considered as an energy dissipation mechanism. Finally, the findings made by previous researchers and how they affected this study are discussed.

2.1 Earthquakes

The earth is composed of four distinct layers. These layers vary in composition, phase and density. The layers are shown in Figure 2.1 as the crust, mantle, outer core and inner core. The crust and the upper part of the mantle is called the lithosphere. The theory of plate tectonics postulates that the lithosphere is not a continuous mass, but is divided into plates of varying size and shape. These plates move in different directions due to the convective transfer of the molten rock in the mantle (Datta, 2010).

Fractures in the rock, called faults, are located at plate boundaries as well as internal to the plates. The faults at plate boundaries are the most common areas for earthquakes to occur (Datta, 2010). In Figure 2.2 the plate boundaries are illustrated as yellow lines and earthquakes with a magnitude of seven or higher are shown as circles, while yellow triangles indicate active volcanoes. It is clear that high seismic activity is generally concentrated at plate boundaries.

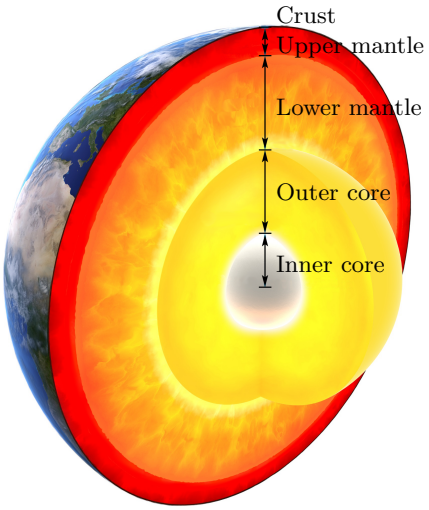

Figure 2.1: Earth's interior (adapted from DESY, 2010)

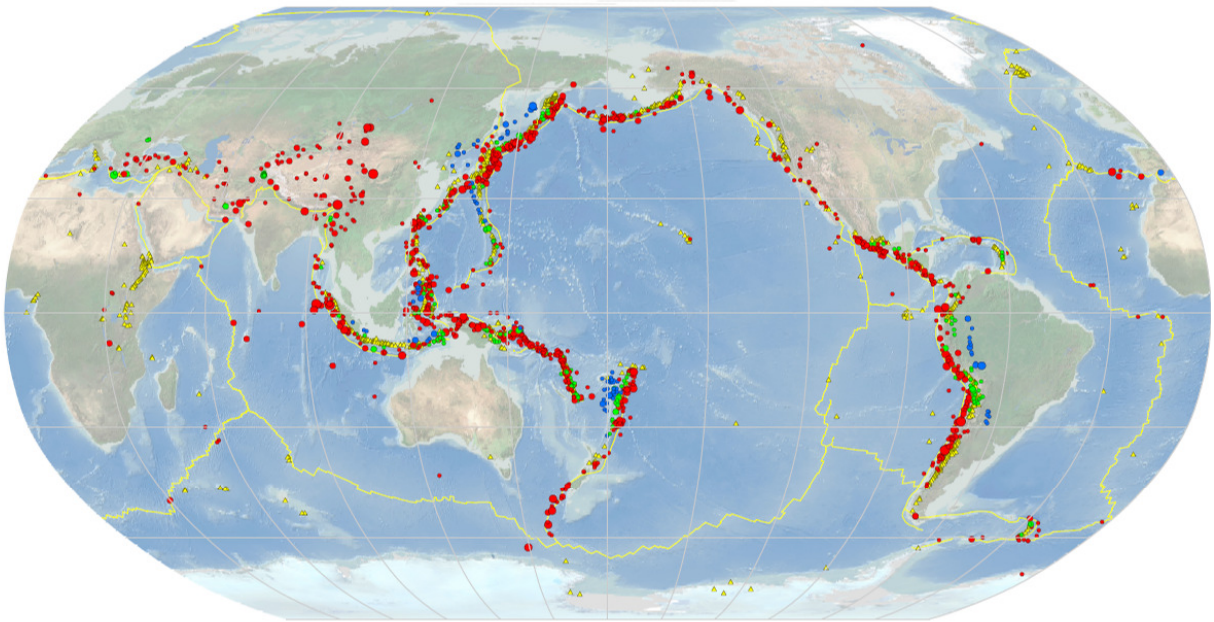

Figure 2.2: Global earthquakes (USGS, 2013)

When tectonic plates move relative to one another, strain energy accumulates as movement is resisted by the rock. This occurs both at plate boundaries and at faults internal to the plates. Slip occurs when the strain increases to such a magnitude that the rock is unable to restrain the movement any longer (Datta, 2010). Energy is then released as radial shock waves that are emitted through the elastic medium of the rock. The waves cause accelerations and displacements on the earth's surface. We perceive these vertical and horizontal movements as an earthquake. The point where slip occurs and energy is released is called the focus while the epicentre is the point directly above this at the earth's surface.

Earthquakes are quantified in various ways. The magnitude of an earthquake is generally measured by the Richter scale. This empirical scale measures the energy released by an earthquake on a base-10 logarithmic scale. The logarithm of the amplitude of the shock waves is used to determine the magnitude. Adjustments are made to allow for distances between seismographic instruments and the epicentre (Ellsworth, 1991). Earthquake intensity on the other hand is a subjective measure and is generally measured by the Modified Mercalli intensity scale. Table 2.1 lists the twelve intensities and their corresponding magnitudes on the Richter scale. The evaluations shown in bold in Table 2.1 correspond to the magnitudes of past and predicted future events in South Africa.

Table 2.1: The Modified Mercalli instensity scale (Datta, 2010)

Intensity	Evaluation	Description	Magnitude (Richter)
I	Insignificant	Only detected by instruments	1-1.9
II	Very light	Only felt by sensitive people; oscillation of hanging objects	2-2.9
III	Light	Small vibratory motion	3-3.9
IV	**Moderate**	Felt inside buildings; noise produced by moving objects	4-4.9
V	**Slightly strong**	Felt by most people; some panic; minor damage	5-5.4
VI	**Strong**	Damage to non-seismic resistant structures	5.5-5.9
VII	**Very strong**	People running; some damage in seismic resistant structures and serious damage to un-reinforced masonry structures	6-6.3
VIII	**Destructive**	Serious damage to structures in general	6.4-6.6
IX	**Ruinous**	Serious damage to well-built structures; almost total destruction of non-seismic resistant structures	6.7-6.9
X	Disastrous	Only seismic resistant structures remain standing	7-7.4
XI	Disastrous in extreme	General panic; almost total destruction; the ground cracks	7.5-7.9
XII	Catastrophic	Total destruction	8-8.9

2.1.1 Earthquakes in South Africa

Public perception is that South Africa is not a seismically active region and that mainly mining-induced seismicity can be expected in the Northern parts of the country. In fact, South Africa is prone to natural earthquakes of low to moderate magnitudes in some regions, particularly the South-Western Cape. Over the period of 1620-1971, seven earthquakes with magnitudes

between 5.1 and 6.5 were recorded in South Africa (Kijko et al., 2002). Early earthquakes were characterised based on accounts of people who experienced the events. Table 2.2 is an excerpt from a database of historical earthquakes of South Africa, compiled by the Council for Geosciences. Table 2.2 lists the five most severe earthquakes of the 20th century as well as a brief description of the effects of each. The worst earthquake in recent South African history occurred in 1969 in the Ceres-Tulbagh region with a magnitude of 6.3. Aftershocks were felt up to a few months after the initial earthquake. The structural damage at the time was estimated at US$24m (Kijko et al., 2002). Kijko et al. (2002) performed a probabilistic seismic hazard assessment of the Tulbagh-Ceres region and concluded that the maximum plausible future event magnitude in this area was 6.99 with a *Peak Ground Acceleration* (PGA) of 0.3g.

Table 2.2: Historical earthquakes of South Africa (Geoscience, 2012)

Year	Location	Intensity	Magnitude	Remarks
1912	Koffiefontein	VII	±6	Felt all over South Africa. Many farm buildings completely destroyed.
1932	Off Cape St Lucia	VIII	6.0-6.5	Poorly constructed buildings badly damaged, one or two collapsed, cracks and fissures in ground reported.
1969	Ceres, Tulbagh, Wolseley	VII-IX	6.3	Serious damage to certain buildings in the area, damage varied from almost total destruction of both old and poorly constructed buildings to large cracks in the better built ones. Twelve people killed and many more injured.
1976	Welkom	VII	5.2	Extensive damage to many buildings and breaking of windows. The most dramatic was the collapse of a block of flats, six storeys high, 75min after the earthquake. Four miners killed.
1992	Carletonville	VII	4.7	Unusual amount of damage recorded, due to the high population density around the epicentre. Houses damaged as far as Pretoria.

The Milnerton fault, shown in Figure 2.3 (a), which is approximately 10 km from the Cape Town CBD is of particular interest to seismologists. According to Dr Chris Hartnady, earthquakes of magnitude 6.0 or larger are “inevitable” along the Milnerton fault (Hartnady, 2003). Figure 2.3 (b) shows the Nubia and Somalia tectonic features of the African continental plate. The Nubia and Somalia plates are separating along the East African Rift Zone. The hatched area is the Lwandle diffuse plate boundary, where deformations take place over an area of hundreds of kilometres wide. This boundary zone extends over the Eastern part of South Africa which is shaded in grey in Figure 2.3 (b). Dr Hartnady believes that movement of the Nubia and Somalia plates constitutes a significant future threat to the whole of Southern Africa.

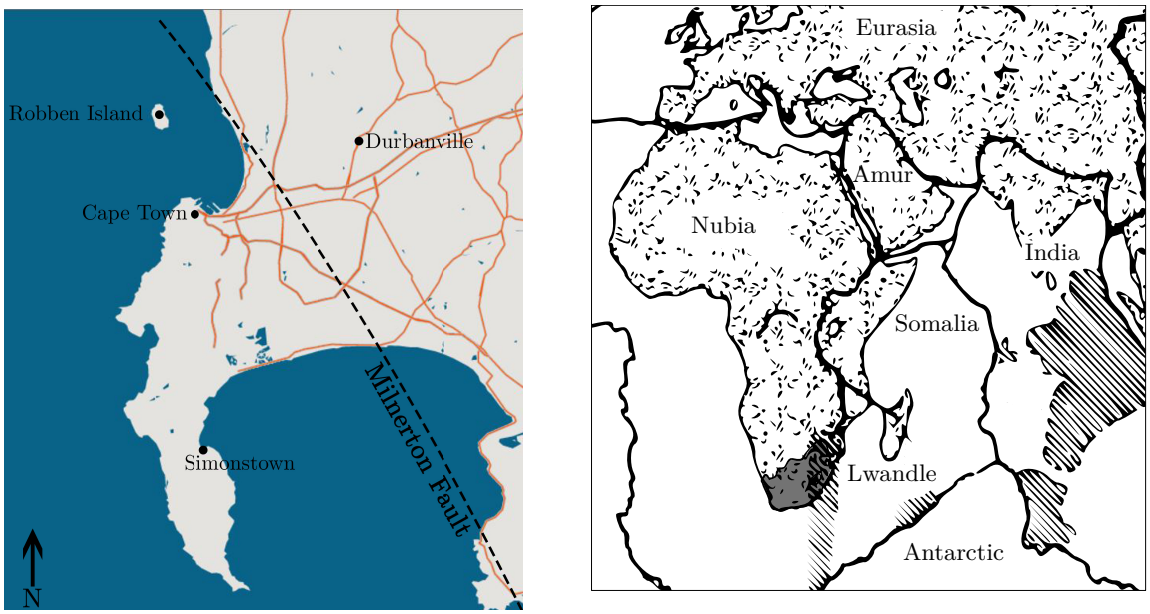

(a) (b)

Figure 2.3: Maps indicating the position of (a) the Milnerton fault and (b) African tectonic features (adapted from Hartnady (2003) and DeMets et al. (2010) respectively)

2.1.2 Seismic risk

According to Munich Re, a global reinsurance company, 29% of natural disasters from 1950-1999 were earthquakes. The death toll from these disasters amounted to 1.4 million with US$960bn in economic losses (Munich-Re, 1999). In this 50 year period, earthquakes caused 45% of the fatalities and 35% of the economic losses.

In more recent years, earthquakes remain devastating in terms of loss of life and the economy. Table 2.3 lists the ten most disastrous natural catastrophes from 1980-2013. In Table 2.3, we see that while earthquakes such as Northridge resulted in significantly less fatalities compared to others, the economic impacts are no less severe.

Table 2.3: The ten most disastrous natural catastrophes from 1980-2013 (Munich Re, 2014)

Date	Event	Area	Losses (US$m)	Fatalities
2011	Earthquake (9.0), tsunami	Japan	210 000	15 880
2005	Hurricane Katrina, storm surge	USA (Southern states)	125 000	1 322
1995	Earthquake (6.9)	Japan (Kobe)	100 000	6 430
2008	Earthquake (7.9)	China	85 000	84 000
2012	Hurricane Sandy, storm surge	USA, Canada, Caribbean	68 500	210
1994	Earthquake (6.7)	USA (Northridge)	44 000	61
2011	Floods	Thailand	43 000	813
2008	Hurricane Ike	USA and Caribbean	38 000	170
1998	Floods	China (Yangtze)	30 700	4 160
2010	Earthquake (8.8), tsunami	Chile	30 000	520

There is a misconception that seismic risk is limited to regions with high levels of seismicity (Bachmann, 2003). Seismic risk is the product of the seismic hazard and the vulnerability of the region (Wang, 2009). Low to moderately active seismic regions such as South Africa might be especially at risk. The high vulnerability of these areas that are not accustomed to seismic events, result in a high seismic risk. In many parts of the world, seismic risk is continually increasing (Bachmann, 2003). Some new structures are built without following specifications stipulated in seismic building codes or general principles of seismic design. This results in structures that are susceptible to collapse or disproportionate damage.

2.2 Damage in Steel Structures

The Northridge (USA) and Kobe (Japan) earthquakes were two of the most destructive earthquakes in recent history which caused an estimated damage of US$150bn. Although collapse of steel buildings was not recorded during Northridge, pronounced damage occurred (Tremblay et al., 1995). Northridge in particular, is well known for the numerous weld-fractures in beam-column connections of MRFs (Miller, 1998). In CBFs, damage was especially localised to braced bays, with predominantly brittle fractures occurring (Di Sarno et al., 2002). Table 2.4 lists some common types of damage in CBFs during these earthquakes. Brace failures occurred in buckling or brace fractures due to *Low-Cycle Fatigue* (LCF), while connection failures ranged from gusset-plate fracture to tear-out. The severe economic losses prompted extensive research into enhancing existing design methods as well as advancing innovative approaches to structural protection.

Table 2.4: Damage to CBFs in Kobe and Northridge earthquakes (Di Sarno et al., 2002)

Element	**Damage**
Braces	Buckling
	Severe brittle fracture (due to LCF)
	Fracture at beam-column connection
	Fracture at bolt holes
	Weld fracture
	Tear-out
Diaphragms	Shear connections
Infills	Fracture at contact points

2.3 Structural control

Buildings that are susceptible to seismic loading must be able to fulfil different requirements under moderate and severe earthquakes. Under moderate earthquakes buildings may be required to have adequate stiffness to avert structural damage. When severe earthquakes do materialise, buildings must have adequate ductility to avert structural collapse (Balendra et al., 2001).

Seismic design requirements have criteria to ensure sufficient ductility in structures. Ductility is defined as the inelastic deformation capacity of structures (Engelhardt, 2009). Conventional design provides ductility by assuming that under severe seismic loading, some members or connections will undergo plastic deformation in order to dissipate energy. This method has, in general, succeeded in collapse prevention, but the high cost of reparation has led to increasing use of alternative energy dissipation measures especially after the economic impacts of the Northridge earthquake (Butterworth, 2000).

In recent years, significant research was conducted on low-damage systems that strive towards the ideal of damage avoidance during an earthquake (MacRae, 2015a). One way in which this can be achieved is by implementing vibrational control systems. These systems include *Passive Energy Dissipation* (PED) systems, fully active systems, hybrid systems and semi-active control systems. The characteristics of these systems are discussed in the following sections.

In order to motivate the use of these control systems, we can start by considering the conservation of energy in a structure subjected to seismicity. This is described by the absolute energy formulation (Uang et al., 1990):

$$E_I = E_K + E_S + E_\mu + E_\zeta \tag{2.1}$$

where:

- E_I - absolute earthquake input energy
- E_K - absolute kinetic energy
- E_S - elastic strain energy

- E_μ - energy dissipation through hysteretic/inelastic action
- E_ζ - energy dissipation through viscous damping

Let us consider a constant amount of earthquake input energy in a structural system. It is clear from Equation 2.1 that if the contribution of hysteretic dissipation (E_μ) and viscous damping (E_ζ) is increased, the energy demand on elastic strain (E_S) and kinetic energy (E_K) decreases (Constantinou et al., 1998). As a direct effect, the structural displacements and accelerations are also decreased. When reviewing Equation 2.1 the rationale behind structural control systems is clear.

Further partitioning of E_μ and E_ζ can be done (Symans et al., 2008):

$$E_\mu = E_{\mu,Structure} + E_{\mu,Devices} \tag{2.2}$$

$$E_\zeta = E_{\zeta,Structure} + E_{\zeta,Devices} \tag{2.3}$$

Equation 2.2 and 2.3 shows that by adding supplemental devices, the demand on the structural and non-structural components can be decreased.

As far as passive control systems are concerned, friction or metallic yielding systems are classified as E_μ, while viscous-based systems are classified as E_ζ (Constantinou et al., 1998). Active and hybrid systems however add energy to the structure so their interactions introduce a new term in the energy balance equation.

2.3.1 Passive Energy Dissipation (PED) systems

A characteristic of these systems is the omission of an external power source. They can be classified as viscous, metallic or friction systems. Viscous and visco-elastic dampers are expensive and require specialised installation. Metallic systems rely on novel materials which are stressed into their post-elastic range in order to dissipate energy. A practical solution which can be employed is to use a SBC that dissipates energy through frictional sliding of the plates (Butterworth, 2000). In structures implementing these systems, instead of designing for some plastic deformation to occur, the focus is on utilising the non-linear strength that arises from the (PED) devices. These devices are placed in certain positions in the structure to obtain the desired performance (Loo et al., 2014). PED devices can be represented by the flow diagram shown in Figure 2.4, which shows that structural vibrations or deflections activate the systems and then affect the structure's response (Constantinou et al., 1998).

Figure 2.4: Structure with passive system (adapted from Di Sarno et al., 2005)

Some examples of PED devices include:

- Metallic yielding dampers: these devices exploit the beneficial inelastic behaviour of certain metals. This provides stable hysteresis loops and energy dissipation that is predictable (Di Sarno et al., 2005). Mild steel or lead is often used for this purpose. These devices have the following shapes; x-shaped, triangular, dog-bone or hourglass. They are commonly placed between braces or at beam-ends. They are idealised by parallelogram-shaped hysteresis loops as shown in Figure 2.5 (a).

- Friction dampers: these devices dissipate energy through friction during sliding between solid interfaces (Symans et al., 2008). Various friction dampers have been developed, namely; the Pall friction damper, the Sumimoto device and the SBC. The SBC is significantly simpler and more economic than other friction dampers since its fabrication is similar to conventional construction. Only a slotted-hole, pre-loaded bolts, spring washers and shim plates (if required) need to be additionally specified. Various materials have been used for the shims of SBCs, namely; mild steel, brass, stainless steel, aluminium and more recently *Abrasion Resistant Steel* (ARS). When friction dampers are idealised by rectangular hysteresis loops as shown in Figure 2.5 (b), it implies that a constant friction force is assumed.

- Shape Memory Alloy (*SMA*) dampers: these devices are composed of special metal alloys such as Nickel-Titanium or Copper-Zinc-Aluminium that exhibit super-elasticity (Di Sarno et al., 2005). Large strains can be achieved without residual deformations after unloading has occurred. This is possible through a reversible phase transformation at crystalline level. These dampers result in stable hysteresis loops, shown in Figure 2.5 (c).

- Visco-fluid dampers: these dampers are analogous to suspension systems in cars and effectively act as linear or non-linear dashpots (Symans et al., 2008). They consist of a viscous fluid in a chamber that is connected to a piston. The piston can translate and causes the fluid to flow through orifices located in or around the piston, which dissipates energy. They are idealised by circular or elliptic hysteresis loops as shown in Figure 2.5 (d).

- Visco-elastic dampers: these dampers are composed of visco-elastic materials such as copolymers which are bonded between steel plates. Copolymers possess a high deformational ability and energy is dissipated through elastic shear deformations when the steel plates move relative to each other (Constantinou et al., 1998). The behaviour of these dampers is temperature dependant. They are idealised by leaf-shaped hysteresis loops as shown in Figure 2.5 (e).

- Base isolation systems: these devices are placed at the base of the structure and are divided into two groups: elastomeric or sliding isolators (Di Sarno et al., 2005). Elastomeric isolators are composed of layers of rubber interposed by steel plates, while sliding isolators utilise friction to dissipate energy and are either flat or curved. Since the structure is isolated from the ground, less energy is absorbed during an earthquake, resulting in less energy that must be dissipated in the structure (Butterworth, 2000).

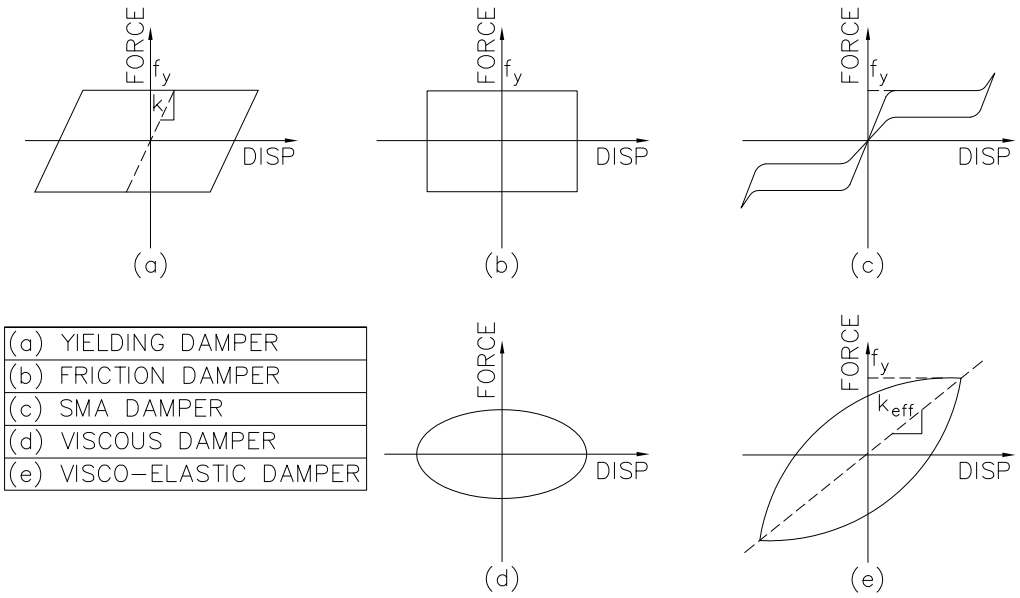

Figure 2.5: Idealised hysteresis loops of PED devices (adapted from Di Sarno et al., 2002)

2.3.2 Active control systems

These systems require an external power source to function. Sensors perceive the earthquake excitation as well as the structural response to the excitation. The signals are processed by a computer which incorporates control algorithms to impart forces onto the structure. Forces are then applied by actuators as shown in the flow diagram in Figure 2.6. Drawbacks of these systems include high complexity, the need for high maintenance and the reliance on power. The *Active Mass Damper* (AMD) is an example of such a system. This system employs an auxiliary mass which is controlled by actuators and is used to reduce the response of the structure to dynamic effects (Chen et al., 2003). The idealisation of an AMD is shown in Figure 2.7.

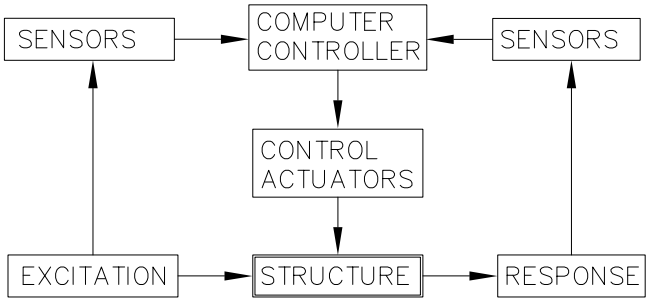

Figure 2.6: Structure equipped with active control (adapted from Di Sarno et al., 2005)

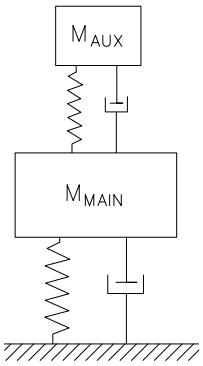

Figure 2.7: AMD principle (adapted from ASME, n.d.)

2.3.3 Hybrid control systems

These systems combine the most advantageous characteristics of passive and active systems and often outperform active systems (Chen et al., 2003). They are however more complex as shown by the flow diagram in Figure 2.8. Examples of hybrid control systems include hybrid mass dampers and hybrid base isolation systems which incorporate active and passive devices.

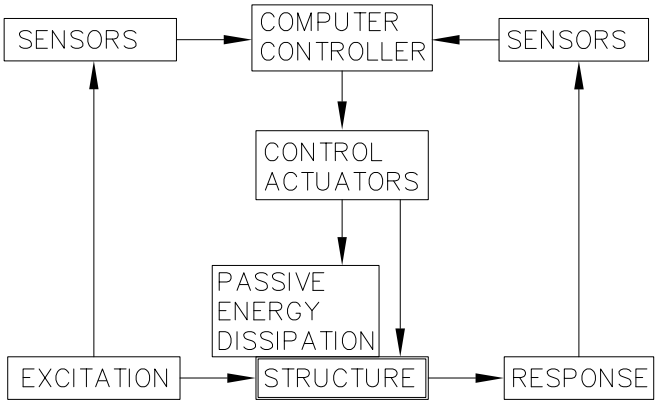

Figure 2.8: Structure equipped with hybrid control (adapted from Di Sarno et al., 2005)

2.3.4 Semi-active control systems

These systems have low power requirements and can often be powered by a battery. They are essentially passive dampers with computer controlled adjustable properties (Chen et al., 2003). This means that energy is not an input to control the behaviour of the structure as with active systems, but energy is rather an input into the passive dampers to obtain the desired structural performance. This is shown in Figure 2.9. Examples of these systems include variable-orifice dampers, variable friction dampers and controllable-fluid dampers.

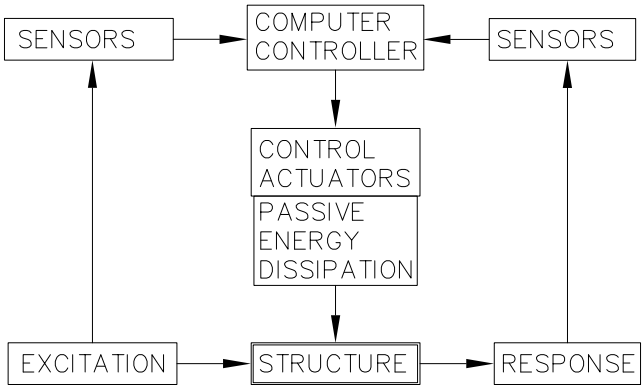

Figure 2.9: Structure equipped with semi-active control (adapted from Di Sarno et al., 2005)

2.4 Slotted connection dissipaters

Section 2.3 indicated that various types of energy dissipation systems are available and have been investigated. In general however, these systems have not been widely implemented in engineering practice. They often require unconventional installation techniques and unfamiliar materials. Systems are usually sold as ready-made, niche solutions leading to high cost. Furthermore, their infrequent use introduces difficulties and uncertainties into design. These factors have all hindered the use of structural control systems in general applications (Grigorian et al., 1993).

SBCs on the other hand, represent a credible method of adding supplemental energy dissipation in a simple manner for general application (Grigorian et al., 1993). Energy dissipation occurs when relative slip takes place between plates in a bolted friction connection. In this manner seismic protection can be offered economically, without using heavier sections to increase the stiffness of the structure (Law et al., 2006). SBCs require minimal deviation from general construction practise and use materials that are commonplace in the industry (Grigorian et al., 1993).

Constantinou et al. (1998), argued that SBCs are restricted by their ability to maintain the properties necessary for their function over the design lifetime of the structure. The concerns were corrosion and bolt-tension maintenance. The friction interfaces could be susceptible to corrosion, depending on the materials used. Bolt-tension loss could also be expected both during sliding and over the lifetime of the structure. In addition, stable friction behaviour during operation was identified as a fundamental requirement for the feasibility of SBCs.

Past research focused on frictional material and SBC testing, full-scale testing, analytical work and bolt-impact considerations. The importance of stable frictional behaviour resulted in a number of studies that investigated different materials for use in the SBC.

Grigorian et al. (1993) performed one of the first studies to evaluate the suitability of SBCs for supplemental energy dissipation during earthquakes. Balendra et al. (2001) proposed implementing the SBC in a low-damage structural system called the *Knee-Braced Frame* (KBF). They performed full-scale testing of a KBF incorporating a SBC in the brace. Butterworth (2000) and Clifton et al. (1998) collaborated to investigate the effect of the ASBC for use in the *Sliding Hinge*

Joint (SHJ) which was developed by Dr Charles Clifton. In addition, a preliminary non-linear dynamic analysis was performed on a case-study building. Lukkunaprasit et al. (2004) performed the only study into the effect of impact between bolt-shanks and slot-ends. They proposed that a type of restrainer be used to prevent bolt-impact. S. Lee et al. (2008) aimed to use the SBC for retrofitting of a damaged building. They used an analytical model to optimise slip-load for the desired response in the retrofitted building. Khoo et al. (2012) continued work by Clifton et al. (1998) with full-scale testing of the beam-column SHJ connection. They aimed to investigate the impact of material hardness on the friction and wear characteristics of SBC components. C. Lee et al. (2013) developed a new friction material with stable behaviour and a high coefficient of friction for use in SBCs. They also investigated the effect of different SBC details on sliding behaviour. Latour et al. (2014) emphasised the need for materials that exhibit stable friction performance. They tested three materials for use in SBCs. Loo et al. (2014) proposed a more simplified connection than previous researchers had used. The simplified SBC was tested with different materials and bolt-tensioning protocols.

A more detailed discussion of work conducted by previous researchers is provided in Section 2.4.1. The discussion is conducted largely in chronological order since significant findings in a particular study often led to trends that carried forward into subsequent research. The objectives, methods and results of their work clarify the areas of interest that motivated this study.

2.4.1 Previous studies

Pre-2000

In the study by Grigorian et al. (1993), the slot in the slotted-plate coincided with the direction of the loading which is shown in Figure 2.10. The slotted-plate is wedged between the outer plates when the bolts are tensioned. Steel and brass slotted-plates were used alternatively with the steel outer-plates. This resulted in steel-steel friction and steel-brass friction. If the loading applied to the connection exceeds the friction, the slotted-plate slips in relation to the outer-plates. When loading is reversed, the same happens in the opposite direction. Earthquake input energy is dissipated through friction when the connection slips.

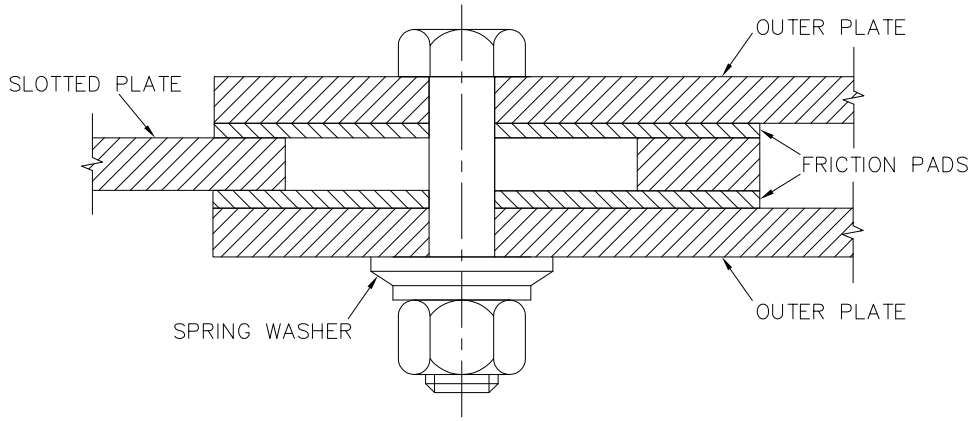

Figure 2.10: Slotted connection detail (adapted from Grigorian et al., 1993)

Forty different samples were tested which included a variety of bolt sizes, layouts and frictional surface conditions. Figure 2.11 shows the typical configuration used for tests. In earlier tests the slip-force diminished quickly due to a loss of bolt-tension when tested for large displacements and cyclic loading. This was remedied by the use of Belleville spring washers. These are conically shaped washers that flatten at a specified load (Davet, 1997). They were used to ensure that the bolt-tension was maintained during sliding.

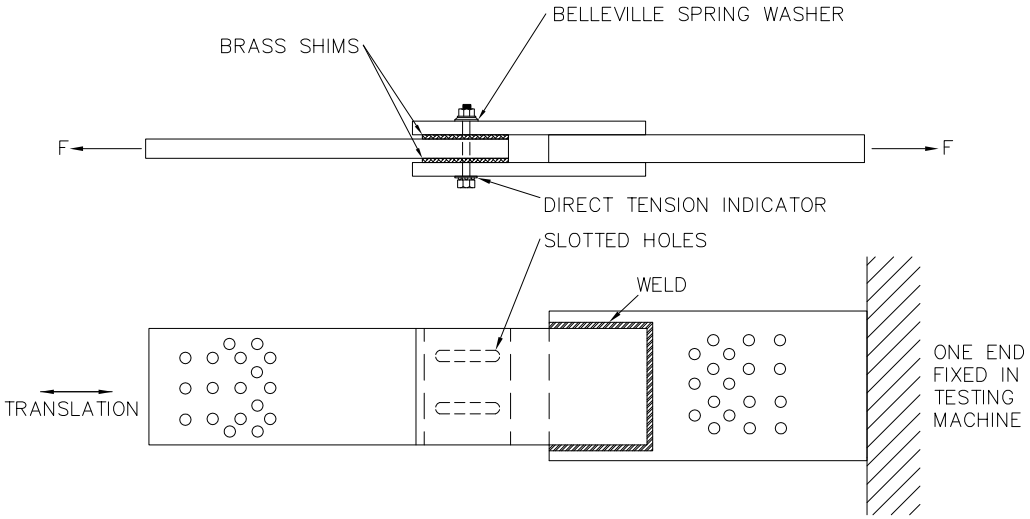

Figure 2.11: Configuration of SBC for testing (adapted from Grigorian et al., 1993)

The samples were tested in a monotonic-testing machine as illustrated in Figure 2.12. The cyclic tests were displacement controlled in order to study the frictional behaviour of the connection. The results for the steel-steel interface exhibited significantly varying friction values with time, which was seen in the majority of the cases. The brass-steel interface delivered a more stable behaviour during sliding. The comparison between the steel-steel interface and steel-brass interface is shown in the hysteresis loops in Figure 2.13. The variable nature of the steel-steel friction is illustrated by the wide distribution of force values in the plot. The brass produced closely spaced force values showing a more reliable slip-force. Thinking that surface conditions were the cause of this behaviour in the steel-steel interface, samples were wire brushed and sand blasted to remove mill scale. This only served to exacerbate the unwanted behaviour. Grigorian et al. (1993) stated that: "the occurrence of this behaviour in SBCs where friction occurs between like steel surfaces renders such SBCs inefficient at best and impractical at worst, as energy dissipaters".

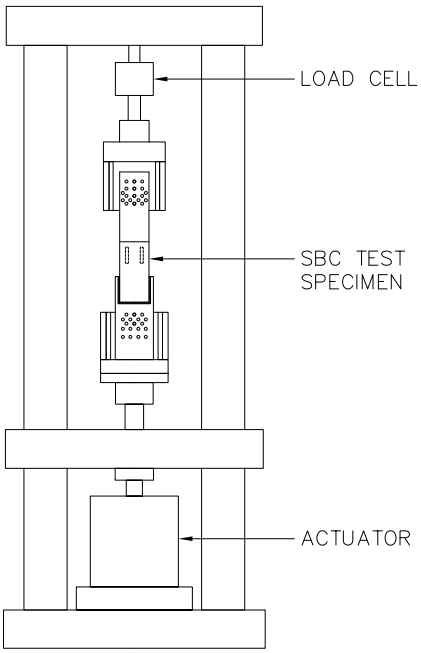

Figure 2.12: SBC in monotonic testing machine (adapted from Grigorian et al., 1993)

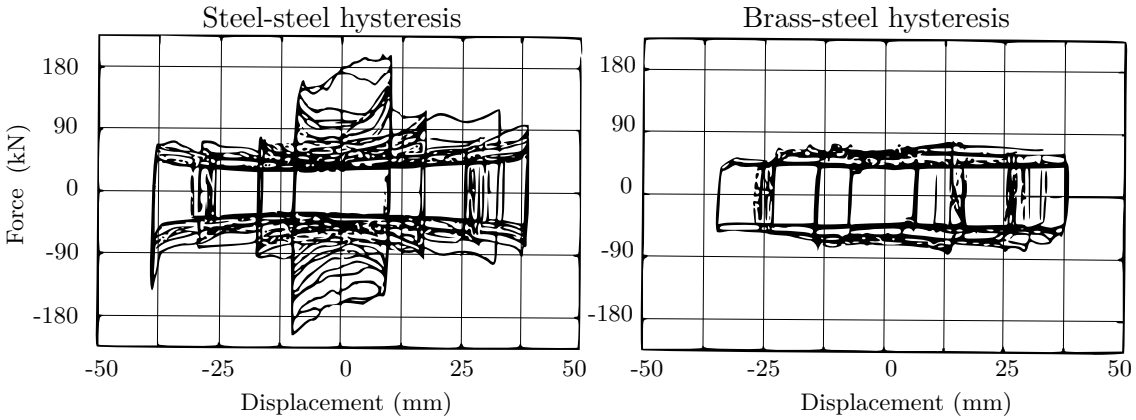

Figure 2.13: Typical SBC hysteresis results (adapted from Grigorian et al., 1993)

Grigorian et al. (1993) believed that this irregular pattern in the hysteresis diagram for the steel-steel was because of the friction and wear characteristics of the surface. They argued that as dynamic loading occurs, adhesive friction is the main mechanism occurring in the connection. Adhesive wear is defined as "when two smooth bodies are slid over each other, and fragments are pulled off one surface to the other", Rabinowicz (1995). Loose particles between the plates increase the bolt tension and therefore the frictional force of the connection. This corresponds to what is seen in the hysteresis diagram. As the connection slides, some of these particles drop out and the bolt tension is decreased. This behaviour was seen independently of the initial smoothness of the surface. The surfaces were described as "severely scratched" after tests. The

steel-brass interface performed significantly better than the steel-steel interface. The authors argued that using other materials, for example ductile cast iron, and inserting these materials as shim plates could result in an improved behaviour. This seemed to be in contrast to one of the original goals of SBCs in that only familiar materials be used.

The study was concluded by mentioning that both types of SBCs were able to dissipate energy. The unstable behaviour of the steel-steel interface is problematic for design since friction can not be bounded with confidence. The steel-brass interface proved more stable and was described as nearly perfectly elastic-plastic (Grigorian et al., 1993). It was agreed that SBCs seemed promising as energy dissipation mechanisms in steel structures. It was also clear that suitable materials should be used.

2000 to 2010

In a subsequent study by Balendra et al. (2001), they considered three frame systems used in earthquake resistant steel structures; the MRF, CBF and *Eccentrically Braced Frame* (EBF). The three systems are shown in Figure 2.14. MRFs are able to dissipate energy by forming plastic hinges in the beams or connections (Hamburger et al., 2009). Plastic hinges must however be avoided in the columns and larger steel sections must be used in MRFs to control lateral drift. CBFs dissipate energy by yielding of braces in tension while diagonals in compression are assumed to buckle (Sabelli et al., 2013). CBFs have a low drift capacity due to their high stiffness. In EBFs, the braced members are connected at eccentricities away from the normal concentric connection positions. Energy is dissipated by forming plastic hinges in the beams attached to the braces (Balendra et al., 2001). The beams are designed to yield in shear or bending.

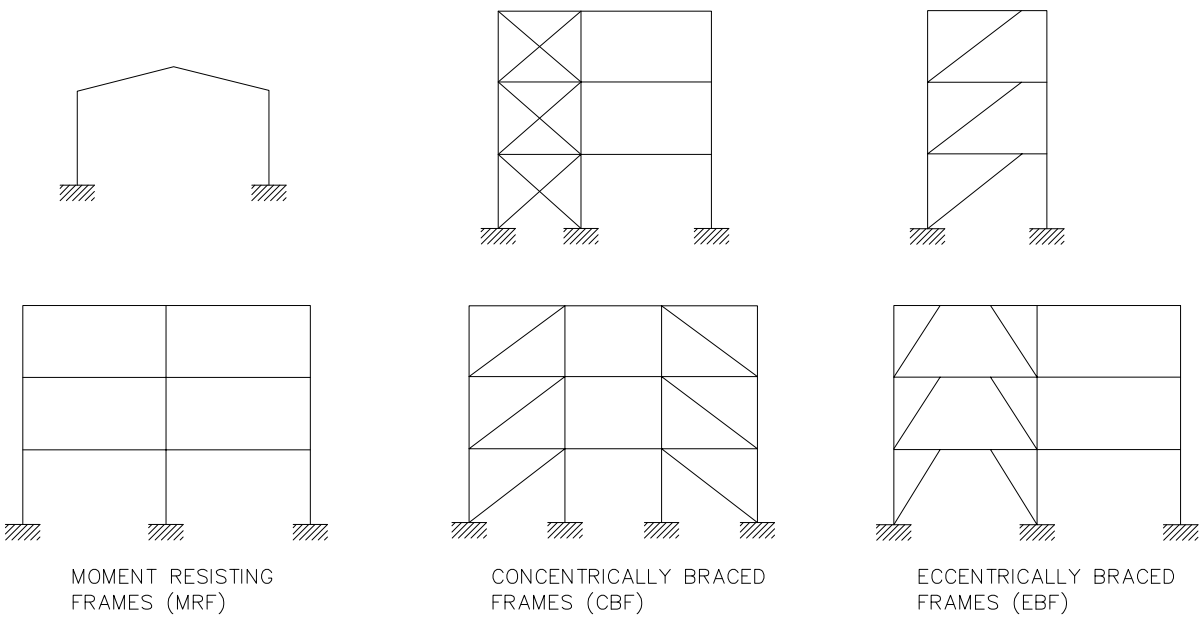

Figure 2.14: Types of earthquake resistant steel frames (adapted from ESDEP-WG17, n.d.)

For the above mentioned systems, the beams or braces would need to be replaced after an earthquake. Since these are principal structural members, reparation would be expensive and occupancy would not be possible during repair. As a solution to achieve low-damage design, Balendra et al. (2001) proposed the KBF. The knee section acts as an intermediary between the bracing element and the member to which it is connected. During a rare earthquake of large magnitude, energy dissipation occurs by the knee yielding in shear and in this manner buckling of the bracing member is averted. Repair is more economical since only the knee will need to be replaced after an earthquake.

Balendra et al. (2001) incorporated a SBC into the brace of the KBF. A pseudo-dynamic testing procedure was used to investigate the behaviour of the frame under earthquake and wind loading. Pseudo-dynamic testing is a method used mainly for seismic testing of full-scale structures. Actuators are used to apply forces simulating the real inertial forces that would be caused by seismic ground accelerations (McClamroch et al., 1987).

The bottom of the brace was connected to the column and column-base by a gusset as shown in Figure 2.15. This connection housed the SBC. The set-up of the SBC itself was similar to that in Figure 2.10. The 10 mm thick gusset plate was bolted to the column and served as the slotted-plate. On either side of the slotted-plate, 3 mm thick brass shims were used.

Slip occurs when forces in the brace exceed the friction in the SBC. The slip-forces were kept sufficiently low so that the knee member remained elastic. Stopper blocks were used to limit the slip-length and to prevent the bolt-shanks from impacting the slot-ends. The blocks could be adjusted depending on the required slip-length. When the slip-length is reached, the force increases in the brace as well as the knee. The sections used for the columns, beam and brace would remain elastic even when the knee was loaded to failure. The knee was designed to fail in shear and not in flexure or buckling.

The setup for the full-scale test is shown in Figure 2.15. A *Linear Variable Displacement Transducer* (LVDT) was used to measure the displacement of the SBC during sliding. Strain measurements were used to determine the force in the SBC. Seismic and wind generated displacements were simulated in the tests in addition to sinusoidal displacement cycles. The maximum slip distance was limited to 3 mm from the reference position. From Figure 2.16 it is observed that in the region of ± 40 kN, energy is dissipated through sliding. Outside of this region energy is dissipated by the knee, either elastically or inelastically. Yielding was verified by the paint starting to crack and peel off of the knee.

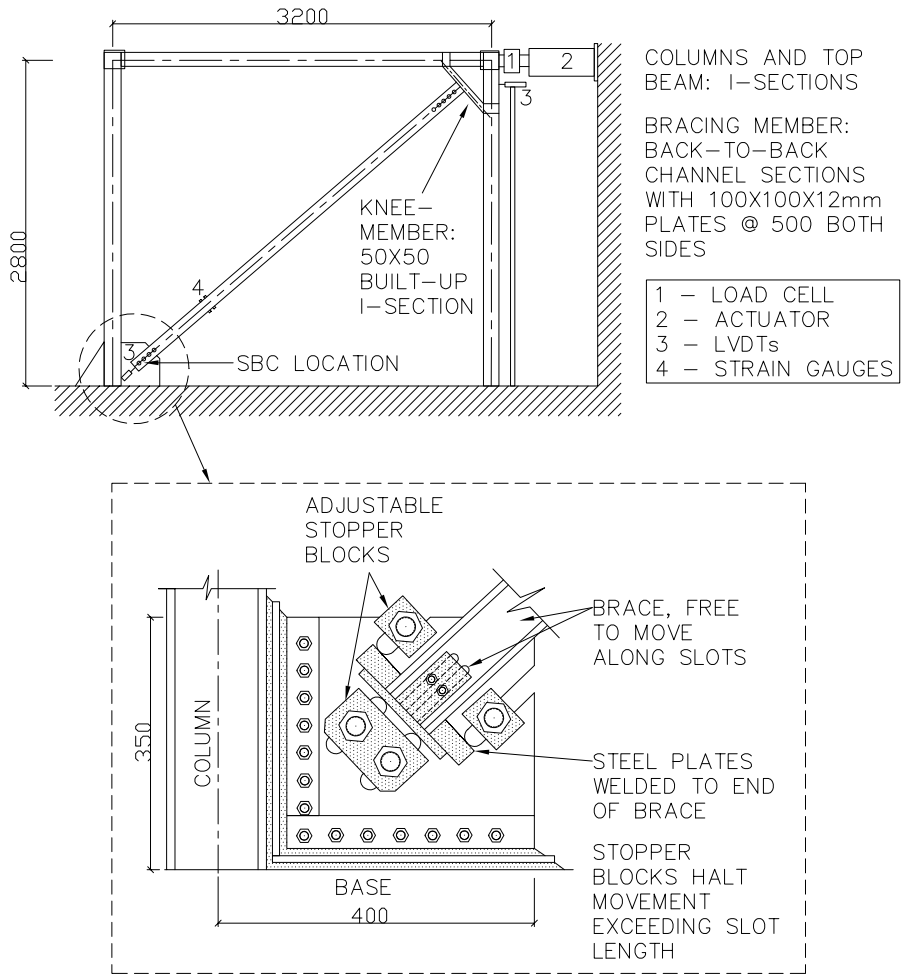

Figure 2.15: KBF for full-scale testing (adapted from Balendra et al., 2001)

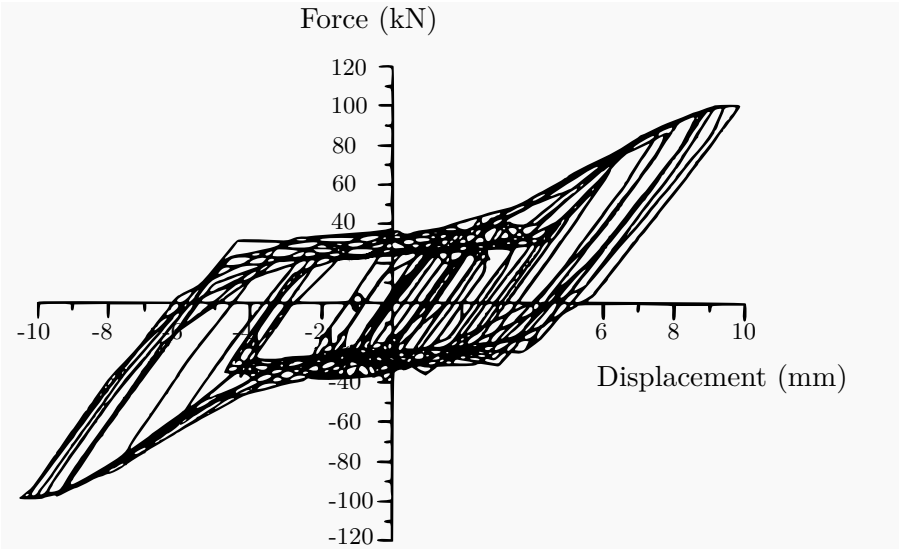

Figure 2.16: Hysteresis of the KBF test (Balendra et al., 2001)

Analytical dynamic software DRAIN-2D (Dynamic Response Analysis of Inelastic 2-Dimensional Structures) was used incorporating subroutines for the SBC and knee element written by Roeder et al. (1977). Experimental and numerical results agree well before the SBC governs the response and after the knee governs the response of the frame. Discrepancies were observed at the times when the SBC controlled the response of the frame. This was because the experiment did not slip at a constant level as was assumed in the analytical model.

It was apparent from this study that the KBF could dissipate energy. The SBC could be incorporated in the design by allowing the connection to slip at an appropriate level thus reducing the strength required in the members. The knee yields during rare events and provides hysteretic dissipation. The knee could be easily removed and replaced. The KBF with the SBC in the bracing was therefore promising in terms of low-damage design.

Butterworth (2000) agreed with Grigorian et al. (1993) in stating that the important aspects in the performance of SBCs were sustained bolt-tension and stable sliding. A brittle failure must also be averted when the bolt-shank makes contact with the slot-end. Butterworth (2000), felt that SBCs were simple to construct and stated that they could dissipate energy either by straight-line or rotational sliding. The two variants of the SBC; SSBC and ASBC are shown in Figure 2.17. In the ASBC, only the slotted-plate and one of the outer-plates of the connection carry loading. The plate that does not carry loading is called the cap-plate and is dragged along during sliding in the ASBC. In a study in which Butterworth was a co-author, Clifton et al. (1998), the ASBC was tested experimentally. The study incorporated the brass shims and spring washers that were shown to be beneficial by Grigorian et al. (1993). It was ensured that the SBC would remain slip free under serviceability loads. Tests for ultimate limit state were conducted with displacement-time histories at rates expected during earthquakes. Neglecting the use of spring washers resulted in up to 40% loss of tension in the bolts after which the connection stabilised. Butterworth (2000) was of the opinion that the omission of spring washers would lead to a simpler connection and was a meaningful trade-off against the associated loss of tension. The ASBC displayed adequate performance despite the large stresses in the bolt-shank and plates adjacent to the bolt holes. When bolts make contact with the edges of the bolt-holes of the cap-plate they start acting in bearing mode.

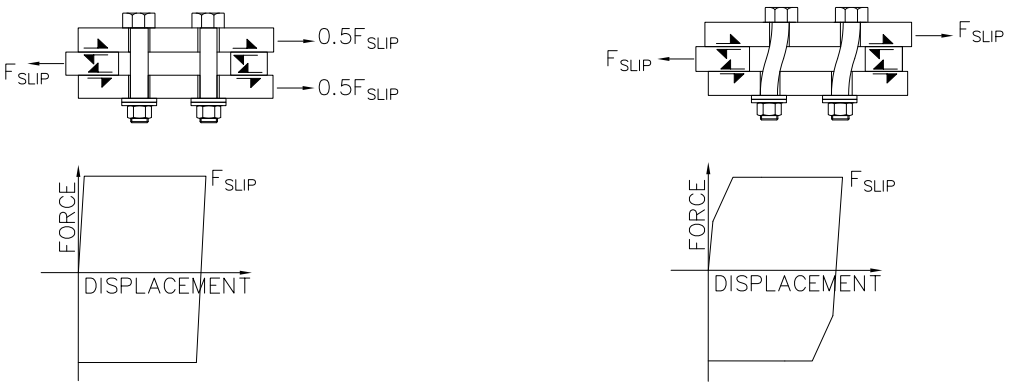

(a) Symmetric SBC

(b) Asymmetric SBC

Figure 2.17: Symmetric (a) and Asymmetric (b) SBC (adapted from Loo et al., 2014)

Diagonally braced frames and K-braces with SBCs incorporated in the braces are shown in Figure 2.18, these were tested experimentally by Yang et al. (1995). A typical detail for such a SBC used in a K-brace was provided by Butterworth (2000) is shown in Figure 2.19. A detail for a rotational SBC in a K-braced frame is shown in Figure 2.20. Systems utilising horizontal sliding for K- and X-arrangements appeared to be promising. The tensile force combined with assistance from the compression member would ensure load reversal. Further, when the lateral bracing reached its ultimate capacity, over-strength could be provided by hinges forming in the surrounding columns and beams of the frame.

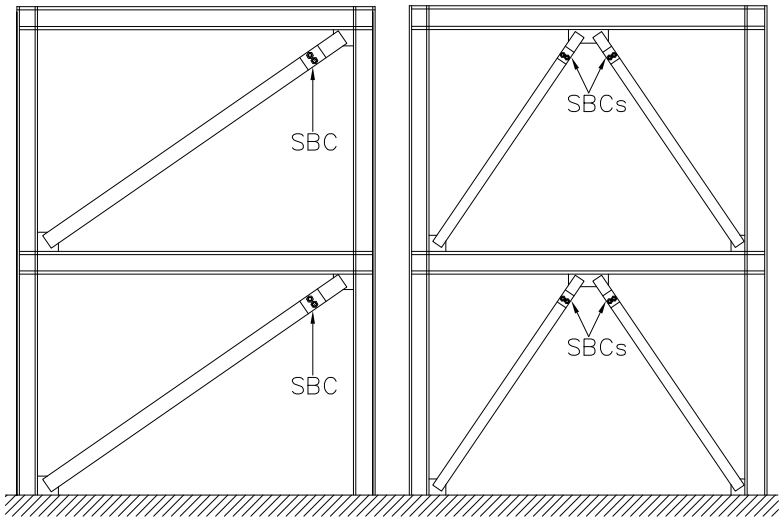

Figure 2.18: Diagonal and K-bracing systems (adapted from Butterworth, 2000)

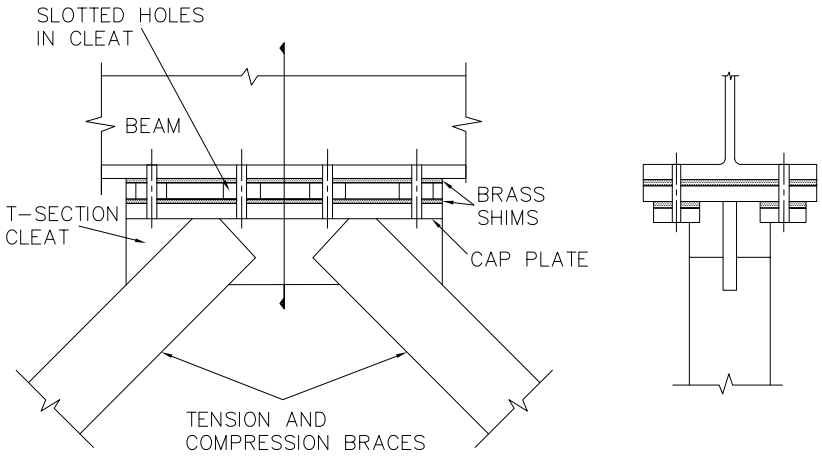

Figure 2.19: T-stub type SBC (adapted from Butterworth, 2000)

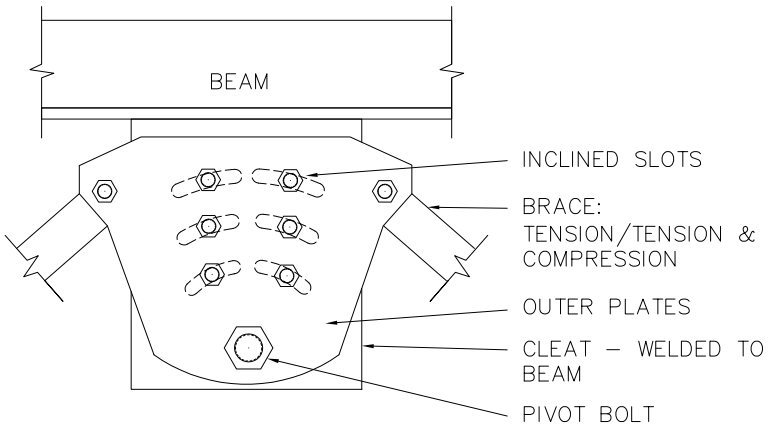

Figure 2.20: Rotational type SBC (adapted from Butterworth, 2000)

Butterworth (2000), performed a simple analytical case study on a frame subjected to earthquake loading. The layout of the frame is shown in Figure 2.21. Earthquake records were incorporated in a non-linear dynamic analysis using SAP2000. Only the non-linear effect of the SBC, assumed to behave in an elastic perfectly plastic manner, was included. Viscous damping of 5% was assumed.

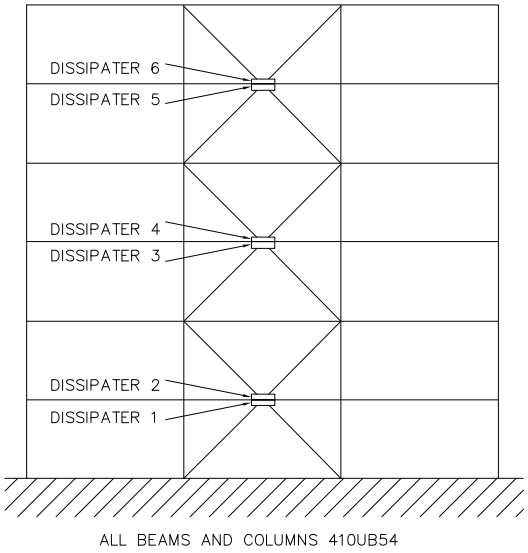

Figure 2.21: Configuration of frame used for case study (adapted from Butterworth, 2000)

It was found that the length of the slotted connections controlled the ductility of the structure. The self-centring capability of the structure after an earthquake was a concern, but it was argued that providing enhanced fixity in beam-column connections could remedy this. Since braces could be made sufficiently strong, the importance of the SBC to provide strength after sliding was noted. Brace forces increased when bolts made contact with the slot-end and generally led to load reversal, decreasing the force in the SBC and brace once more. Decreasing the slot-length resulted in higher storey-shear. Forces in the SBCs were up to six times the slip-force when

bolt-impact occurred, albeit for short durations. This increase in force would be less with more refinement in the post-slip behaviour of the model. Butterworth (2000), stated that general conclusions could not be made from the research, since a single simple structure was considered. Additionally, only slight changes were made in the boundary conditions, slot-length, slip-force, and only three earthquake records were employed. Further research was therefore necessary.

Lukkunaprasit et al. (2004), motivated their study by stating that previous research had not inspected bolt-shank impact with the slot-end of the SBC. They argued that in many cases a long slot-length would not be achieved due to the congested nature of beam-column-brace connections. This implies that sliding that exceeds the slot-length of the SBC is likely and consequently, impact of the bolt-shanks with the slot-ends could occur.

A SBC with brass shims and spring washers was tested experimentally. Displacement controlled testing was performed considering the connection both with and without bolt-impact. By selecting an appropriate thickness for the slotted-plate, it was ensured that the failure mode was that of bearing deformation, and not shear failure of the bolts.

Tests of the SBC without bolt-impact yielded similar results to previous studies. The brass-steel interface provided relatively stable sliding as well as strengthening behaviour with the final friction being double that of the initial friction. During tests with bolt-impact, the force in the connection increased dramatically upon impact. Figure 2.22 shows that the initial force in the connection during sliding was approximately 100 kN. When bolt impact occurred, the force increased to approximately 125 kN until the applied displacements changed direction and load reversal occurred. In successive cycles, approximately only half of the initial friction force of the connection remained. This occurred after less than 5 mm of displacement was prescribed past the slot-ends. The bolts experienced permanent deformation in their shanks due to bearing. This resulted in a loss of bolt-tension causing friction loss in successive cycles. It should therefore be ensured that the plates deform in bearing and not the bolts.

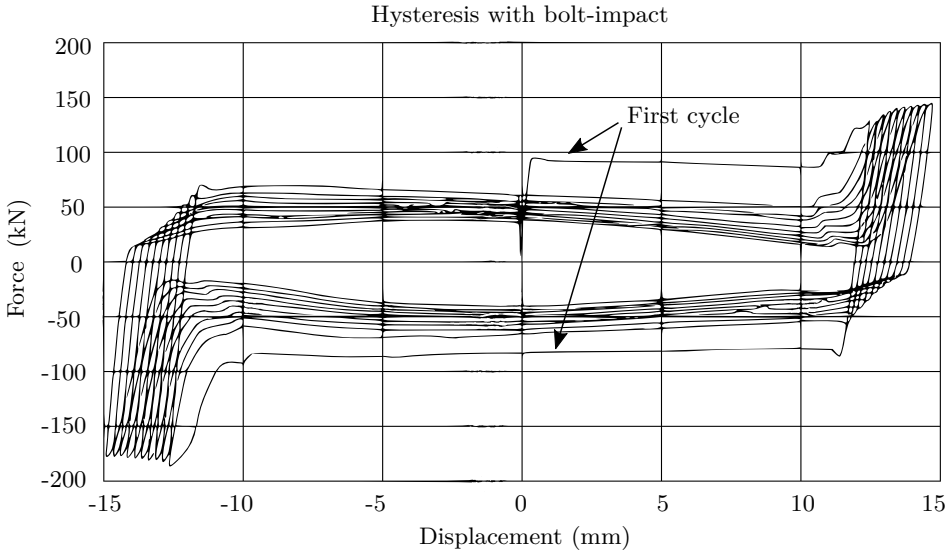

Figure 2.22: Hysteresis of SBC with bolt-impact (adapted from Lukkunaprasit et al., 2004)

They proposed using a restrainer to protect the SBC by limiting the maximum force that could be transferred. They failed however to discuss any details of what the device was composed of and how it functioned.

A non-linear dynamic analysis was performed on a case study building. The 6-story steel MRF would collapse during a large earthquake through weld fracture of the beam-column connections. Chevron bracing was considered for the model in the central bay of the MRF. These connections included SBCs with restrainers in each brace.

Lukkunaprasit et al. (2004), concluded from their results that the SBCs with restrainers performed better than the original connections. With the restrainers they observed a reduction in the inter-storey drift. Although this meant that less energy was dissipated in the SBC, they felt that it was necessary to prevent bolt-impact. They concluded by expressing the need for more studies to determine the optimal characteristics of the connection including the restrainers.

S. Lee et al. (2008) investigated the use of SBCs for retrofitting. They aimed at finding the optimal slip-force for retrofitting the multi-storey building they considered. This optimum was based on performance indexes for the reduction of acceleration and inter-storey drift of the structure.

Tests were conducted to validate the characteristics of the connection before an analytical model was created. Brass shims were incorporated into a SSBC with a similar set-up to Grigorian et al. (1993). Bolts were tightened using a torque wrench.

Linear loading tests were performed to determine the slip-force of bolts tightened to different torques. The tests indicated that the slip-force was proportional to the bolt torque. The relationship between bolt torque and slip-force was used to predict the slip-force for the analytical model. It is unclear whether this relationship that was used in the analytical model was based on only the six experimental tests listed.

For the analytical model, the SBC and brace was modelled as shown in Figure 2.23. Using this model, the results from the cyclic experiments were compared to the analytical values and the results compared well.

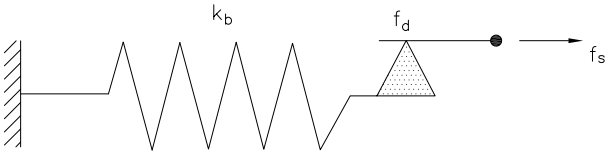

Figure 2.23: Friction damper model (adapted from S. Lee et al., 2008)

The symbols used in Figure 2.23 are:

- k_b - stiffness of bracing member
- f_d - friction force of damper
- f_s - force in entire configuration

S. Lee et al. (2008) conducted a comparative analytical study of the seismic response of a damaged 10-storey structure with and without the SBC-braces. Newmark's method was used to obtain the response of the structure to a seismic record for both cases. In order to investigate the analytical response of the structures, two indices were examined:

- R_d - the ratio of the maximum retrofitted to the maximum reference inter-storey drift.
- R_a - the ratio of the maximum retrofitted to the maximum reference acceleration.

Since the SBCs were considered for retrofitting the damaged building, the optimisation aimed at minimising these response indices. Two slip-force distribution techniques were considered:

- Case (i) - slip-force over the maximum base shear of the reference building.
- Case (ii) - slip-force over the maximum inter-storey shear force of the reference building.

For Case (i), the slip-force was equal over all stories. For Case (ii), each storey had slip-forces proportional to the inter-storey shear of the reference structure.

The inter-storey drift performance indicated that the SBC-braces improved the structural response irrespective of the slip-force distribution technique. This is shown in Figure 2.24 (b). It is important to note that increasing the magnitude of the slip-force beyond its optimal value could affect the response of the structure negatively as shown in Figure 2.24 (a). It is clear that when the slip-forces are larger, the structure exhibits a stiffer response causing higher accelerations. During high accelerations in the reference structure, permanent deformations may have occurred in some areas. They concluded from the numerical results that the SBC-braces could be effective for retrofitting of a damaged building, especially in terms of inter-storey drift reduction.

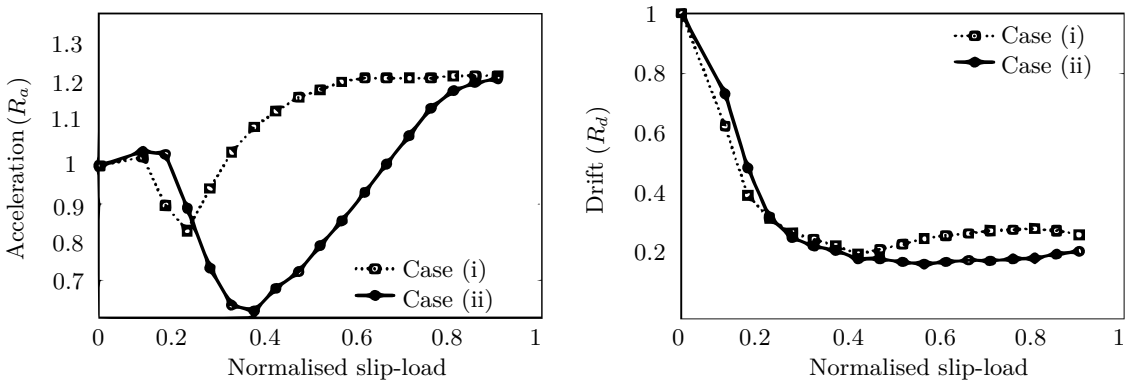

(a) Acceleration performance index (R_a) (b) Drift performance index (R_d)

Figure 2.24: Optimisation of the selected performance indices (adapted from S. Lee et al., 2008)

Post-2010

Khoo et al. (2012), studied the effect of the hardness of shim materials on a specific connection detail, namely; the *Sliding Hinge Joint* (SHJ). The SHJ is a beam-column connection for

MRFs developed by Dr Charles Clifton from 1995-2002. The SHJ proposed to solve problems encountered in preceding details where SBCs were present in both top and bottom flanges of beam-column connections. These details exhibited positive dissipative qualities, but were problematic because of the ability of gaps to form between the beam and column face. This impacted negatively on the structural frame and floor slabs.

The SHJ connection is illustrated in Figure 2.25. The connection consists of a pinned top-flange to column connection. The top flange plate is welded to the column face, while the bottom-flange and web connections are incorporated into the ASBCs. It was designed to experience plastic rotations facilitated by the pinned connection while maintaining excellent energy dissipation characteristics through the ASBCs in the web and bottom-flange.

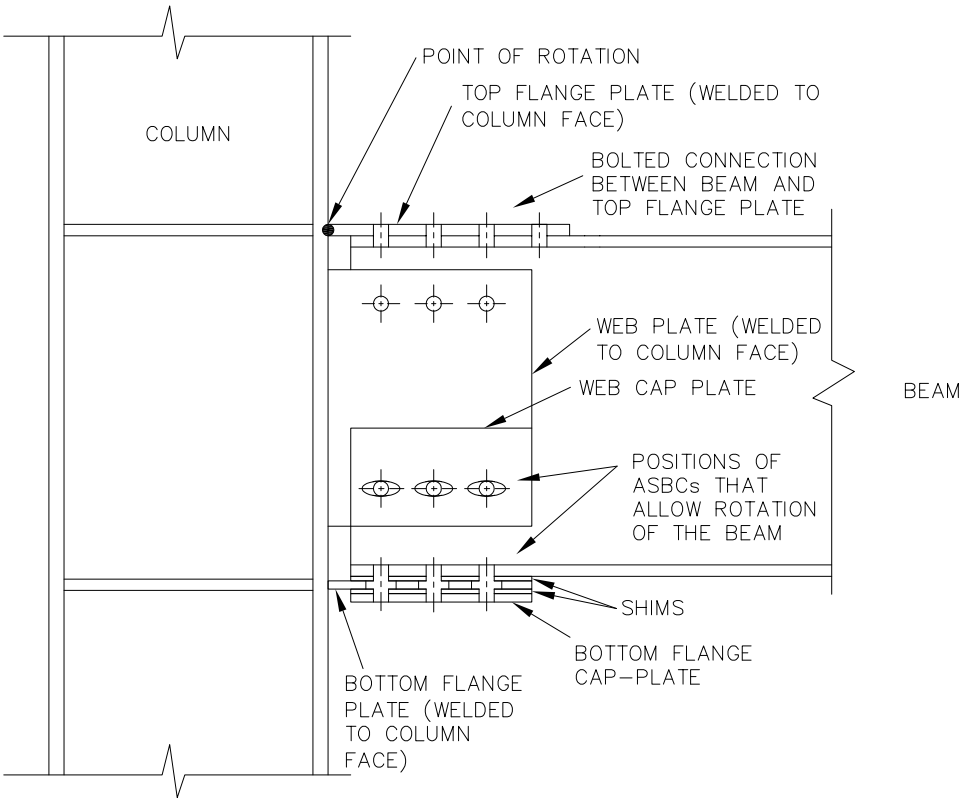

Figure 2.25: Layout of the Sliding Hinge Joint for MRFs (adapted from Khoo et al., 2012)

Their research aimed to clarify the frictional modes at the interfaces of the SBC. In this manner an understanding of the problems encountered with steel-steel sliding could be obtained. They examined the influence of the material hardness on the sliding stability and wear mechanisms of the SBC. In addition they investigated which material exhibited the most stable behaviour with the highest initial to dynamic slip ratio.

The moment-rotation curve of the SHJ is shown in Figure 2.26. The SHJ has a linear stiffness in zone (A) of the curve. When the slip-force in the web and the bottom flange is exceeded, rotation in the pinned top-flange commences. The first interface of the ASBC slips (B) until the rotation reaches such a point where the second interface also slips, doubling the frictional force (C). When the load is reversed, the opposite occurs. For a negative rotation a slightly higher

frictional force was observed which was attributed to the bottom flange plate coming into the beam at an angle and increasing bolt tension. The SHJ is able to undergo a rotation of more than 0.04 radians which corresponds to class “high ductility” for MRFs in Eurocode 8 (Khoo et al., 2012).

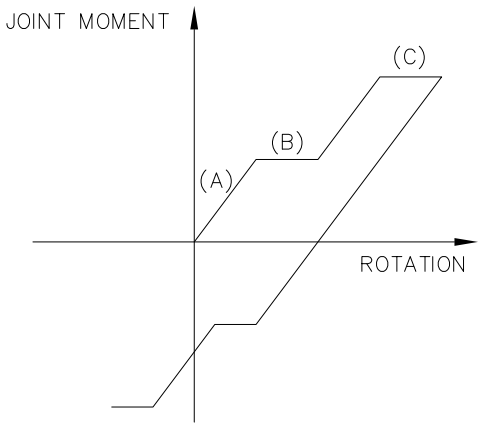

Figure 2.26: SHJ moment-rotation curve (adapted from Khoo et al., 2012)

The manner in which the bolt-shanks of the ASBC make contact with the bolt-holes of the outer-plate and cap-plate during normal sliding can be explained by Figure 2.27. In Figure 2.27 (a), slip occurs between only the slotted-plate and the outer-plate while no relative movement occurs between the cap-plate and the slotted-plate. When the construction tolerance between the bolt-hole of the outer-plate and the bolt-shank is closed, the bolt is shifted until the bolt-shank contacts the bolt-hole of the cap-plate as well, this corresponds to Figure 2.27 (b). In Figure 2.27 (c), the ASBC is fully activated and the outer- and cap-plates move relative to the slotted-plate.

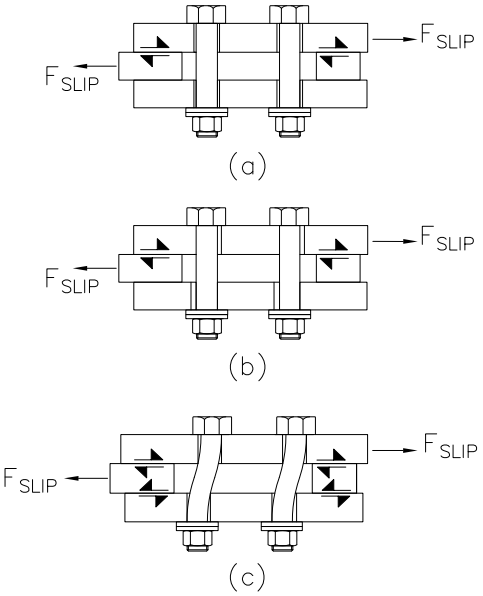

Figure 2.27: Mechanism of the ASBC during normal sliding (adapted from Loo et al., 2014)

The complex forces and interactions that the bolts experience in the ASBC were investigated and a mathematical model was developed by Dr Clifton. The forces and moments on the bolts were idealised as shown in Figure 2.28 which considers the ASBC in the bottom flange of the SHJ.

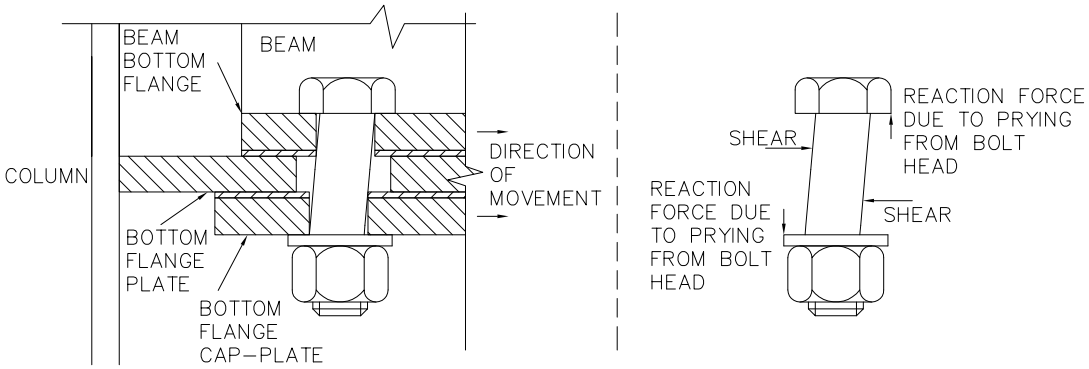

Figure 2.28: Idealised bolt deformation and force distribution due to ASBC in SHJ (adapted from Khoo et al., 2012)

The test setup modelled the bottom flange of the SHJ connection. This is shown at C in Figure 2.29. The distance of 460 mm between A and C represented an inverted I-beam section. Rotation took place around A which represented the pinned top flange of the SHJ. Loading was applied by a linear actuator at B.

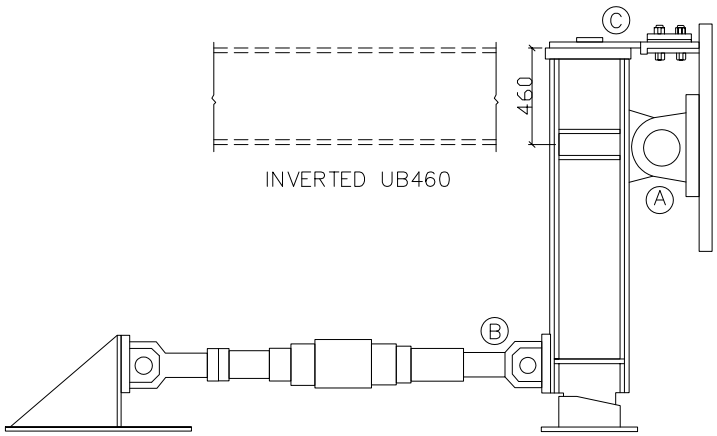

Figure 2.29: Experimental setup for SHJ test (adapted from Khoo et al., 2012)

The different shims that were tested are listed in Table 2.5. The material used for the beam and plates was G300 mild-steel. The turn-of-the-nut method was used with 120° rotation in compliance with New Zealand standards to achieve a bolt proof load of 210 kN. When spring washers were utilised, an additional 115° rotation was implemented to ensure flattening of the washers which was verified by the load-cell. The tests were displacement-controlled with a sinusoidal displacement function.

Table 2.5: Different steels tested by Khoo et al. (2012)

Steel:	Code:	f_y(MPa)	f_u(MPa)	Brinell hardness (HB)	thickness (mm)
Mild	G300	300	430	168	3
High strength	G80	690	790-930	266	3
Abrasion resistant	G400	1070	1320	382	5

In terms of friction and wear, the SBC must possess a high slip-force, stable behaviour, low friction variation and minimal wear of the interfaces. The stability and longevity of SBCs are related to the compatibility of the friction materials. It is necessary to have some understanding of the wear mechanisms present when metals slide over each other. Firstly, it is important to understand the real area of contact between metals. Figure 2.30 illustrates a contact interface between two metals on a microscopic level. The area over which the metals seem to be in contact is called the apparent contact area (A_a). In reality, the metals will only be in contact at the microscopic "joints" where actual contact occurs. The sum of these smaller areas is the real contact area (A_r). Even though A_a is much larger than A_r, the areas where no contact occurs play no part in friction (Rabinowicz, 1995).

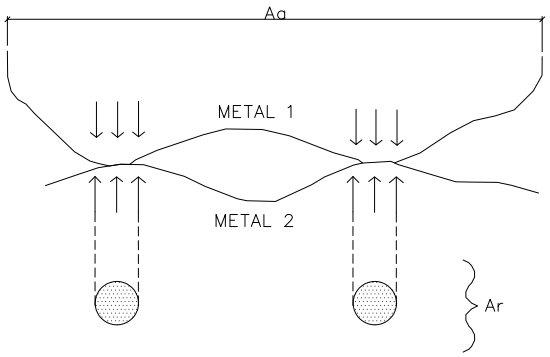

Figure 2.30: Real and apparent contact areas in metals (adapted from Rabinowicz, 1995)

Adhesive wear occurs whenever metals slide against each other. Particles disintegrate and are transferred from one metal to the other to which they then adhere. Figure 2.31 illustrates this wear mechanism between two metals on a microscopic level. The break in the material surface usually occurs at the interface between the materials, which corresponds to "Path 1" in Figure 2.31. If this interface is stronger than some internal surface, the break occurs in the solid, shown as "Path 2" in Figure 2.31, and material is transferred.

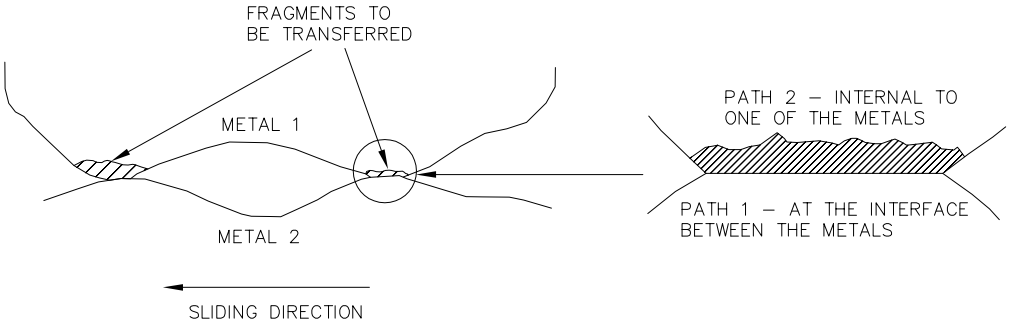

Figure 2.31: The adhesive wear mechanism in metals (adapted from Rabinowicz, 1995)

Abrasive wear occurs at a frictional interface where a harder and softer material is present. The harder material gouges out a rut in the softer material. The softer material disintegrates or forms mounds next to the rut and is removed through continued sliding. Figure 2.32 shows that abrasive wear between two metals on a microscopic level can occur as "two-body abrasion" or between independent particles which have been removed as "three-body abrasion". This mechanism is a function of the hardness of the materials involved.

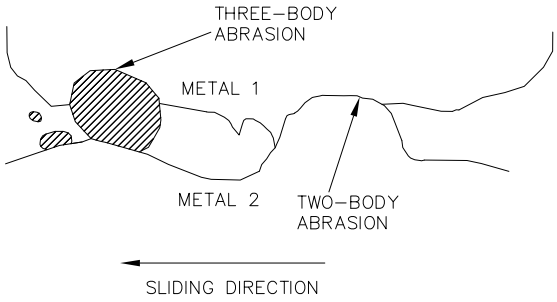

Figure 2.32: The abrasive wear mechanism in metals (adapted from Rabinowicz, 1995)

As material hardness increases, it becomes more resistant to wear (Rabinowicz, 1995). Materials with dissimilar hardnesses therefore yield better performance. The harder material dictates the mechanism while the softer material adapts. The loose particles of the harder material are embedded into the softer material. Where materials of equal hardness are used, the particles cannot implant and will cause rutting in both materials. This results in the unstable behaviour observed in the steel-steel interface. The test results were interpreted with cognisance to the different wear mechanisms.

The test results of the G300 shims displayed the same unstable sliding behaviour as in the studies of Grigorian et al. (1993), Latour et al. (2014) and Loo et al. (2014). For the ASBC, an increase in the friction was found as the test continued. This was in contrast to the decrease that Grigorian et al. (1993) observed. This unwanted force increase poses a problem for design. The G80 shims in which the spring washers were used provided more stable behaviour than the

G300 shims. There was also a lower increase in strength throughout the tests. The G400 shims produced the best behaviour in terms of stability, highest shear capacity per bolt and the least amount of strength gain during continued cycles.

The material wear was inspected after testing. The G300 shims exhibited the most wear with severely scratched surfaces and uneven wear on the plates. The G80 shims exhibited less wear, with moderate scratches evenly distributed over the surface. Scratches on the softer connecting plates were deeper than those on the shims. The G400 shims exhibited the least wear, scratches on the surface could not be felt by touch and were evenly distributed. The wear on the connecting plates was also seen to be less than with the other materials.

Khoo et al. (2012) concluded that the G400 shims were the best solution for the SHJ. The ARS is more economic and available compared to the brass used earlier. It can be welded to beams where necessary, while corrosion is also not a problem. They proposed that the G400 shims be tested in the SSBC.

C. Lee et al. (2013) underlined the need for reliable slip-force in SBCs. In previous studies, stable slip was diminished due to incompatible materials and the associated adverse wear mechanisms. The coefficients of friction (μ) found by earlier work ranged from 0.2 to 0.4. The study aimed at creating a new composite material with stable behaviour and a higher μ. Unfortunately, no specific information on the composition of the material was provided.

The SBC was comparable to the details used in previous studies. The shims were composed of the composite material and aimed at operation under a maximum slip-load of 150 kN. The shim had chamfered corners as shown in Figure 2.33, which was done to decrease stress concentrations at the edges and increase durability. Initial FEM analysis indicated that larger washers were required to assist in the distribution of the clamping force to the plate surface. The SBC allowed movements of 20 mm in both directions. In order to prevent bolt-impact, a stopper block was situated between the slotted holes as illustrated in Figure 2.34. In previous studies, the test setup meant that the actuator applied forces concentrically as shown earlier in Figure 2.11. Here the actuator applied transverse force at the top of the SBC as shown in Figure 2.34. This was argued to result in a more uniformly distributed slip force which was unaffected by eccentricities.

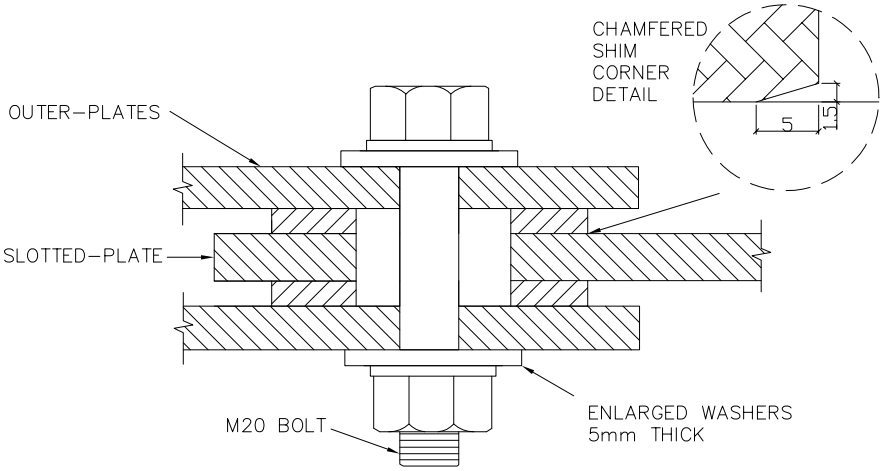

Figure 2.33: Initial SBC for experimental tests (adapted from C. Lee et al., 2013)

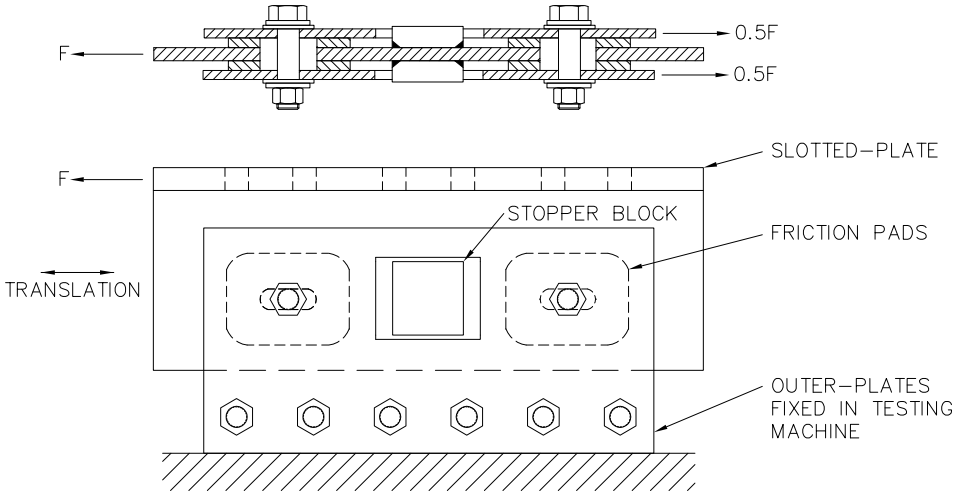

Figure 2.34: SBC assembly in test machine (adapted from C. Lee et al., 2013)

Tests were displacement controlled using an actuator with an internal load cell to measure the horizontal force. LVDTs were mounted on both the slotted- and outer-plates to determine the displacements during sliding. In preliminary tests, spring washers were not used and bolt-tension loss was observed as in previous research. For further testing they considered three details:

- Detail 1 - No spring washers.
- Detail 2 - A single spring washer under the bolt-head and the nut.
- Detail 3 - Two spring washers stacked in series under the bolt-head and the nut.

This is illustrated in Figure 2.35. A load-cell through which the bolt-shank passes was used. The load-cell was positioned under the bolt-head to measure the bolt-tension forces throughout the tests. The nut could therefore be tightened until the required bolt-tension was achieved.

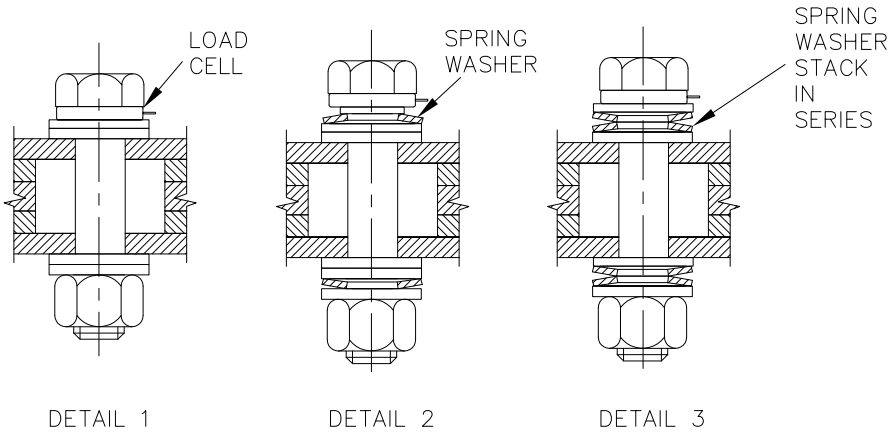

Figure 2.35: Spring washer details tested (adapted from C. Lee et al., 2013)

Results indicated that the composite material possessed stable friction behaviour. The material was also free from significant friction variation with continuing cycles. Detail 2 performed the best with double the friction of the other connections.

It was found that although bolt-tension varied during sliding, the friction of the different connections remained stable. During the initial cycles of loading there was a reduction in bolt tension regardless of the connection detail used. They suggested that the connection undergoes a "phase change" from zero displacement to sliding. It was thought that this "phase change" led to the drop in bolt-tension. The loss of bolt-tension only occurred in the first cycle and stabilised thereafter. They found that μ varied according to the connection detail employed. Detail 2 again exhibited the most promising behaviour. It resulted in the highest μ which meant the most energy was dissipated in this detail. They stated that by using the values obtained for μ, the SBC could be modelled using the Coulomb friction model. The final μ values found are listed in Table 2.6.

Table 2.6: Results for μ (C. Lee et al., 2013)

Connection Detail	μ
1	0.27
2	0.52
3	0.24

Figure 2.36 is an excerpt from the manual for the use of Belleville spring washers which shows how the arrangement of the spring washers affect the flat-load and deflections (Davet, 1997). The torques required for bolt tensions of 100 kN were found to be 270 Nm, 340 Nm and 190 Nm for details 1 to 3, respectively. This seems counter-intuitive, since according to Figure 2.36 details 2 and 3 should have the same flat-load but different flat-deflections. Detail 3 should therefore have had a higher torque than detail 2 to achieve the same bolt-tension. This was ascribed to the non-linear behaviour of the spring washers. C. Lee et al. (2013) stated that the use of spring washers in series should be avoided since it is improbable that the loads will be transferred as idealised through the inside diameters of the washers when placed crown-to-crown.

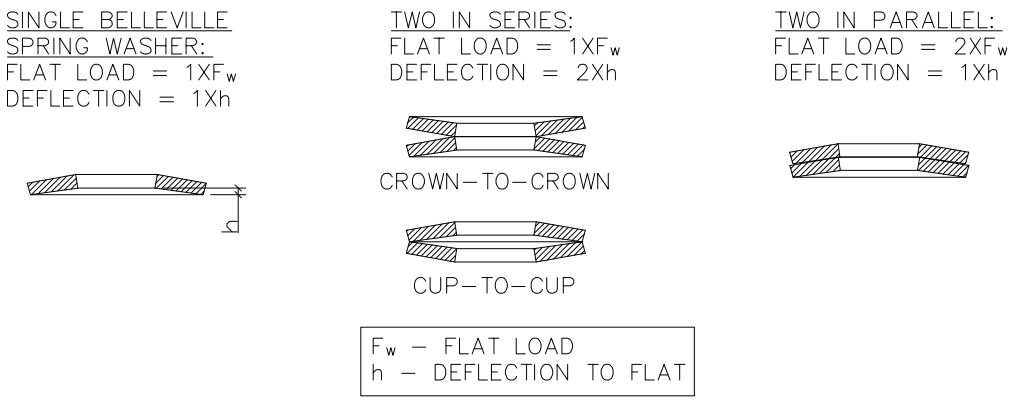

Figure 2.36: Spring washer layouts (adapted from Davet, 1997)

The material exhibited beneficial wear characteristics with surfaces remaining without deep scratches or ploughing. Consequently, the shims would not have to be replaced after an earthquake. C. Lee et al. (2013) felt that they successfully obtained a material with stable hysteresis behaviour and a high μ. It is questionable however, whether developing a new friction material for use in structures is economical or practical.

Latour et al. (2014) stated that a great advantage of the SBC is that the slip-force is the only variable that the designer must assume. It is imperative however, that the slip-force be predictable for design. In order to provide enhanced predictability, they studied the use of different friction materials for use in SBCs.

The study investigated steel-steel, brass-steel and *Thermally Sprayed Aluminium* (TSA)-steel interfaces. Figure 2.37 illustrates the setup of the connection they employed. They aimed at determining the coefficients of static (μ_s) and kinetic friction (μ_k) for the materials. This was done in the range of slip-forces adequate for seismic design. In addition, they investigated the effect of different material interfaces on friction variation during sliding. This was shown by previous research to be either a degradation in friction or an increase followed by a degradation.

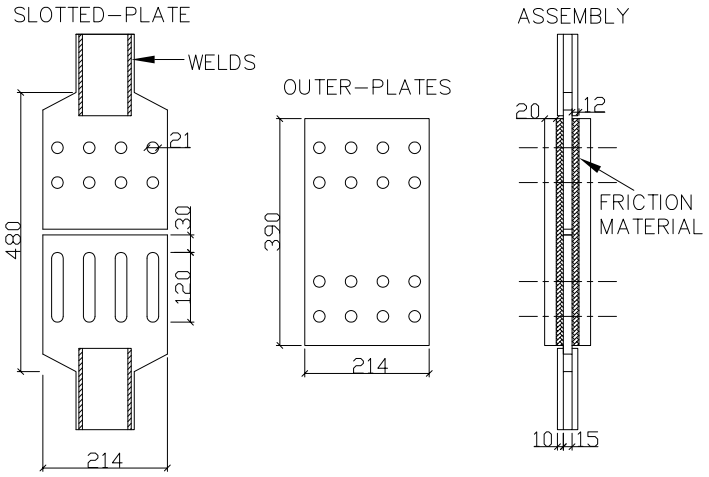

Figure 2.37: Layout of SBC for material testing (adapted from Latour et al., 2014)

For the steel-steel SBC they recognised unstable behaviour which is illustrated by the variation of force values in the hysteresis diagram in Figure 2.38. An increase followed by a loss of strength was observed for the steel-steel interface. A significant correlation between μ_k and pressure on the steel-steel friction interface was not found and the average μ_k for the steel-steel interface was 0.37.

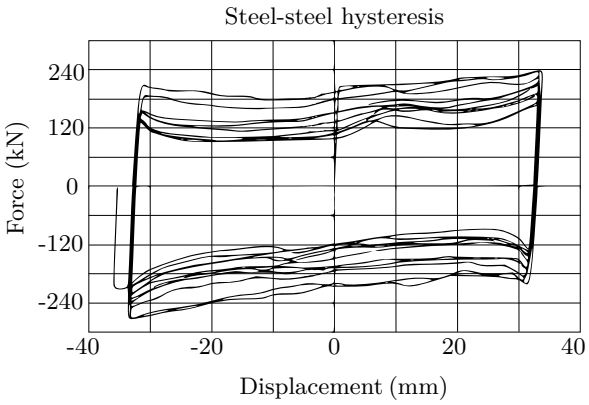

Figure 2.38: Steel-steel hysteresis curve (adapted from Latour et al., 2014)

The brass-steel SBC had a lower slip-force than the steel-steel SBC, but exhibited more stability. The hysteresis loops in Figure 2.39 show closely spaced force values compared to the steel-steel interface. A hardening behaviour during increasing cycles was observed which is in contrast to the steel-steel interface behaviour.

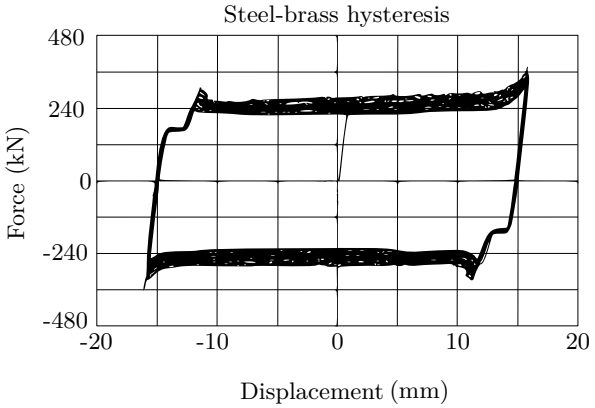

Figure 2.39: Steel-brass hysteresis curve (adapted from Latour et al., 2014)

The TSA-steel interface was composed of a 300 μm thick coating. Results indicated that this interface had superior stability compared to the other materials. This is easily noticed from the narrow band in which the friction values lie in Figure 2.40. There was only a minor difference between the μ_s and μ_k for the TSA-steel interface. The slip-force was found to be inversely proportional to bolt-tension and as the interface pressure increased, μ decreased. This was explained by the increased wear behaviour associated with the higher interface pressure. There was no correlation between the loss of strength after subsequent force cycles and pressure applied to the friction interface.

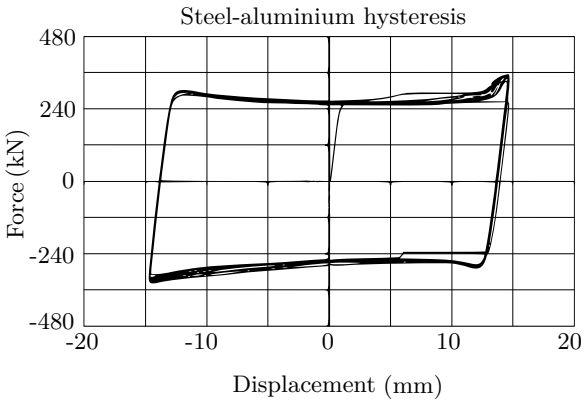

Figure 2.40: Steel-aluminium hysteresis curve (adapted from Latour et al., 2014)

From the overall test results, the steel-steel interface resulted in a high μ combined with unstable friction behaviour. The brass-steel interface yielded a low μ with stable energy dissipation and hardening behaviour over increasing cycles. The TSA-steel interface displayed the best performance with a high coefficient of friction and no significant degradation during cyclic loading. Latour et al. (2014), attempted to find a material with a high μ and stable sliding behaviour. They claimed that the TSA would be economical since only a thin layer is required and was therefore a suitable alternative to the brass which was previously used.

Loo et al. (2014) investigated the necessity of the shims that researchers such as Grigorian et al. (1993), Balendra et al. (2001) and Butterworth (2000) used in their SBCs. They incorporated a slotted-plate of ARS. ARS was shown to be effective by Khoo et al. (2012), although they had used it for the shim material. Using a shim-less SBC would result in more economical fabrication and easier construction. ARS is also corrosion resistant so this would not be a concern.

In exploratory tests, Bisalloy-400 was used between the mild-steel outer-plates. Bisalloy-400 is an ARS usually implemented in areas of high impact and abrasion. The results indicated that ARS-steel interface was able to achieve the stable behaviour required. They decided to increase the accuracy of the bolt-tension by using bolts with a finer thread for detailed testing. A depth micrometer, which is a precision measuring instrument, was also used to measure the deflections of the Belleville spring washers. This ensured more accurate bolt-tension, since the turn-of-the-nut method was used to pre-load the bolts. The washers were stacked as shown in Figure 2.41.

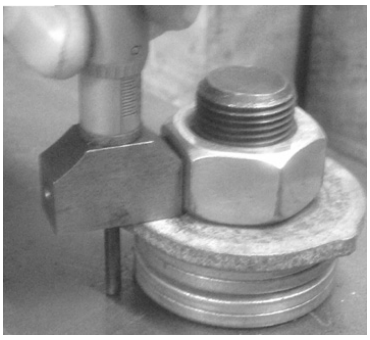

Figure 2.41: Belleville washer stack and depth micrometer (Loo et al., 2014)

The setup that was used for the detailed testing is shown in Figure 2.42, mild-steel outer-plates were used throughout. During the tests of different slotted-plates, four mild-steel, three Bisalloy-60 and twelve Bisalloy-400 plates were used. The four steel-steel interfaces were tested in order to confirm the results of Grigorian et al. (1993), as well as for comparison to the ARS-steel interface. The displacement-time schedule only allowed the bolts to displace 40 mm in both directions and in this manner bolt-impact was prevented. A displacement schedule similar to that used by Grigorian et al. (1993) was incorporated.

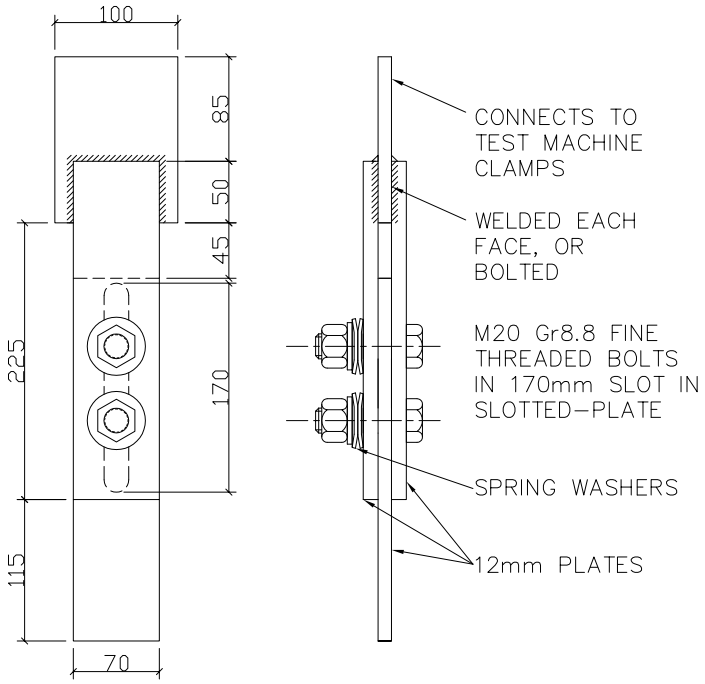

Figure 2.42: Shim-less SBC detail for testing (Loo et al., 2014)

For the steel-steel interface, unstable friction behaviour similar to what was found in previous research was recognised. These findings originally led to the use of brass shims for friction interfaces. The performance of the ARS-steel interface was excellent and stable behaviour was obtained. The depth micrometer resulted in more accurate bolt-tension calculation than when only the number of rotations of the turn-of-the-nut method was used. Visual observation between the test results of brass shims from Grigorian et al. (1993) and ARS used in this study showed that the ARS compared well. In successive tests the connections did lose strength, but their behaviour was still outstanding.

Tests were also conducted on a worst case scenario that most likely would be more strenuous than in earthquake conditions. The ARS exhibited performance that was for all practical purposes equal to the brass connections. The SBC exhibited increased strength in the middle of the test, doubtless caused by heating and expansion increasing the bolt-tension, at the end of the final test the connection maintained at least 75% of its strength.

They concluded that the shim-less SBC with an ARS slotted-plate resulted in sustained strength and stability which was equal to or better than the SBC with brass shims used previously. The

rate of loading had no significant effect on the shim-less SBC. They believed that the shim-less SBC could be used for energy dissipation in a cheaper and more durable manner than previous SBCs that included shims.

2.4.2 Conclusion

Previous research covered a broad spectrum of investigations and applications. Even so, the friction material performance was arguably the only area that was significantly studied.

Grigorian et al. (1993) noted the concerning loss of bolt-tension in the SBC in addition to the unstable friction behaviour of steel-steel interfaces. By introducing spring washers and brass shims, they managed to obtain enhanced performance and these components became relatively standard parts of the SBC. Full-scale testing of the KBF incorporating a SBC in the brace introduced by Balendra et al. (2001) displayed beneficial characteristics in terms of energy dissipation. Their aim of low-damage construction was achieved since the knee member could easily be replaced after an earthquake. Butterworth (2000) believed that the loss of bolt-tension associated with omitting the spring washers was necessary in the pursuit of a simpler SBC. When considering the ASBC, it was found that stress concentrations occurred in the bolt-shanks and plates around the bolts during sliding. From the non-linear analysis, Butterworth (2000) observed that the slip-length governed the structural response during earthquake ground accelerations. Lukkunaprasit et al. (2004) were the only researchers to consider the possible negative effects of bolt-impact. Their research showed that if detailed incorrectly, bolt-impact could affect the SBC detrimentally. The analytical model used by S. Lee et al. (2008) illustrated that SBCs could adequately be used in the braces of a structure. Khoo et al. (2012) investigated the effect of hardness of the shims used in the SHJ through full-scale testing. They found that the wear characteristics of high hardness ARS resulted in less friction variation than other materials. The ARS would have better availability and economy than the brass used earlier. C. Lee et al. (2013) created a new composite material to be used in SBCs. Their material exhibited excellent frictional performance, but the economy and practicality thereof was unclear. Additionally, in their comparison of different SBC details, they found that a single spring washer under the bolt-head and nut resulted in superior behaviour. They discouraged the use of spring washers in series. Latour et al. (2014) found that from the three materials they considered, the TSA exhibited superior stability and predictability. They claimed that TSA would be economical since only a thin layer is necessary. Loo et al. (2014) tested a shim-less SBC with slotted-plates of ARS and observed behaviour equal to or better than materials previously used. They argued that the shim-less SBC would be cheaper, more durable and easier to fabricate and construct than the SBCs with shim-plates previously used.

The advances made by Loo et al. (2014) amongst others, meant that braces connected with SBCs became practical for construction. Literature indicated that more research was necessary before a design procedure for braces with SBCs could be compiled. More understanding was necessary in terms of: bolt-impact behaviour, the differences between SSBC and ASBC and how they affect performance and the effect of the SBC on brace behaviour. A modelling approach for

non-linear dynamic analysis of a building with SBC-braces was also required. The comprehensive information on the shim-less SBC that Loo et al. (2014) designed and tested meant that it could be modelled with sufficient accuracy that results could be used to calibrate a FE model. This is discussed in Section 3 and serves as the point of departure for the study.

Chapter 3

SBC Model Verification

The SBC was modelled using Abaqus, a commercially available *Finite Element Analysis* (FEA) software package. This was performed to obtain similar results to experimental results and ensured that the modelling approach used was suitable. The shim-less SBC incorporating ARS as tested by Loo et al. (2014) was used for the model verification. Once this was accomplished, further study of the SBC was performed.

The experimental work performed by Loo et al. (2014) indicated that ARS in the SBC was preferable to brass shims. This is supported by the findings of Khoo et al. (2012) using ARS in the SHJ. Further, information regarding the materials and testing provided by Loo et al. (2014) was sufficiently detailed that the experimentally tested SBC could be used to calibrate the *Finite Element* (FE) model.

3.1 Abaqus Model

Two modules of the Abaqus FEA software were used:

- Abaqus/Standard, a general-purpose FEA program.
- Abaqus/CAE, a user interface for modelling, analysis and interpretation of results.

Abaqus/Standard can be executed through the Abaqus/CAE interface or as a batch application through the Abaqus command line using text format input files to define model data (SIMULIA, 2012a).

The SBC was modelled using 3D solids in Abaqus. It consisted of a slotted-plate, outer-plates and bolts, which are shown in Figure 3.1. The dimensions of the plates were based directly on the details provided by Loo et al. (2014). Refer to Appendix A for detailed drawings of the parts of the connection. For the bolts, it was assumed that the pre-load is transferred at one end through the "across flats" dimension of the head and at the other end through the spring washers. The spring washers were assumed to be at the flat position with their inside and outside diameters on the same plane. The effect of bolt thread in the shear plane was disregarded.

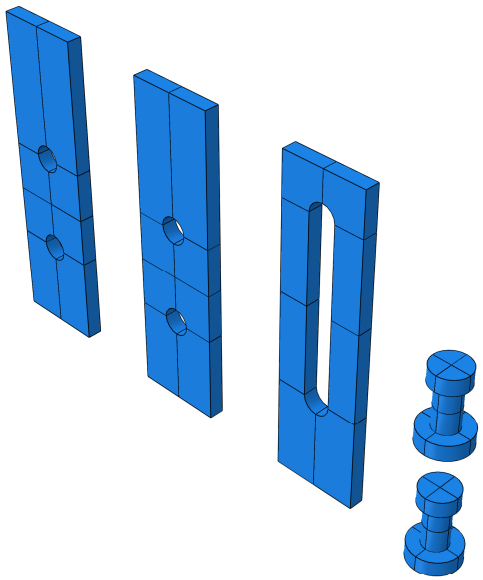

Figure 3.1: Parts of the SBC model

The SBC was modelled as a perfectly elastic isotropic material with the properties: $E = 200\,\text{GPa}$ and $\nu = 0.3$. Damaged material behaviour was not included in this model, since the tests did not consider bolt-impact.

The parts were assembled as shown in Figure 3.2, which is equivalent to the SBC of Loo et al. (2014). Figure 3.2 (a) shows the full connection while Figure 3.2 (b) shows the inside of the connection with one outer-plate removed. Modelling the complex interactions present in the SBC required the use of contact modelling in Abaqus. "General contact" was used for the contact definition, which is discussed in Section 3.1.1. The coefficient of friction $\mu = 0.36$ was used for the friction property definition, which is discussed in Section 3.1.1; the value was based on the average value of μ for the Bisalloy-400 ARS.

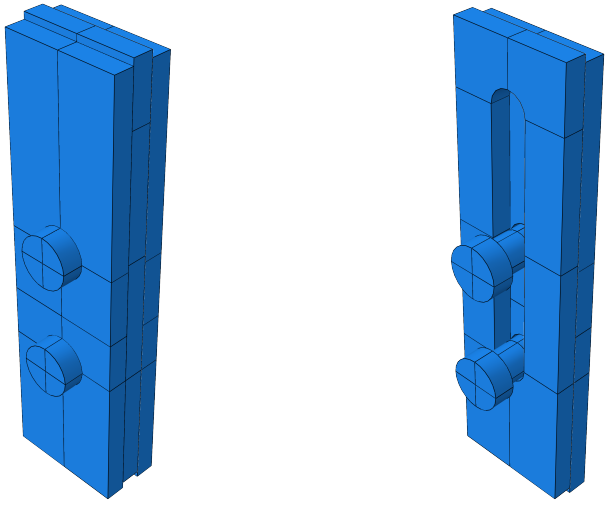

(a) (b)

Figure 3.2: The assembled SBC model

3.1.1 Contact modelling in Abaqus/Standard

Three approaches are available for contact modelling in Abaqus: general contact, contact pairs and contact elements. The first two approaches use surface-based contact definitions, where these are not applicable, usually in specialised applications such as tube-to-tube contact, contact elements are used. The Abaqus documentation advocates the use of the general contact algorithm or contact pairs where possible (SIMULIA, 2012d).

The difference between general contact and contact pairs lies in the user implementation as well as numerical controls. General contact offers simple implementation while contact pairs allow for improved analysis performance (SIMULIA, 2012d). The general contact algorithm provides a means of specifying contact definitions simply and effectively.

The characteristics needed to define a contact modelling approach are shown in the first column in Table 3.1. The default settings for general contact with respect to these characteristics are also listed in Table 3.1 and are discussed in the following sections.

Table 3.1: Requirements for contact implementation

Contact modelling characteristic:		General contact:
Contact formulation	-	Finite-sliding, surface-to-surface
Contact constraint enforcement	-	Penalty method
Treatment of initial overclosures	-	Strain-free adjustments
Master-slave assignments	-	Pure master and slave roles

Contact formulation

The contact formulation refers firstly to the contact discretization and secondly to the tracking approach used. Contact discretization here refers to the manner in which contact is incorporated in the elements of the mesh. Two types of discretization are available in Abaqus: node-to-surface and surface-to-surface (SIMULIA, 2012d).

With node-to-surface discretization the master surface nodes can penetrate the slave surface, but the opposite does not apply. This is presented in Figure 3.3 (a) and (b). Surface-to-surface discretization prescribes contact over averaged regions near slave nodes rather than at slave nodes themselves. While penetration may occur at individual nodes, as in Figure 3.3 (d), large penetrations of master nodes into slave surfaces do not occur with surface-to-surface discretization. Stress and pressure results from surface-to-surface are more accurate than node-to-surface if the contact surfaces represent the surface geometry well (SIMULIA, 2012d).

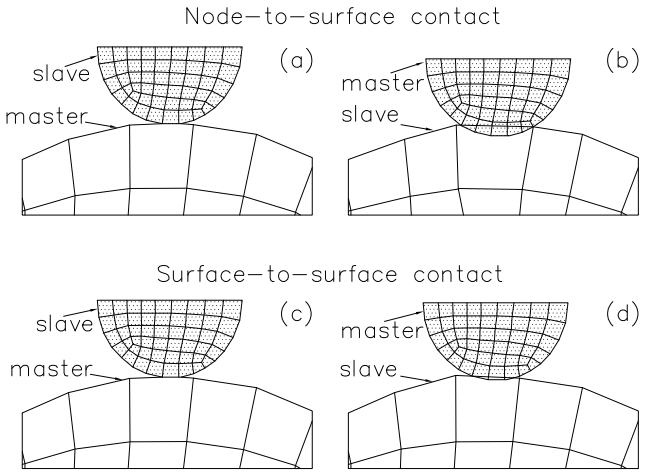

Figure 3.3: Contact discretization (adapted from SIMULIA, 2012d)

The tracking approach refers to consideration of relative motion between surfaces to enforce contact conditions during analysis. Two tracking approaches are available: small-sliding and finite-sliding. Small-sliding is only suitable where relative sliding is small, usually less than the length of a single mesh element (SIMULIA, 2012d). The small-sliding approach tracks nodes in contact only at the commencement of analysis. Finite-sliding permits separation, sliding and rotation of the contact surfaces throughout analysis. This approach tracks relative motion between surfaces in contact in each increment of the analysis which adds to the computational cost of contact analysis.

Contact constraint enforcement

A mechanical contact property model is defined by a pressure-overclosure relationship. The default pressure-overclosure relationship is hard contact between surfaces in Abaqus, but three types of softened contact relationships are also available. Hard contact is clarified by Figure 3.4. If clearance exists between two bodies, there is no contact and no contact pressure. When clearance between the bodies reduces to zero, they come into contact and any contact pressure can be transferred (SIMULIA, 2012d). It is clear that hard contact does not permit tensile stress transfer over the interface. It also minimises the ability of slave surfaces to penetrate master surfaces. Figure 3.5 shows an example of a softened pressure-overclosure relationship. This type of relationship might be used to model a soft layer as one of the surfaces involved in contact.

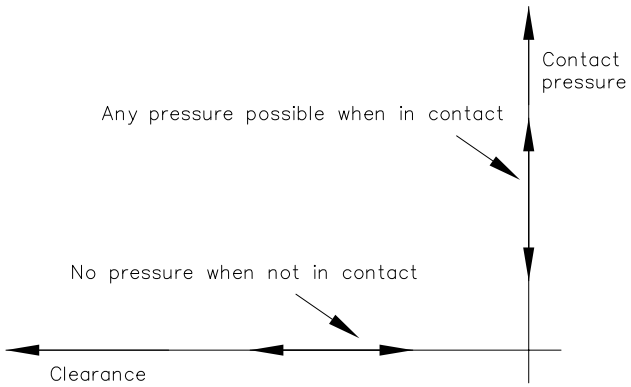

Figure 3.4: Hard contact (adapted from SIMULIA, 2012d)

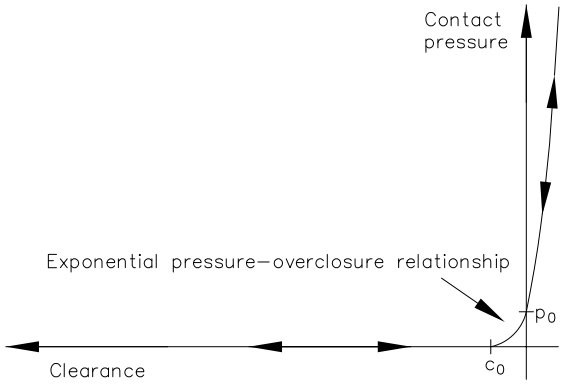

Figure 3.5: Softened contact (adapted from SIMULIA, 2012d)

Contact constraint enforcement dictates how the mechanical contact property model is resolved numerically in an analysis (SIMULIA, 2012d). Three enforcement methods are available: the direct method, the penalty method, and the augmented Lagrange method.

The direct method enforces the contact constraints in a strict manner, Lagrange multipliers are used depending on the type of pressure-overclosure relationship involved. The penalty method approximates hard pressure-overclosure. With this method an extent of penetration is present, since contact force is proportional to the penetration distance. The approximation of the penalty method can reduce the cost of an analysis. In addition to this, it does not use Lagrange multipliers which can lead to improved accuracy (SIMULIA, 2012d). The augmented Lagrange method has similarities to the penalty method and uses augmentation iterations to improve solution accuracy.

Treatment of initial overclosures

The clearance between bodies in the initial geometry determines the contact state present at the outset of analysis. Mesh generation, particularly with curved surfaces may cause minor initial overclosure in a model as shown in Figure 3.6. Figure 3.6 shows how these initial overclosures are resolved by adjusting the initial nodal positions to a “just touching” state (SIMULIA, 2012d).

The default method used by the general contact algorithm is by strain-free adjustments of the nodal positions.

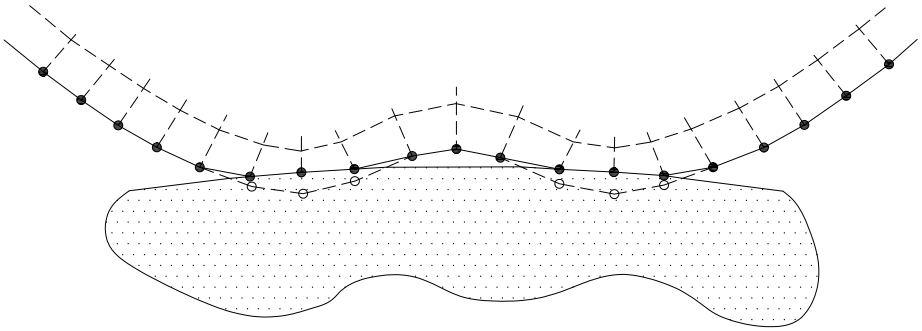

Figure 3.6: Initial overclosure of surfaces (adapted from SIMULIA, 2012d)

Master-slave assignments

The default method of master-slave assignment for general contact is by automatically prescribing pure master and slave roles for most contact interactions. Pure master-slave contact means that the master nodes can penetrate the slave surface unopposed. This is displayed in Figure 3.7, where the coarse discretization causes the master surface to penetrate the slave surface. This method works well in most cases and should not be modified from the default settings (SIMULIA, 2012d).

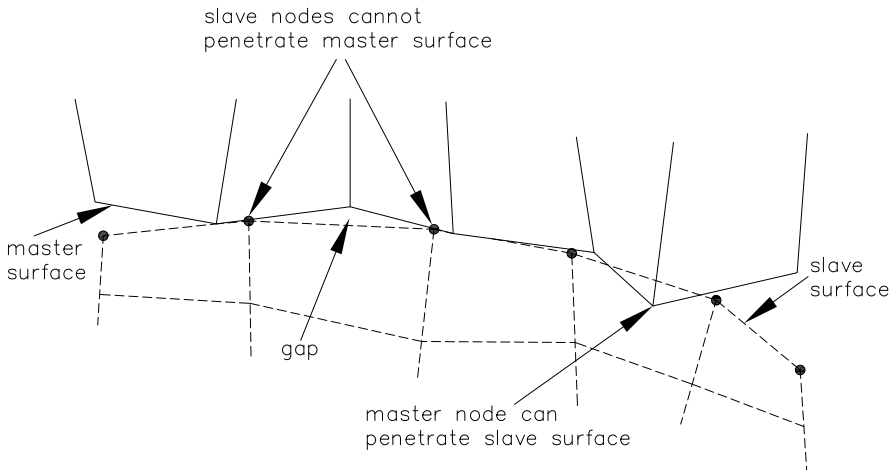

Figure 3.7: Pure master-slave contact (adapted from SIMULIA, 2012d)

General contact definition in Abaqus/CAE

The default settings used for general contact with regards to the contact formulation, contact constraint enforcement, treatment of initial overclosures as well as master-slave assignments were discussed. The definition of general contact for inclusion into the SBC analysis can now be described.

Only a single general contact definition can be performed and this definition is present for the entire analysis (SIMULIA, 2012d). The contact domain specified for general contact was defined as "self-contact" for the entire model. Self-contact entails contact between all the bodies in the model as well as each body with itself. The global contact surface property was defined as "Friction" and is discussed in the following paragraph.

The "Friction" contact property defined in the contact analysis consisted of a "hard" contact pressure-overclosure relationship for normal behaviour. This contact constraint was enforced by the default penalty method. Tangential behaviour was isotropic friction defined simply by the friction coefficient and enforced by the penalty method. The Coulomb friction model was used for this contact property. This model states that surfaces in contact can transmit shear stress of a certain magnitude without sliding of one surface relative to the other (SIMULIA, 2012e). Sliding occurs at the critical shear stress. Below this stress, "sticking" occurs shown as the hatched region in Figure 3.8.

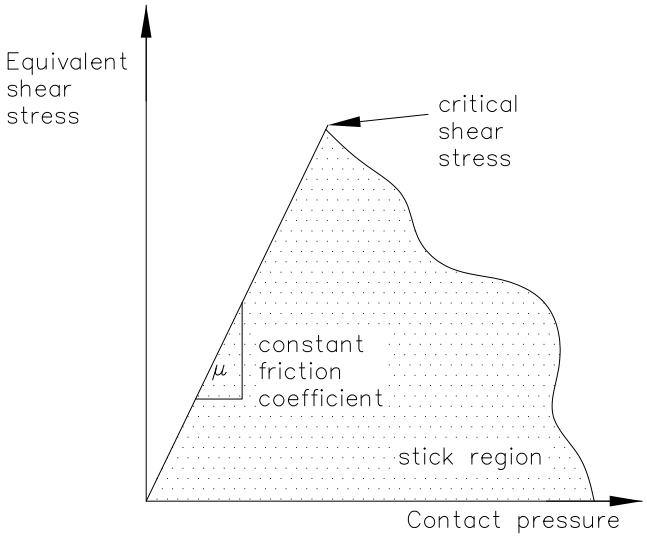

Figure 3.8: Coulomb friction model (adapted from (SIMULIA, 2012e))

Critical shear stress is the product of the coefficient of friction and the contact pressure when slip occurs. This calculation, shown in Equation 3.1, is used during analysis to determine if there are points where the state has changed from sticking to slipping or vice versa.

$$\tau_{crit} = \mu \times p \tag{3.1}$$

3.1.2 Boundary conditions and loads

The test setup of Loo et al. (2014) had the outer-plates connected by welds or bolts to a plate connected to the test machine. This was idealised by boundary conditions with translational fixity in all directions at the top surfaces of the outer-plates, as shown in Figures 3.9 and 3.10. A constraint was used to couple the displacements of the bottom surface of the slotted-plate to a

reference point as presented in Figure 3.11. This point was used to apply the displacements to the slotted-plate and to obtain the frictional force.

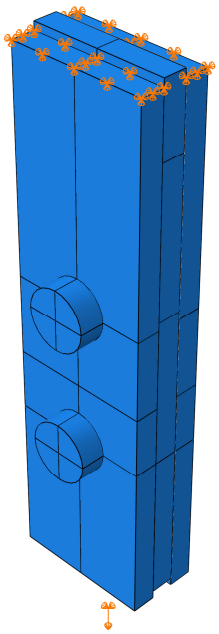

Figure 3.9: Boundary Conditions

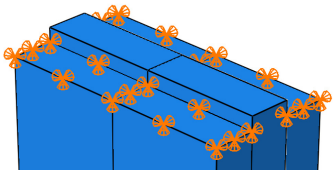

Figure 3.10: Outer plates translational fixity

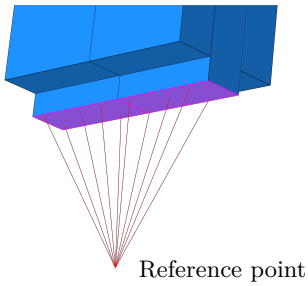

Figure 3.11: Slotted-plate displacement control

The tension in the preloaded bolts was the only load applied to the SBC. Using “Bolt loads” in Abaqus/CAE, pre-loaded bolts are defined by a concentrated load or by adjusting the bolt length to a specified value (SIMULIA, 2012f). The load is applied to a plane through the cross-section of the bolt-shank as shown in Figure 3.12 and is able to interact with other components of the assembly. The tension in the bolts that Loo et al. (2014) used in the majority of the tests was applied to the model.

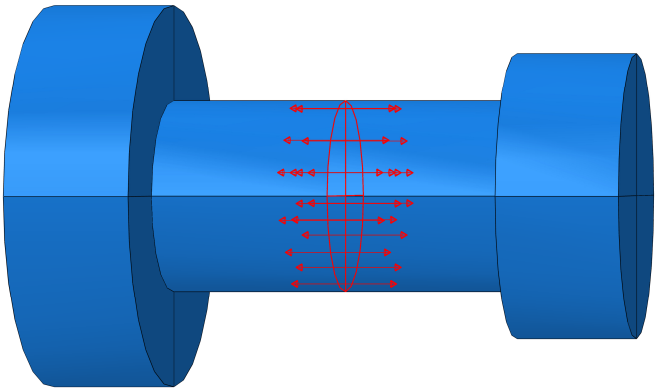

Figure 3.12: Bolt load application

As stated in Section 2.4.1, Loo et al. (2014) measured deflection of the spring washer stack with a depth micrometer. The properties and configuration of the spring washers used in their tests are

shown in Table 3.2. These parameters are used with Equations 3.2 to 3.4 to determine the bolt tension T_b and slip force F_{slip}. $T_b = 32.5\,\text{kN}$ was used for the bolt loads in the model, resulting in an expected $F_{slip} = 46.8\,\text{kN}$ for the connection.

Table 3.2: Washer properties and configuration for Bisalloy-400 test

Used with bolt	M20	Washer thickness	3.4 mm
Inside diameter	20.6 mm	Outside diameter	40 mm
Number of bolts - n_b	2	Flat deflection - $\delta_{Belleville}$	0.914 mm
Washers in parallel stack - n_p	1	Flat load - P_{flat}	37.81 kN
Washers in series stack - n_s	4	Washer group deflection - δ	3.14 mm
Total washers - $(n_p \times n_s)$	4	Coefficient of friction - μ	0.36

$$\delta_{flat} = n_s \times \delta_{Belleville} \tag{3.2}$$

$$T_b = n_p \times P_{flat} \times \frac{\delta}{\delta_{flat}} \tag{3.3}$$

$$F_{slip} = 2 \times n_b \times T_b \times \mu \tag{3.4}$$

3.1.3 Mesh

The configuration of the mesh elements used in a model can affect the computational cost and the results of an analysis significantly. Appropriate element types must be selected carefully with respect to: first- or second-order elements, full or reduced integration and hexahedral or tetrahedral elements.

Although tetrahedral elements can mesh complex shapes more easily, hexahedral elements were selected for the mesh. When hex elements are able to mesh the geometry sufficiently, they provide equivalent solution accuracy, less computational cost and a better convergence rate (SIMULIA, 2012c). Second-order elements are suitable for surfaces with the surface-to-surface contact formulation (SIMULIA, 2012d). They provide better accuracy than their first-order counterparts for applications where element distortion is not excessive. Since no bolt impact or severe deformation was expected in the analysis, second-order elements were selected. Reduced integration was selected since full integration may cause volumetric locking behaviour in the elements (SIMULIA, 2012c). Reduced integration also reduces analysis running time.

C3D20R elements were subsequently used in the mesh. These are 20 node, three-dimensional continuum stress/displacement elements with reduced integration. The meshes of all the parts of the assembly were verified and checked with the mesh verification tool in Abaqus/CAE. Element quality is verified according to default criteria such as aspect ratio and element distortions which may cause problems during analysis (SIMULIA, 2012f). Elements that do not pass the quality tests are highlighted and the mesh in these regions can be refined accordingly. Table 3.3 lists the two meshes that were considered: a finer mesh where all parts had an element size of 4 mm and a coarser mesh, which is shown in Figure 3.13, with 4 mm seeds in the bolts and 6 mm in the plates. In the preliminary analyses the two meshes produced equivalent results but with

significant savings in computational time with the coarser mesh. The coarser mesh was therefore suitable for the results verification since no plasticity was involved in the testing.

Table 3.3: Seed sizes of parts in the meshes considered

Part	Coarse mesh	Fine mesh
Outer-plates	6 mm	4 mm
Slotted-plate	6 mm	4 mm
Bolts	4 mm	4 mm

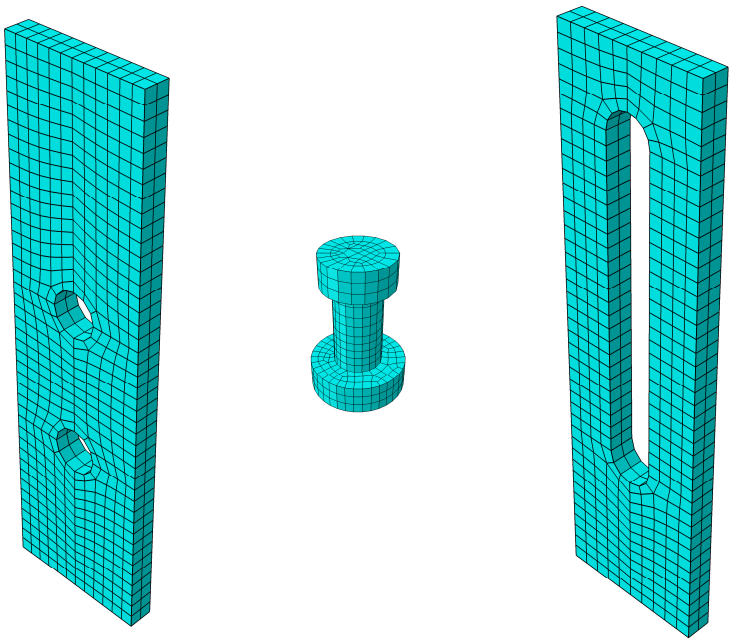

Figure 3.13: The meshed parts of the assembly

Symmetry in the connection could be taken advantage of for simplification. Although this would decrease computational cost, the full connection was modelled for the verification of the results of Loo et al. (2014). Symmetry was however employed in later investigations.

3.2 Analysis

A Static Stress/Displacement step was selected for the analysis. The assumption was that as only the connection was tested dynamically, inertia effects would play an insignificant role and could be neglected. Static stress analysis takes into account rate-dependent plasticity and hysteretic behaviour (SIMULIA, 2012b). As discussed in Section 3.1, displacements were applied to the connection through the control point. Figure 3.14 shows the displacement schedule that Loo et al. (2014) employed in their tests. The displacement schedule has seven sets of ten cycles each with varying amplitudes and loading frequencies which are listed in Table 3.4. This is based on the displacements originally used for testing by Grigorian et al. (1993). A truncated version of this displacement schedule, shown in Figure 3.15, was used for the analysis. The truncated

displacement schedule had seven sets of one cycle each with the same loading frequency used by Loo et al. (2014). The truncated displacement schedule could be used since a constant μ was assigned and slip would reliably occur at the appropriate critical shear stress. In experimental testing however, long displacement schedules were used because the stability of sliding was investigated. The main output value of interest for this analysis was the friction force throughout sliding. This was obtained by a history output request of the reaction force "RF2" in the direction of the sliding motion through the control point. Results are discussed in Section 3.3

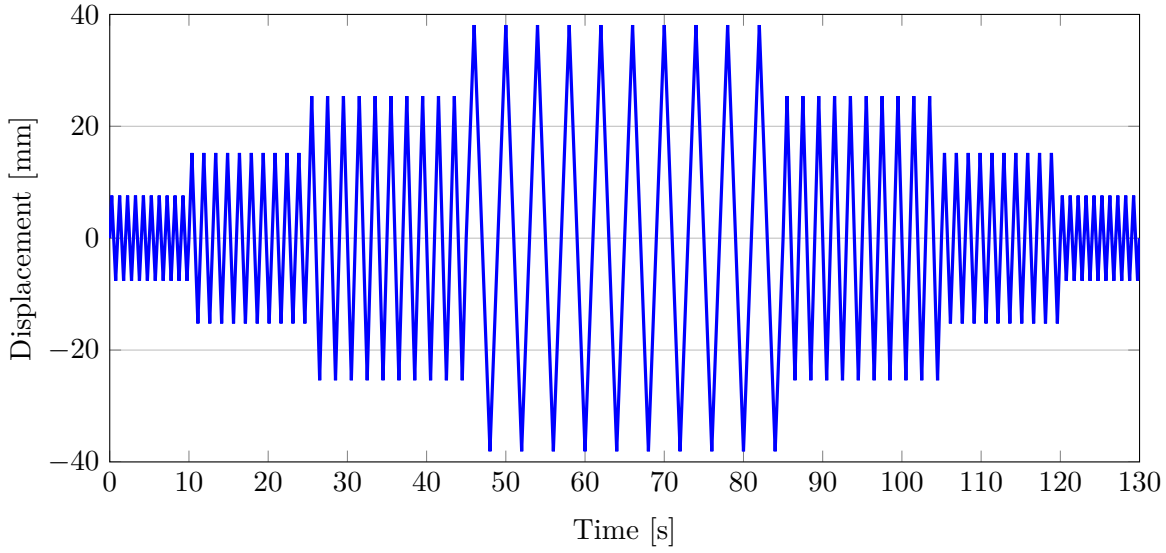

Figure 3.14: Full displacement-time history used by Loo et al. (2014) and Grigorian et al. (1993) for experimental tests

Table 3.4: Amplitudes and frequencies of Loo et al. (2014) tests

Set number	Amplitude [mm]	Loading frequency [Hz]
1st	7.62	1
2nd	15.24	0.67
3rd	25.4	0.5
4th	38.1	0.25
5th	25.4	0.5
6th	15.24	0.67
7th	7.62	1

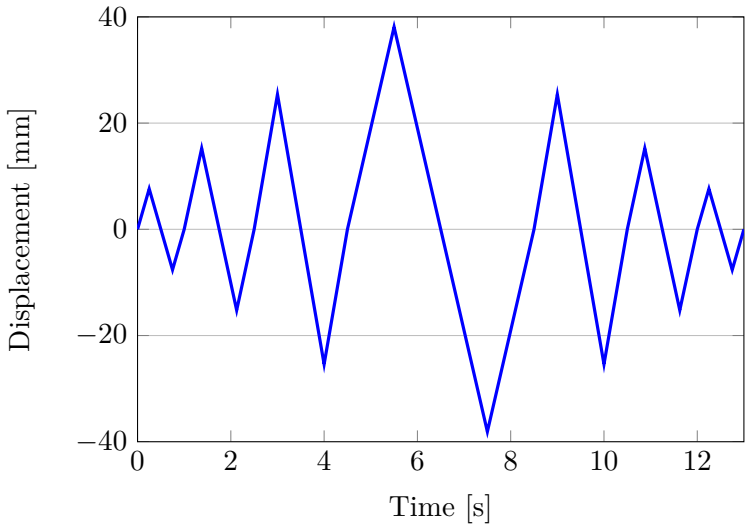

Figure 3.15: Truncated displacement schedule used for Abaqus analysis

3.3 Results comparison

The force-displacement and force-time results from the analysis described in Section 3.2 are shown in Figures 3.16 and 3.17. Figures 3.16 and 3.17 show that the slip force from the analysis is similar to the expected $F_{slip} = 46.8\,\text{kN}$ calculated in Section 3.1. The hysteresis results of Figure 3.16 compare well to the original results of Loo et al. (2014) shown in Figure 3.18 (a). These results are of the SBC with an ARS slotted-plate, tested with the full displacement schedule shown in Figure 3.14. The "pinched" regions of these test results were due to slight slippage in the bolts connecting the assembly to the testing machine. Without these "pinched" areas an even better comparison could be drawn between experimental and numerical results. Further, as discussed in Section 3.2, since a constant μ was assigned no variation is present in F_{slip} from analysis results. Test results in Figure 3.18 (a) and (b) however display a slight variation in μ and consequently in F_{slip}. Subsequently, an analysis was performed where variation of μ was introduced to illustrate that tests and analysis results can be correlated exactly with minor adjustments to μ. The values for the μ variation were obtained from values listed by Loo et al. (2014). The results, which are shown in Figure 3.19, replicate the test results in Figure 3.18 favourably.

Table 3.5 shows the computational cost of the meshes that were considered. The computer that was used had a processor speed of 3.3 GHz and 16 GB RAM. Using the "parallelization" option in Abaqus, eight processors were used in parallel during analysis. It is clear that the coarse mesh resulted in a significant improvement in the running time of the analysis.

Table 3.5: Computational cost of meshes considered

	Running time
Fine mesh	5.5 h
Coarse mesh	1.5 h

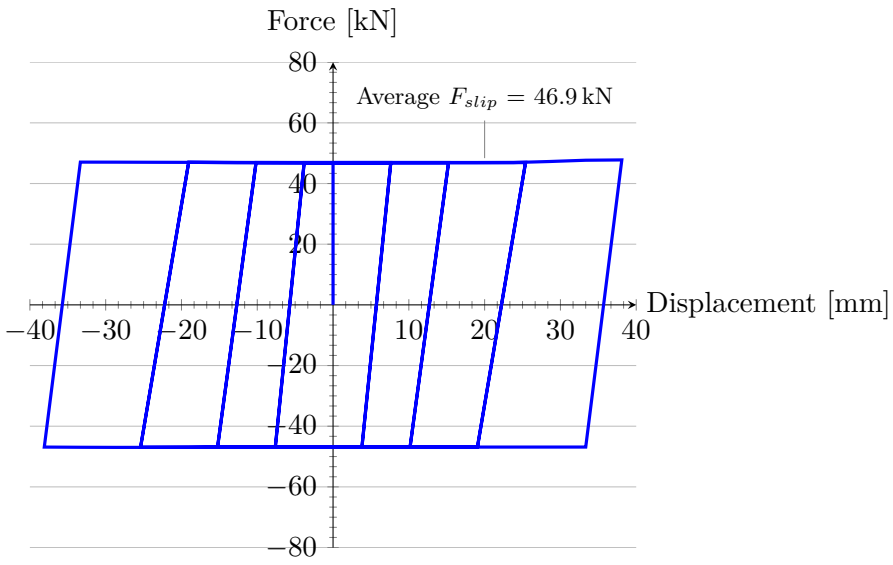

Figure 3.16: SBC hysteresis loops from Abaqus results

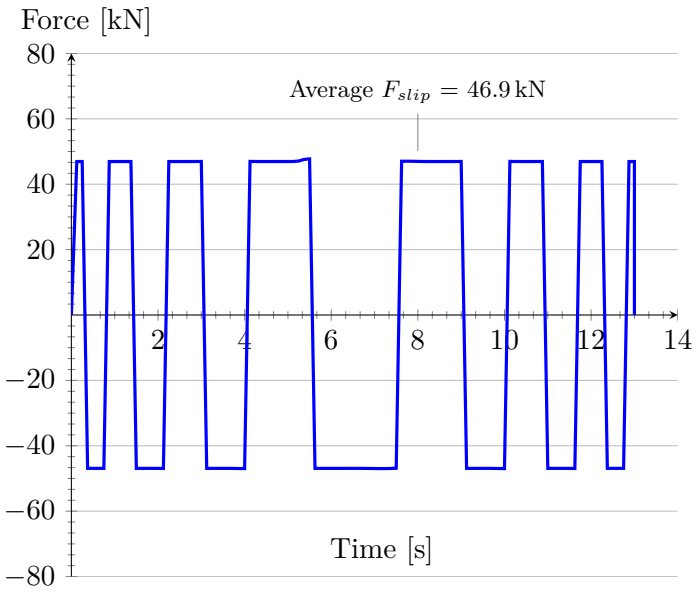

Figure 3.17: SBC force-time results from Abaqus

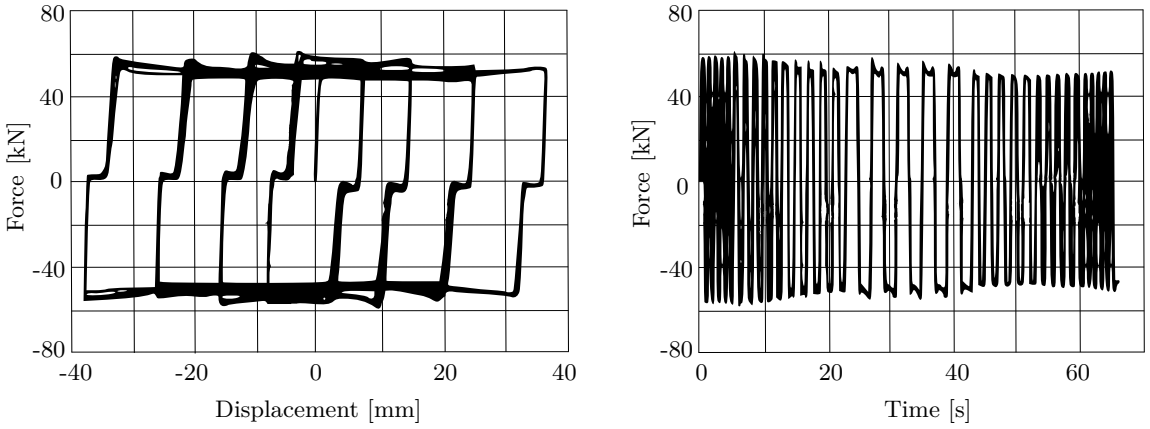

(a) (b)

Figure 3.18: Corresponding hysteresis and force-time results from test by Loo et al. (2014)

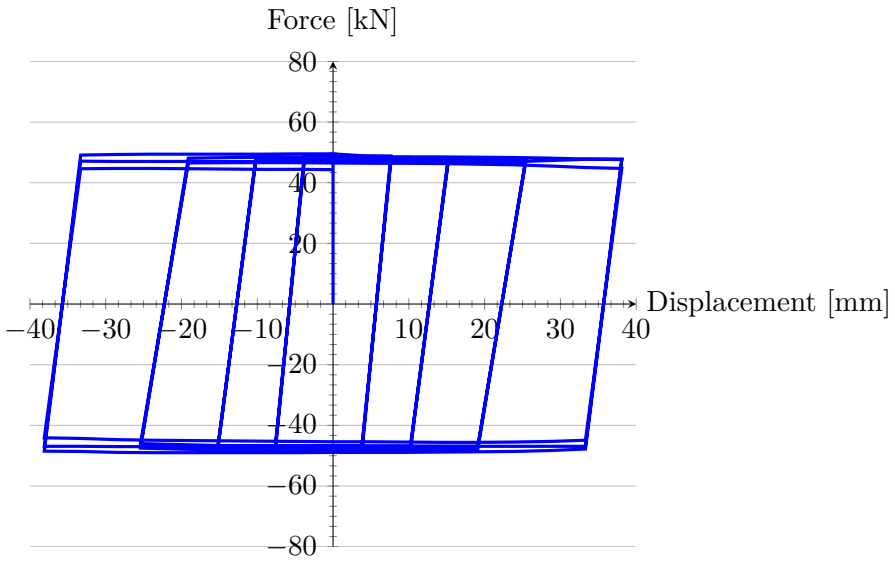

Figure 3.19: SBC hysteresis loops from Abaqus with variation in μ

3.4 Model validity

The SBC was modelled and analysed in Abaqus to replicate test results of Loo et al. (2014). This served as model verification showing that the results from FE analysis and experimental work compared favourably. With further calibration to vary the friction coefficient, the FE model captured the experimental behaviour of the SBC accurately. This created a basis from which further investigation into the behaviour of the connection could be performed.

Chapter 4

Further SBC investigations

4.1 Bolt Impact

The effect of the slot-end impacting the bolt-shank was analysed in Abaqus and compared to bolt-impact test results from Lukkunaprasit et al. (2004). This was conducted to qualitatively verify the modelling with the experimental work. In this manner, the effect of bolt impact on the behaviour of the SBC could be studied. The model developed in Section 3.1 was used for this study. A damaged material model was implemented and refined meshes with appropriate elements were used. Due to a lack of information in the paper by Lukkunaprasit et al. (2004), the SBC used in their tests could not be recreated. It was therefore decided to replicate their results in principle using the SBC already verified in Section 3.1.

4.1.1 Model

The SBC model of Section 3.1 was used with adjustments to the material properties, mesh and element type used. In addition to this, a model that utilised the symmetry of the connection was prepared. The symmetry model was equivalent to the model of Section 3.1 although only half the connection was modelled and consequently only half the bolt loads used in the previous analysis were applied. This model would therefore yield half the force of the full connection models

Damaged material behaviour

During bolt-impact, materials are unlikely to remain in their elastic range. A damaged material model was included to allow for plastic deformation in the SBC. The idealised stress-strain behaviour of structural steel is shown in Figure 4.1. Elastic behaviour ceases at the yield stress, which is depicted by the linear part of the graph. Plastic behaviour is initiated and stress remains at yield point while inelastic strain occurs. This is followed by strain hardening where stress increases with strain. At ultimate strain the ultimate tensile stress is reached. After this point the strength of the material degrades until necking and ultimately fracture occurs. To model

this stress-strain behaviour, a bilinear stress-strain model was assumed with linear elasticity and plasticity.

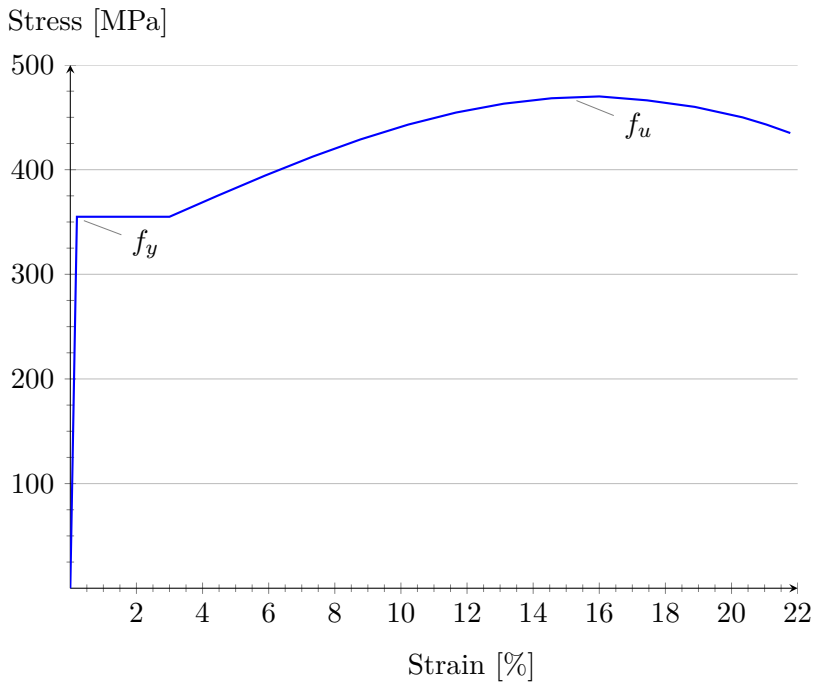

Figure 4.1: Idealised stress-strain behaviour for structural steel (adapted from Hibbeler, 2008)

The characteristic yield and ultimate strengths for the steel plate and bolts are shown in Table 4.1. These values represent the 5th percentile strengths and are used in design to account for material variability. When modelling the SBC however, the expected strength of the material properties should be used.

Table 4.1: Characteristic strengths for steel plate and bolts

	f_y [MPa]	f_u [MPa]	ε_y [%]	ε_u [%]
S355JR plate	355	470	0.2	16
Class 8.8 Bolts	660	830	0.2	12

A log-normal distribution can be used to represent the material variability of structural steel (Holicky, 2009). The relationship between the 5th percentile (f_{yk}) and the standard deviation (σ_x) can be used to obtain a mean value (μ_x) as shown by Equation 4.1. Literature suggests that an acceptable value for the coefficient of variation (c_v) of structural steel is 0.08. Equation 4.2 shows how c_v is determined. By estimating a value for σ_x, a mean can be determined with Equation 4.1. This value is used with Equation 4.3 to calculate a new σ_x. This process is continued until values for σ_x converge and an acceptable mean value is reached. This approach was followed for the mean values of the yield and ultimate tensile strengths of the steel plate and the bolts of the model, as shown in Table 4.2. Although the value of 0.08 is specifically used for structural steel, the assumption was that this value would be sufficient for the bolts. The accompanying yield strain and ultimate tensile strain values are listed in Table 4.2. These values were obtained from the South African Steel Construction Handbook (SAISC, 2013), with the

16% of the plate being a conservative assumption based on the ±20% recommendation. The resulting bilinear curves used for the damaged material model are shown in Figure 4.2.

$$\mu_x = f_{yk} + (2 \times \sigma_x) \tag{4.1}$$

$$c_v = \frac{\sigma_x}{\mu_x} \tag{4.2}$$

$$\sigma_x = 0.08 \times \mu_x \tag{4.3}$$

Table 4.2: Expected strengths for steel plate and bolts

	f_y [MPa]	f_u [MPa]	ε_y [%]	ε_u [%]
S355JR plate	423	560	0.2	16
Class 8.8 Bolts	786	988	0.2	12

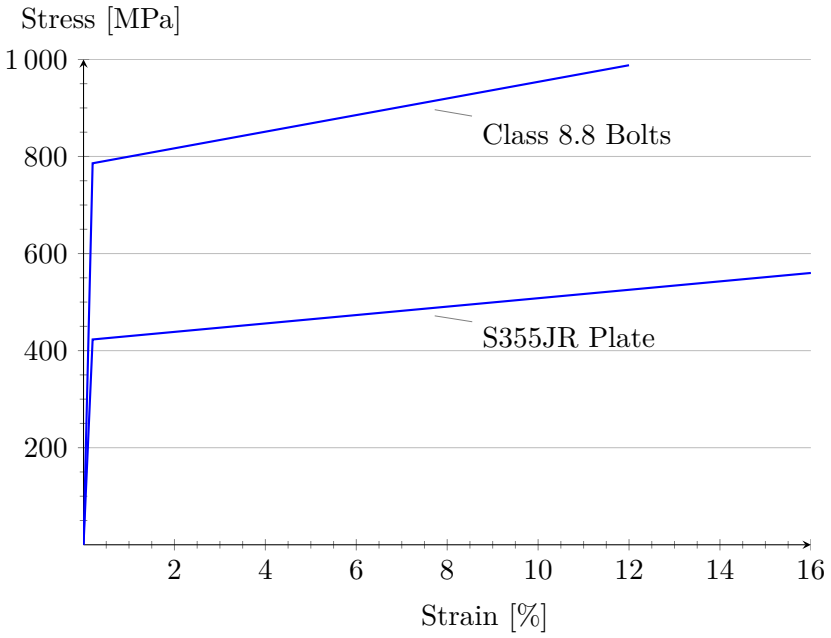

Figure 4.2: Idealised bilinear stress-strain curves for steel plate and bolts

Mesh

As discussed in Section 3.1, the elements and mesh size selected can have a significant influence on the results of an analysis. Consequently, elements were chosen according to the recommendations of the Abaqus documentation. Meshes were refined in areas of interest and element sizes were varied to inspect the influence on results and computational cost. The effect of using symmetry in the connection to be computationally efficient was also investigated.

The advantages of hexahedral elements over tetrahedral elements were discussed in Section 3.1. The C3D20R hex elements were therefore retained as one option for the element type with the bolt impact analysis. Alternatively, C3D10I tet elements were considered. These are 10-node, three-dimensional continuum stress/displacement elements with improved surface stress

formulation. The C3D10I elements are appropriate for modelling metal plasticity and provide more accurate stress visualizations (SIMULIA, 2012c). Unfortunately, they are computationally expensive in comparison to conventional tet elements since they use a unique integration scheme that prevents extrapolation errors from integration points.

Four meshes were considered. Table 4.3 lists the details of the two hexahedral meshes used. Figure 4.3 shows a comparison of the mesh around the edges of the bolt-holes and the slot, (a) and (c) are Hex-1 while (b) and (d) are Hex-2 as defined in Table 4.3. Hex-1 is more refined than Hex-2 with three and four elements through the outer- and slotted-plates respectively, which is shown in Figure 4.3 (a) and (b). The meshes in the bolts were equivalent for Hex-1 and Hex-2. The refinement of the mesh around the-bolt holes and the slot is in contrast to the very coarse hexahedral mesh used in Section 3.1.

Table 4.3: Details of hexahedral meshes considered

Mesh	Size	Outer-plate	Slotted-plate	Bolts
Hex - 1	Around holes (mm)	3	3	-
	Rest of part (mm)	5	5	-
	Shank (mm)	-	-	3
	Head & End (mm)	-	-	6
	No. of elements per part	3000	1696	864
	No. of elements through thickness	3	4	-
Hex - 2	Around holes (mm)	2.88	2.88	-
	Rest of part (mm)	6	6	-
	Shank (mm)	-	-	2.88
	Head & End (mm)	-	-	6
	No. of elements per part	1156	840	864
	No. of elements through thickness	2	2	-

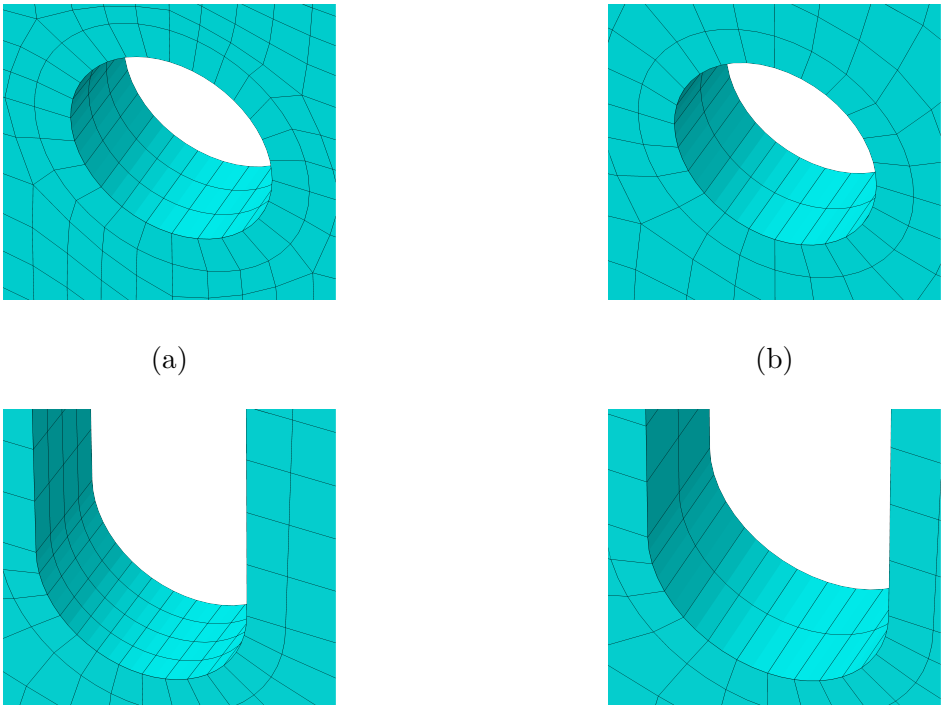

(a) (b)

(c) (d)

Hex-1 Hex-2

Figure 4.3: Hexahedral meshes in the outer- and slotted-plates

Table 4.4 lists the details of the two tetrahedral meshes used. Figure 4.4 shows a comparison of the mesh around the edges of the bolt-holes and the slot, (a) and (c) are Tet-1 while (b) and (d) are Tet-2. Tet-2 is a coarse mesh with a global element size of 6 mm while Tet-1 is significantly finer. The bolts have different element sizes unlike with the hex meshes. The finer Tet-1 mesh in the bolt is shown in Figure 4.5 (a) while the coarser Tet-2 mesh is shown in Figure 4.5 (b).

Table 4.4: Details of tetrahedral meshes considered

Mesh	Size	Outer-plate	Slotted-plate	Bolts
Tet-1 & Sym-1	Around holes (mm)	2.88	2.88	-
	Rest of part (mm)	6	6	-
	Shank (mm)	-	-	2.88
	Head & End (mm)	-	-	6
	No. of elements per part	10296	8006	4811
	No. of elements through thickness	4	4	-
Tet-2 & Sym-2	Around holes (mm)	6	6	-
	Rest of part (mm)	6	6	-
	Shank (mm)	-	-	6
	Head & End (mm)	-	-	6
	No. of elements per part	8057	6783	2158
	No. of elements through thickness	4	4	-

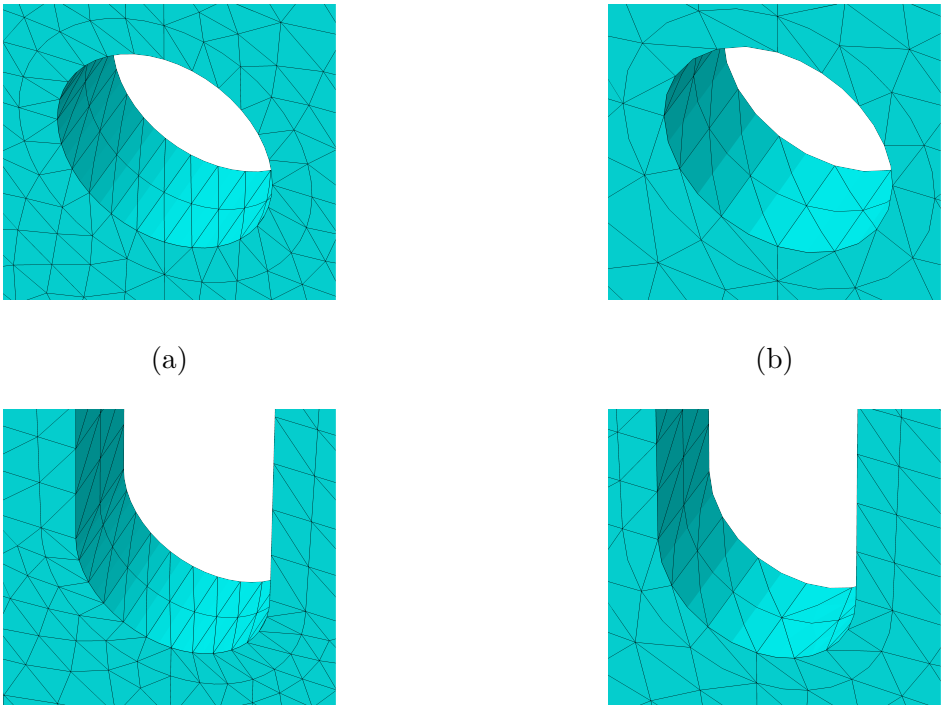

(a) (b)

(c) (d)

Tet-1 Tet-2

Figure 4.4: Tetrahedral meshes in the outer- and slotted-plates

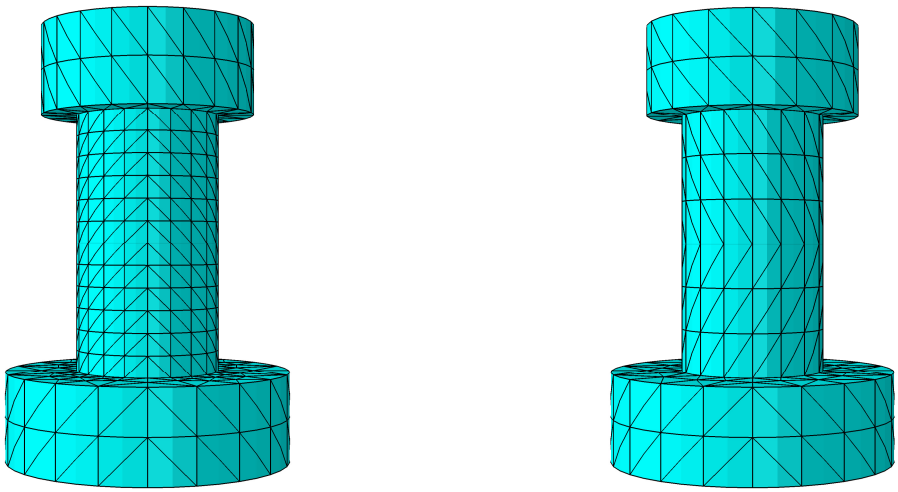

(a) Fine mesh (b) Coarse mesh

Figure 4.5: Tetrahedral meshes in the bolts

The number of mesh elements for the respective parts of the assembly are listed in Tables 4.3 and 4.4. Tables 4.3 and 4.4 show that the use of tetrahedral elements result in an increased number of elements compared to hexahedral elements. This is due to the pyramid shape of tetrahedral elements instead of the brick shaped hexahedral elements. The number of elements have an

effect on computational time of an analysis as well as the size of the output file needed to store the results. Contact tracking and contact constraint enforcement must take place throughout the analysis as explained in Section 3.1.1. Models with many elements necessarily mean longer computational times since more checks and calculations must be performed. Therefore, in addition to the meshes described above, a model that incorporated symmetry was considered. The two tetrahedral meshes were used with this model with the same properties as listed in Table 4.4. Figure 4.6 shows the meshed parts of the symmetry model. Only half the number of elements listed in Table 4.4 are included in the analysis of the symmetry model. The impact of the meshes and symmetry on results and computational cost is discussed in Section 4.1.3.

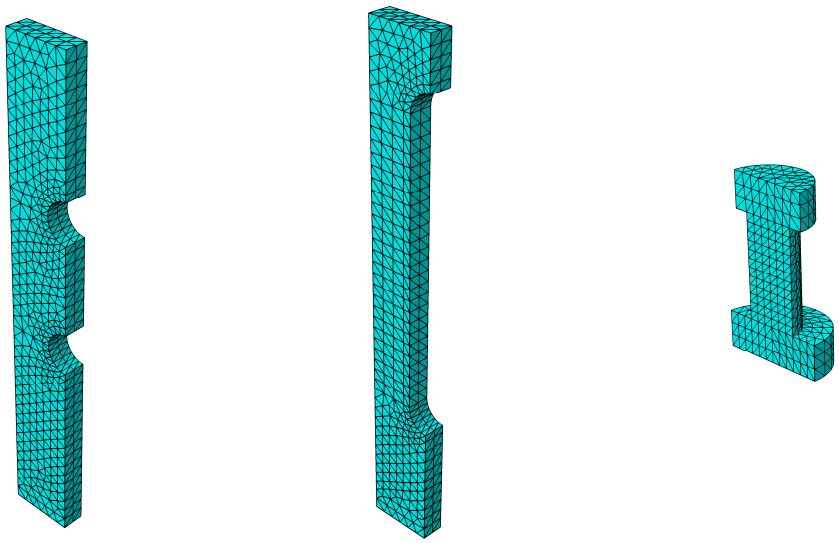

Figure 4.6: Tetrahedrally meshed parts of the symmetry model

4.1.2 Analysis

The bolt-impact analysis was similar to the analysis described in Section 3.1. In the previous analysis, it was ensured that bolt-impact would not occur since the maximum amplitude was 38.1 mm as in the experimental test. The displacement schedule for bolt-impact was structured such that a single cycle would be completed with impact at both ends of the slot. For bolt-impact to occur, the 40 mm slot-length available to both sides must be exceeded, this is illustrated in Figure 4.7 (b). In Figure 4.7 (a), the regions at the peaks of the displacement series between the dashed lines represent the areas where impact occurs. For the particular schedule shown in Figure 4.7 (a), 3 mm displacement beyond the slot-length is prescribed.

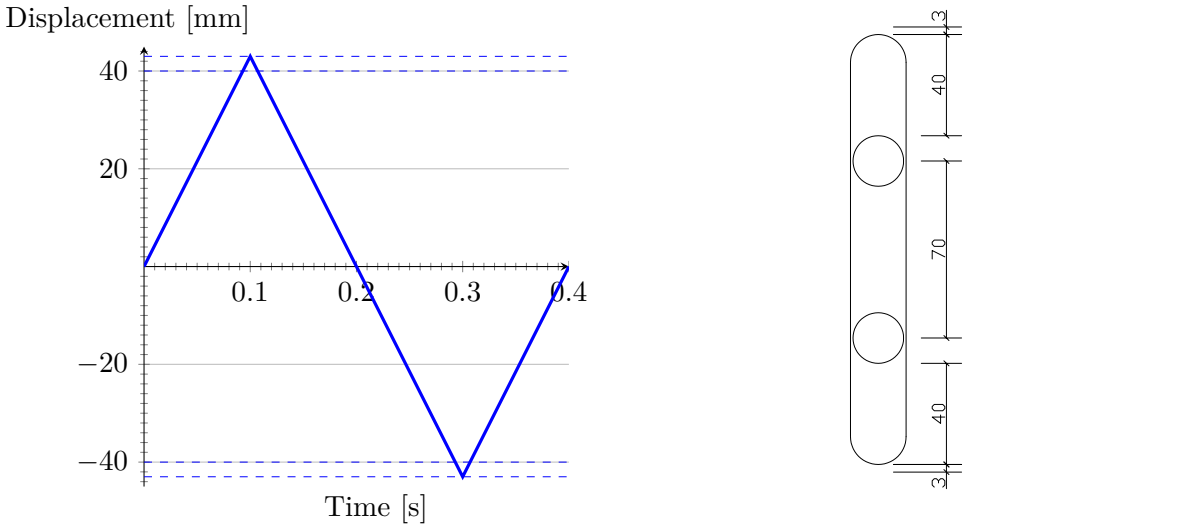

(a) Displacement schedule employed (b) Slotted-hole with bolt-shanks

Figure 4.7: Displacement schedule for bolt-impact analysis and illustration of slotted-hole

4.1.3 Results and discussion

The typical hysteresis curve of the SBC with bolt-impact is shown in Figure 4.8. It is characterised by a rectangular loop with a plateau at the slip-load and a sharp increase in stiffness where impact occurs. Figure 4.9 shows a section through the SBC to explain the interaction between the bolt-shank and the plates of the connection during bolt-impact. The slotted-plate displaces towards the bolt-shank in the successive parts of Figure 4.9 . Initially, as presented in Figure 4.9 (a), there is no contact between the plates of the SBC and the bolt-shank. Upon impact, the slot-end of the slotted-plate makes contact with the bolt-shank, which is shown in Figure 4.9 (b). After the slot-end has made contact with the bolt-shank, the 1 mm construction tolerance between the bolt-shank and the bolt-holes in the outer-plates is closed, which is shown in Figure 4.9 (c). The initial contact between the slot-end and the subsequent shift of the bolt to close the tolerance leads to the second plateau in the hysteresis graph after 40 mm displacement. After the construction tolerance has been closed, the bolt enters a bearing mode which is shown in Figure 4.9 (c). The holes in the outer-plates as well as the slot-end are in contact with the bolt-shank and a sharp increase in the stiffness of the connection is observed. The hysteresis results can be compared qualitatively to experimental results obtained by Lukkunaprasit et al. (2004) in Figure 4.10. In terms of shape, the bolt-impact hysteresis compares favourably to that of Lukkunaprasit et al. (2004), both sets of results exhibit a primary and secondary plateau followed by a significant gain in stiffness during bolt-impact.

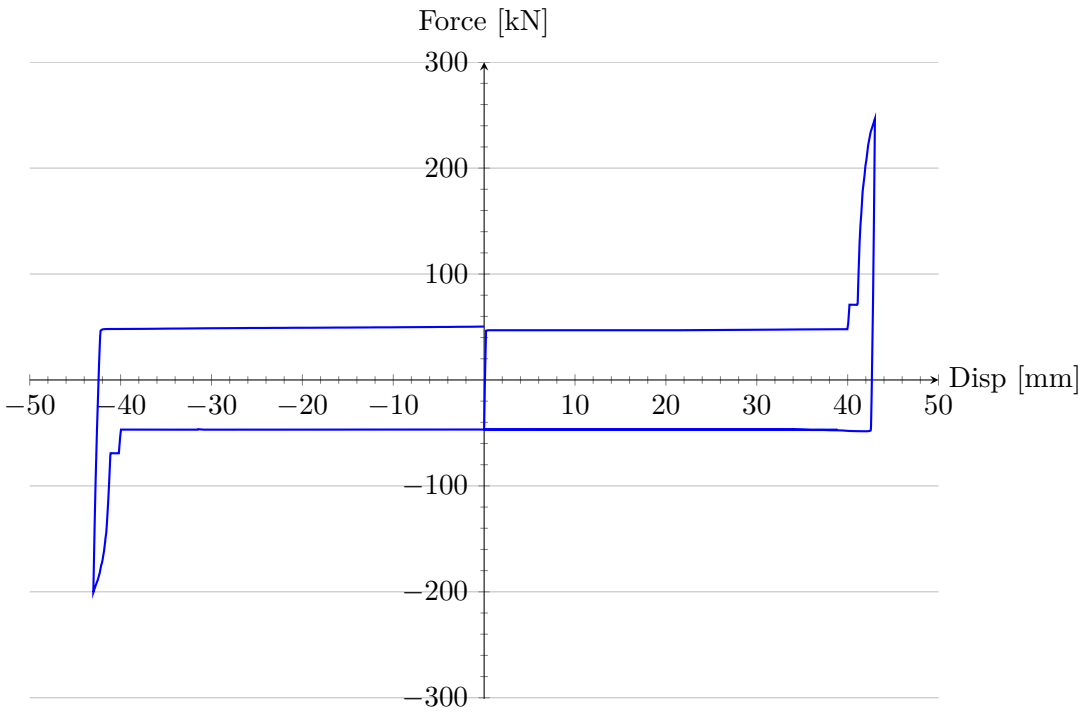

Figure 4.8: Bolt impact hysteresis for Hex-1 mesh

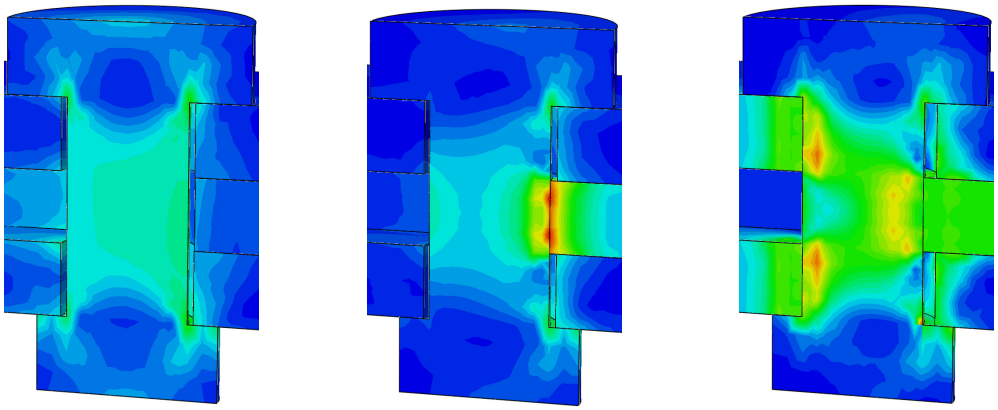

(a) No contact and 1 mm construction tolerance open

(b) Contact between slot-end and shank

(c) Tolerance closed initiating the bearing mode

Figure 4.9: Shift of bolts into bearing mechanism

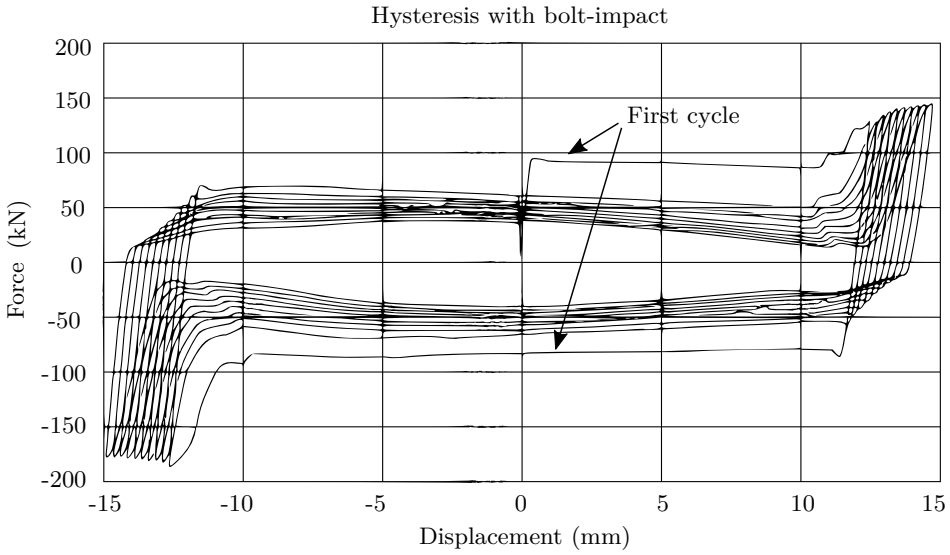

Figure 4.10: Experimental hysteresis results from Lukkunaprasit et al. (2004)

Mesh impacts

In terms of forces, the meshes considered obtained practically the same maximum and minimum force results for the bolt-impact analyses. The results listed in Table 4.5 are from the positive and negative peaks of the bolt-impact hysteresis results for the various meshes. The force values obtained from the symmetry models were doubled and also compare favourably. Similar force values for different elements and meshes should be expected since the same amount of displacement beyond the slot-end is prescribed. The same inelastic deformation should require the same amount of force regardless of the element type or mesh selected, provided that the mesh is sufficiently fine and a suitable element type is used.

The meshes differ slightly with regards to stress results, but overall the results are similar across the different meshes and element types. The results of the symmetry models are also similar to those of the full connection. The coarser Hex-2 mesh results in the highest stresses, while the fine Hex-1 mesh results in slightly lower stresses. The results of the two Tet meshes are similar and assumed to be accurate since the Abaqus documentation recommends the use of these elements. A comparison between the stress results of the meshes considered and the symmetry models are provided in Appendix B.

Table 4.5: Peak force results for meshes considered

Mesh	Max (kN)	Min (kN)
Hex-1	246	−200
Hex-2	246	−200
Tet-1	247	−200
Tet-2	244	−199
Sym-1	$123 \times 2 = 246$	$-100 \times 2 = -200$
Sym-2	$120 \times 2 = 240$	$-100 \times 2 = -200$

The use of refined meshes resulted in computationally expensive analyses. This caused longer analysis duration and larger output files than with the analysis of Section 3.1 even though the displacement history was significantly shorter. Table 4.6 shows the running time for the bolt-impact analyses as well as the size of the output files generated. Table 4.6 shows that these output files become tedious to work with and running times become excessively long. The beneficial use of symmetry to improve computational efficiency is clear from Table 4.6. Although the symmetry models contained exactly half of the elements to the corresponding full connection models, the running times reduced much more significantly.

Table 4.6: Computational cost of different meshes

Mesh	Running time (h)	Output file size (GB)
Hex-1	15	3.7
Hex-2	9	1.5
Tet-1	16	13.4
Tet-2	13	8.5
Sym-Tet1	3	8
Sym-Tet2	1.7	4.7

Stresses and deformations

The Abaqus results in Figure 4.11 indicate the Von Mises stress in units of Pascal that developed in the slotted-plate and bolt when compressive contact occurred. The top outer-plate was omitted from view in Figure 4.11 (b). The pink lines represent the coupling constraint between the reference point and the sliding plate. Figure 4.11 corresponds to the point of maximum positive prescribed displacement in Figure 4.7 and therefore to the maximum positive force in Figure 4.8. The high stresses in the slotted-plate in Figure 4.11 (b) are close to the yield stress of 423 MPa in the region between the bolt-shank and the edge of the plate. Around the slot-end of the slotted-plate, the stresses have exceeded the yield stress of the plate. Figure 4.11 (a) indicates that stress in the bolt is close to the yield stress of 786 MPa at certain locations. As expected, stress concentrations occur in the central region of the bolt where the slotted-plate

impacts and also at the top and bottom surfaces of the shank. This is caused by a combination of the outer-plates being pushed outwards due to bulging around the slot-end, which is shown in Figure 4.13, as well as the sustained bolt tension due to the bolt-loading applied as discussed in Section 3.1.

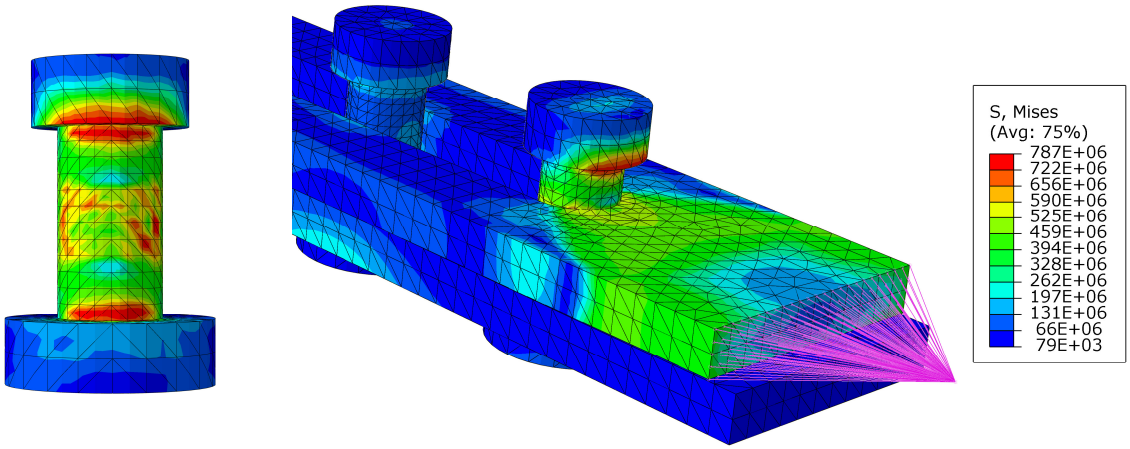

(a) (b)

Figure 4.11: Stresses in slotted-plate and bolt in contact

Figure 4.12 (a) and (b) shows the deformation of the slot-end due to bolt-impact. The deformations in the "U3" direction are shown in metres and were exaggerated for the plot. The maximum deformation is less than a millimetre and is expected since only 3 mm of displacement beyond the slot-end was prescribed. With greater displacements beyond the slot-end, more bearing deformation would occur. The deformations cause the outer-plates to bulge outward as shown in Figure 4.13, deformations were exaggerated for the plot. This bulging contributes to the high stress regions in the bolts as shown in Figure 4.11 (a).

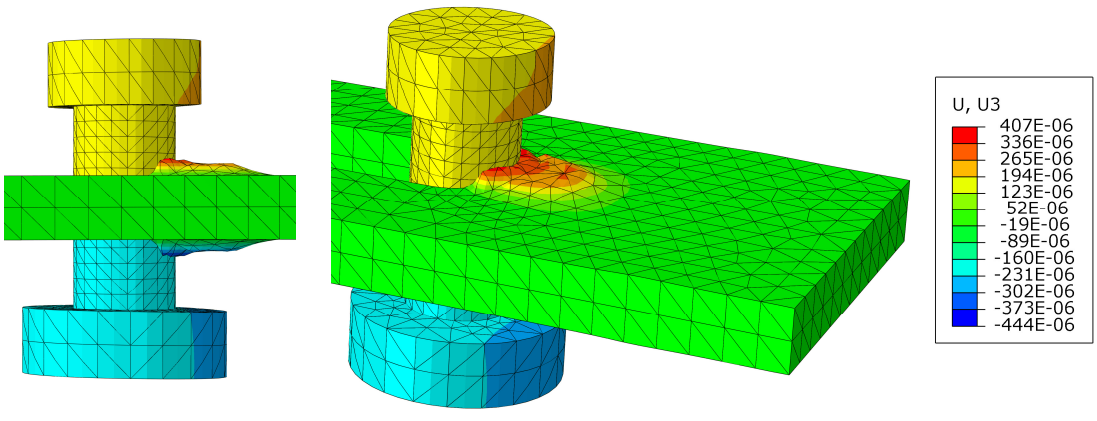

(a) (b)

Figure 4.12: Bulging of steel into mounds around slotted-hole

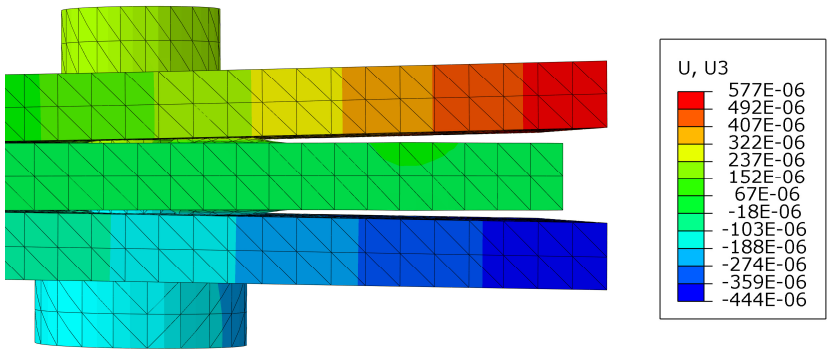

Figure 4.13: Bearing deformation causing outer-plates to displace laterally

Figure 4.14 (a) and (b) shows the results for Von Mises stress in Pascal when the SBC is at its maximum negative displacement and the connection is in tension. Deformations were exaggerated to show how the slotted-plate deforms during bolt-impact. Slight necking is shown in the slotted-plate when in tension in Figure 4.14 (b). The hysteresis results in Figure 4.8 indicate that the force carried by the connection in tension is lower than in compression. When in tension, stress can distribute through the entire slotted-plate, as in Figure 4.14 (b), limiting the force that occurs. When in compression, all the stress is concentrated in the region between the surface through which displacements are applied and the point of impact with the bolt, which is shown in Figure 4.11 (b). This leads to higher stresses and deformations as well as a higher force for the SBC.

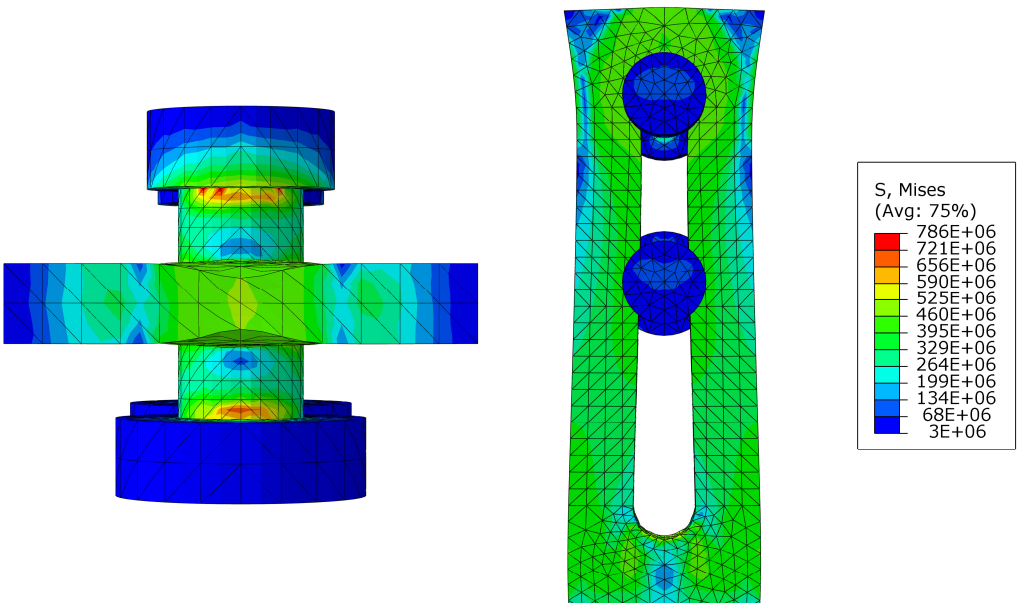

(a) (b)

Figure 4.14: Tensile deformation of the slotted-plate

Lukkunaprasit et al. (2004) tested subsequent cycles of bolt impact. They observed deterioration in the friction force of the connection caused by permanent deformation of the bolts due to

impact. The bolt-impact analysis presented in this section employed the SBC developed by Loo et al. (2014) and indicated that deformations were concentrated in the slotted-plate and not in the bolts. It must be noted that Lukkunaprasit et al. (2004) used M12 bolts together with outer-plates and slotted-plates of 11 mm each as well as two 6 mm shim plates. This resulted in a rather bulky connection with light bolts which could have exacerbated the loss of strength in the connection after impact. The deformation in the bolts noticed by Lukkunaprasit et al. (2004) means that if tested to failure, the bolts would have failed in shear. This is clearly an unwanted failure mode for the SBC. Deformations in the bolts will affect their ability to retain pre-load and must therefore be averted. Shear failure and deformation of the bolts must be precluded by bearing deformation in the plates. Bearing deformation in the slotted-plate is desirable since this mode is ductile and deformations in the order of 10 mm can be expected (SAISC, 2013). When detailing the connection this is a vital consideration.

The use of more bolts in a transverse line is beneficial in the case where bolt-impact occurs. During impact in the connection of Loo et al. (2014), all the force travels through the bolt that is impacted. In this condition, the other bolts in the longitudinal direction play no part in the strength of the connection. Naturally, the SBC detail used by Loo et al. (2014) was not designed to be tested for bolt-impact, but to limit the eccentricities in the connection and use a setup that agreed with their testing machine. The SBC of Lukkunaprasit et al. (2004) had two bolts in a transverse line to prevent shear failure. It is plain that a preferred detail for the slotted-plate of the SBC is one as shown in Figure 4.15 with multiple bolts in a transverse line. The combined shear resistance of the bolts are significantly higher and if necessary, bearing deformation can occur in more areas.

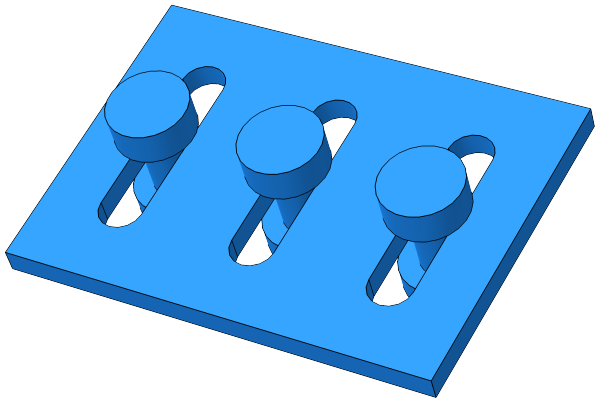

Figure 4.15: Preferred connection detail type for SBC slotted-plate

4.2 Symmetric and Asymmetric SBC performance

The differences between the SSBC and the ASBC, which are the two variants of the SBC, are discussed in this section. Abaqus analysis raised important issues with regards to the behaviour of the ASBC during sliding and bolt-impact. The expanded and symmetry models used in

Section 4.1 were analysed with alterations made to the fixity conditions for the ASBC. This was conducted to better understand the differences between the ASBC and the SSBC. It was motivated by the focus on the ASBC in research by Golondrino et al. (2014), as opposed to the SSBC.

4.2.1 Performance differences

The main difference between the two layouts is that in the ASBC, only one of the outer-plates carries loading and not both as with the SSBC, which is shown in Figure 4.16. Slip initiation in the ASBC consists of different stages, which are shown in Figure 4.16 (a) to (c). Initially, relative movement is present only between the slotted- and outer-plate and the cap-plate is dragged along, which is shown in Figure 4.16 (a). The initial slip of the connection therefore occurs at a lower force than when fully activated, albeit for a short duration of time, which is shown in Figure 4.17 (b). When the bolt-shank contacts the outer-plate as well as the cap-plate, which is shown in Figure 4.16 (b), the cap-plate stops moving and two frictional interfaces are present, which is shown in Figure 4.16 (c). At this stage, the connection is fully activated and is at its maximum sliding force. In the SSBC on the other hand, both frictional interfaces are always involved with slip and the slip-force is constant, which is shown in Figure 4.17 (a).

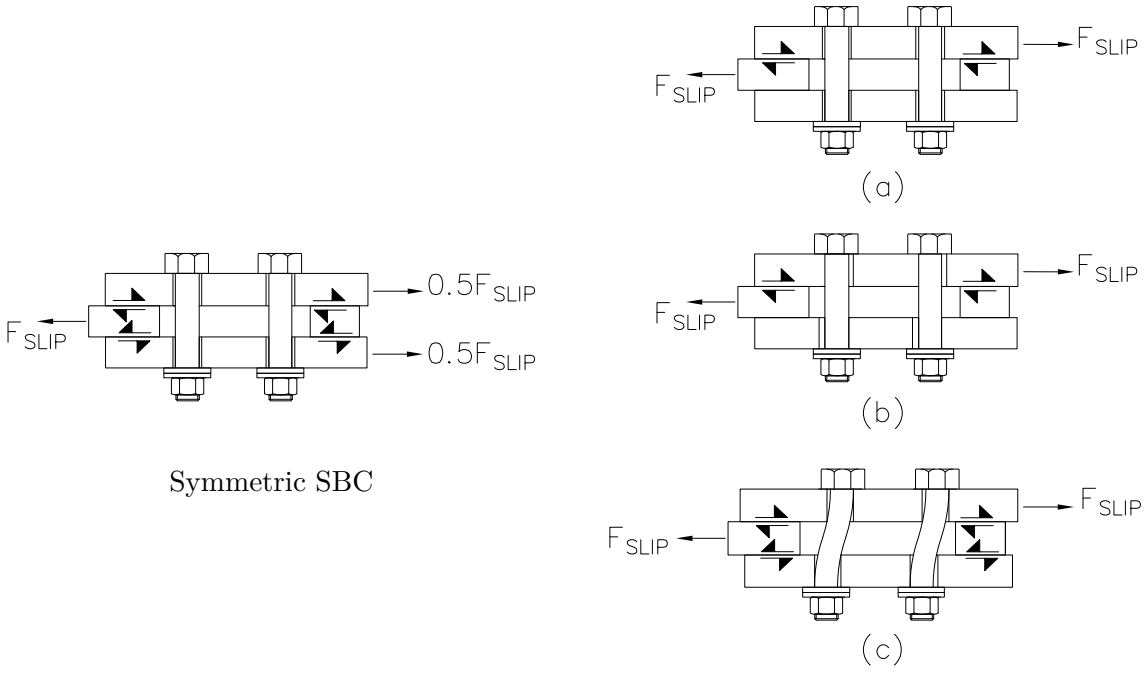

Figure 4.16: Differing load paths and layout for SSBC and ASBC (adapted from Loo et al., 2014)

(a) Symmetric SBC (b) Asymmetric SBC

Figure 4.17: Differing hysteretic behaviour for SSBCs and ASBCs (adapted from Loo et al., 2014)

During normal sliding of the SSBC, the bolt-shank and the plates of the connection do not make contact. If impact with the slot-end does not occur, the tensile stress in the bolts due to the applied pre-load remains constant. With the ASBC however, the bolt-shanks make contact with the outer- and cap-plate during normal sliding. The resulting stress concentrations in the bolts may negatively affect the bolt pre-load as well as the SBC as a whole. In the event of bolt-impact, the SSBC has two shear planes while the ASBC only has one. This results in an unfavourable stress distribution in the ASBC-bolt which is discussed in Section 4.2.4.

4.2.2 Model

The model of Loo et al. (2014) explained in Section 4.1 was used for the SSBC model. The only alteration made to the ASBC was that one of the outer-plates retained the boundary conditions of the original connection. A comparison between the boundary conditions of the SSBC and the ASBC is shown in Figure 4.18 (a) and (b).

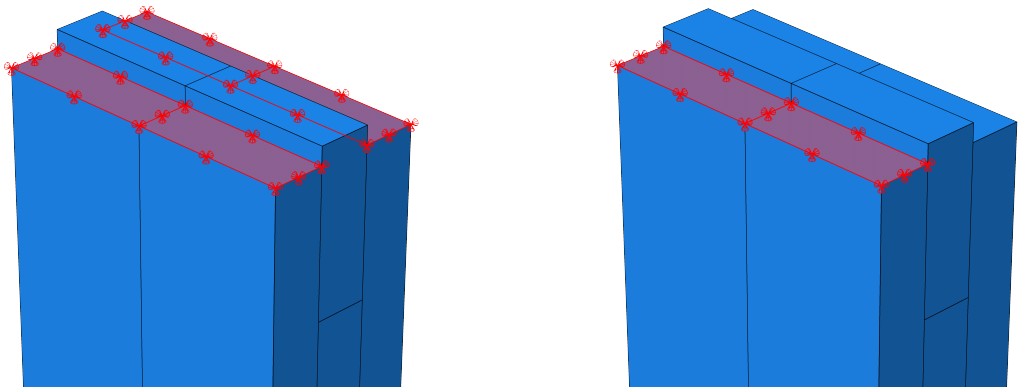

(a) Symmetric SBC (b) Asymmetric SBC

Figure 4.18: Boundary conditions of the SSBC and ASBC models

4.2.3 Analysis

Two analyses were performed. For normal cyclic behaviour, the SSBC and ASBC were analysed as performed in Section 3.2 with only a single displacement cycle and no bolt-impact. This was conducted to understand the effects on the normal hysteretic behaviour of the two connections. The bolt-impact analysis used the same displacement control as in Section 4.1.2 for a single cycle and impact on both sides of the connection.

4.2.4 Results and Discussion

Figure 4.19 shows that there is an insignificant difference between the overall hysteresis behaviour of the two layouts. The difference is that the ASBC has a lower initial slip-force when the cap-plate moves as explained in Figure 4.16 (a). When the bolts make contact with the outer- and cap-plate, the force stabilises at the slip-force. The enlarged part of Figure 4.19 shows a part of the transition from initial to full slip-force. This transition occurs quickly since the clearance between the bolt-shanks and bolt holes are small and the displacements applied to the connection are large in comparison. As soon as slip occurs in the SSBC, it is at the slip-force level shown by the clear transition from sticking to slipping behaviour in Figure 4.19.

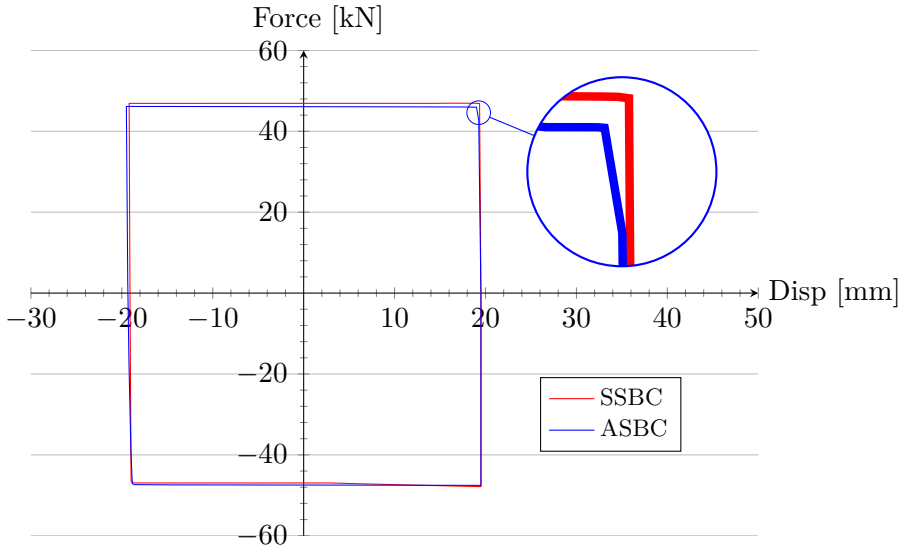

Figure 4.19: Hysteresis behaviour of SSBC and ASBC

As explained in Section 4.2.1, bolts work in a bearing mode during normal sliding in the ASBC. For this reason, the stresses in the bolts are expected to be higher than those of the SSBC. The results of the analysis for normal sliding is shown in Figure 4.20 in terms of the Von Mises equivalent stress in Pascal. The plates have been omitted and a section through the bolts is shown. The bolt in Figure 4.20 (a) experiences stress only from the pre-load while the bolt in Figure 4.20 (b) experiences an unequal stress distribution due to bearing. The results of the ASBC bolt corresponds to condition (c) in Figure 4.16. From a strength perspective, the higher

stresses is not concerning, but the higher stresses combined with bearing on the bolt-shank could certainly impact the bolt pre-load negatively.

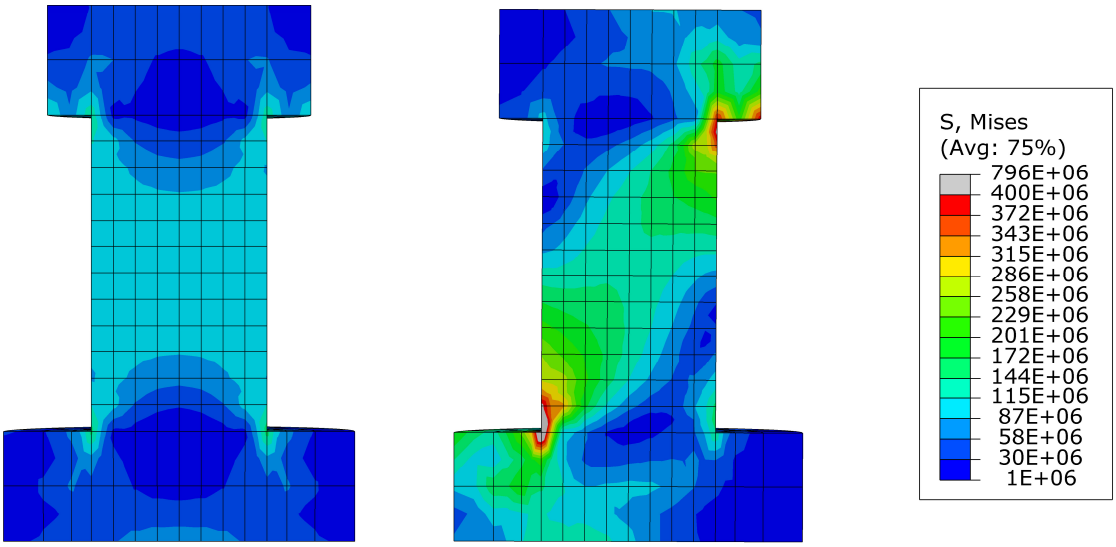

(a) Symmetric SBC bolt (b) Asymmetric SBC bolt

Figure 4.20: Stresses in bolts under normal sliding conditions

The advantage of the SSBC over the ASBC during bolt-impact is clear, two shear planes are present instead of the single shear plane with the ASBC. This means that the bolt capacity is effectively doubled. Figures 4.21 and 4.22 show the Von Mises stress at the stage of maximum prescribed displacement for the full connection and for the bolts, respectively. An unequal stress distribution through the ASBC bolt in Figure 4.22 (b) due to single shear means that connection failure may occur due to bolt shear before bearing deformation of the plates can result in a more ductile failure. This is seen from the high stresses throughout cross-section of the ASBC bolt in Figure 4.22 (b). At this stage of the analysis, the bolt of the ASBC is no longer in its elastic range. Under subsequent cycles of impact, the unequal distribution of high stresses in the bolt of the ASBC will have a more severe effect on the bolt pre-load than the SSBC under similar conditions.

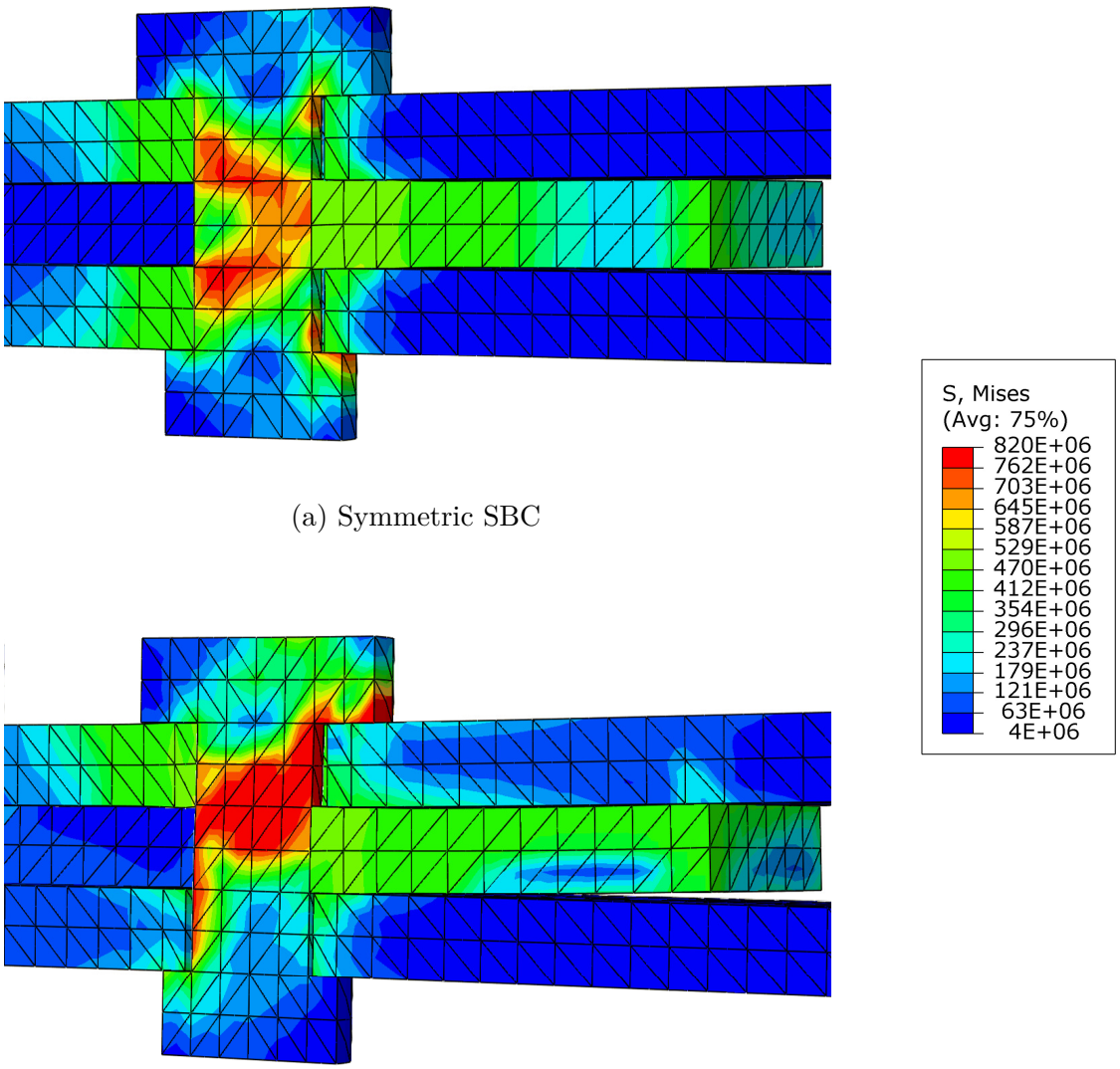

(a) Symmetric SBC

(b) Asymmetric SBC

Figure 4.21: Stress distribution in bolt of SSBC and ASBC due to impact

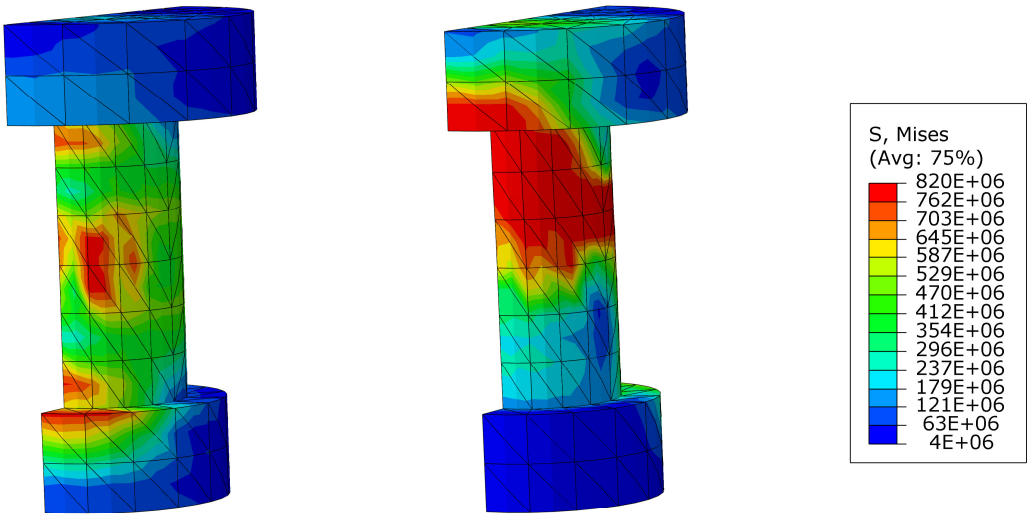

(a) Symmetric SBC (b) Asymmetric SBC

Figure 4.22: Stress distribution through bolt cross-sections due to impact

Further, the layout of the ASBC introduces an eccentricity into the connection. If the ASBC is used to connect a bracing member to a gusset plate, the eccentricity will cause side-sway of the gusset during compressive loading. This may cause sway buckling failure of the gusset plate.

The only area in which the ASBC is preferable to the SSBC is in terms of detailing. Detailing an ASBC between a gusset and a bracing member is more straightforward than a SSBC. ASBC detailing is similar to general practice except for the slotted-holes, spring washers, bolt pre-load and the addition of the cap-plate. Both the gusset and the bracing element can function as the slotted-plate depending on easier constructability. The SSBC poses detailing challenges depending on the sections used as bracing members. If equal leg angles or channel sections are used on either side of the gusset functioning as the slotted-plate, detailing would be simple. If more brace member capacity is required and CHS for example are used, the detailing becomes more involved. Either two gusset plates or two spade-plates must be used with the other functioning as the slotted-plate. It is clear that detailing and constructability with heavier sections is non-standard and requires more careful consideration.

The comparison between the SSBC and the ASBC was motivated by the work of Golondrino et al. (2014) on Asymmetrical Friction Connections for use in low-damage braces. The reason for their focus on the ASBC was unclear since the SSBC seemed to exhibit better qualities. Following the analysis and discussion above, it is clear that the SSBC is superior to the ASBC. It is believed that the focus on the ASBC in their research was prompted by the work conducted by Dr Charles Clifton on the ASBC for use in beam-column connections as mentioned in Section 2. In the case of Dr Clifton's SHJ beam-column connection, the ASBC performs better than the SSBC. The availability of information, test data and proposed design models for the ASBC meant that there might have been bias towards continuing work on the ASBC while the SSBC is clearly more suitable for connecting bracing elements.

4.3 Sliding direction and braces with SBCs

The interactions between the bolt-shanks and slot-sides were investigated in this section. This was conducted in Abaqus with the SBC connected to a structural frame. Horizontal displacements were applied to the top chord of the frame. The possibility of adverse behaviour when the direction of sliding was not collinear with the slot-direction was examined.

Loads passing through the SBC are not always collinear with the slot-direction. Most experimental tests considered only collinear sliding where the loading-direction and the slot-direction aligned perfectly. Base accelerations due to earthquakes cause structures to deflect laterally. Sway modes are dominant, resulting in horizontal deflections being several orders larger than vertical deflections. There was therefore a concern that the interaction between the bolt-shank and the slot-sides could have a significant effect in the performance of the SBC when used in a structural frame as a connection to bracing elements.

A single braced bay of a structural frame was modelled. 3D solid elements were used to model a SBC between the brace and the gusset plates at the column-base-to-bracing connection. Displacements were prescribed to the top chord of the frame and the behaviour of the components of the SBC was studied. With satisfactory modelling of the SBC with reference to experimental tests as discussed in Sections 3 and 4.1, the assembly of the SBC into a structural frame could be completed. Investigating the SBC within a frame with FEA software provides great advantages over full-scale testing. The stresses developed in the SBC can be visualised and parametric studies can be performed more easily than with full-scale testing.

4.3.1 Non-Collinear Sliding

Ground accelerations during seismic excitation cause structures to drift laterally. In multi-storey buildings, horizontal deflections take place to various degrees on different levels. With simple construction, beams are not moment-restrained and horizontal deflections of the structure are larger than vertical deflections. This is what causes bracing members or connections to fail. Figure 4.23 shows that the bracing member of a simply constructed, diagonally-braced bay experiences mainly horizontal deflection due to storey-drift. If the brace was attached by a SBC, the slotted-plate of the SBC should experience greater horizontal than vertical sliding. There was thus a concern that the interaction between the bolt-shanks and the slot-sides could affect the performance of the SBC with braces.

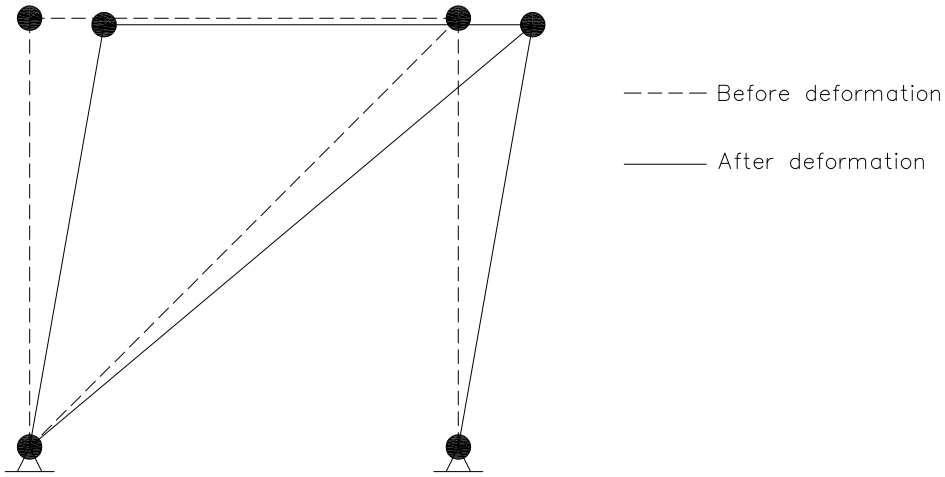

Figure 4.23: Storey-drift in a single bay of a diagonally-braced frame

In SBC experimental tests to date, most forces applied to the SBC were in the same direction as sliding. When the SBC is present in a bracing member, this will clearly not be the case. While the slot is parallel to the bracing member, the direction of movement is not. In the study by Balendra et al. (2001), their SBC was part of a structural frame that was tested pseudo-dynamically. Unfortunately, the small sliding distance (3 mm to each side) together with the bulky halting blocks used around the connection, restrained their SBC in such a way that the impact of non-collinear sliding could not be established.

Admittedly, non-collinear sliding is a layout-specific problem. The global structural layout affects slot-inclinations, bolt layout and bolt pre-tension, amongst others. This means that the effect of non-collinear sliding will be more pronounced in certain situations than others. Please note that this section therefore is not intended as a study of all situations and their effects on the SBC's performance, but rather a simple evaluation of the possible impact of this behaviour. The influence of bolt impact with slot-ends was negated and only normal sliding was considered. This section does not consider the impact of different magnitudes of lateral deflections present on different levels in a multi-storey structure.

4.3.2 Model

The model used in this section was a single bay of a diagonally-braced frame. A SBC was used between the bracing element and gusset plates. The SBC was composed of 3D solid elements, while beam elements were used for the columns, beam and brace. A layout drawing of the frame that was modelled is provided in Figure 4.24, while detailed drawings of the SBC are provided in Appendix C.

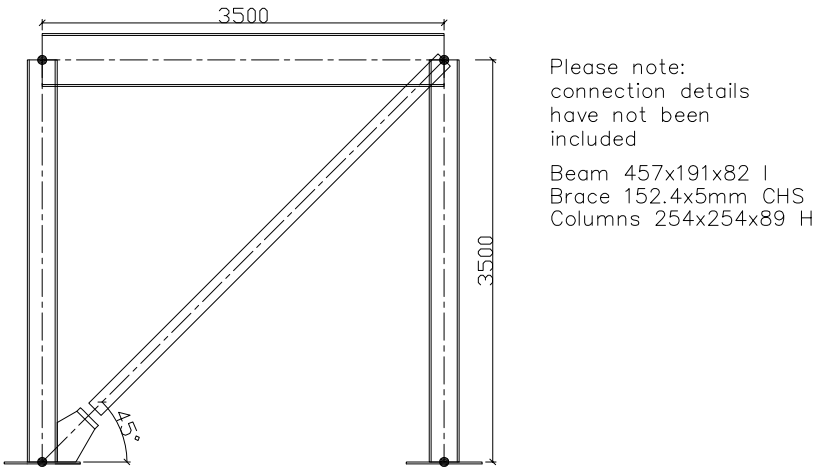

Figure 4.24: Layout and element sizing for the model

Since pin supports were modelled for simple construction, no moments and minimal shear and axial forces are present in the frame. The section sizes were therefore arbitrarily selected which is shown in Figure 4.24. It was assumed that in general, braced bays are longer horizontally than vertically. A 3.5 m storey height was selected and an angle of 45° from the horizontal was selected for the slot inclination. This would be the "worst case" for non-collinear sliding with inclinations less than 45° being more favourable. As the inclination angle approaches zero, the slot direction coincides with the horizontal displacement direction. Figure 4.25 shows the Abaqus model with the beams rendered for illustrative purposes.

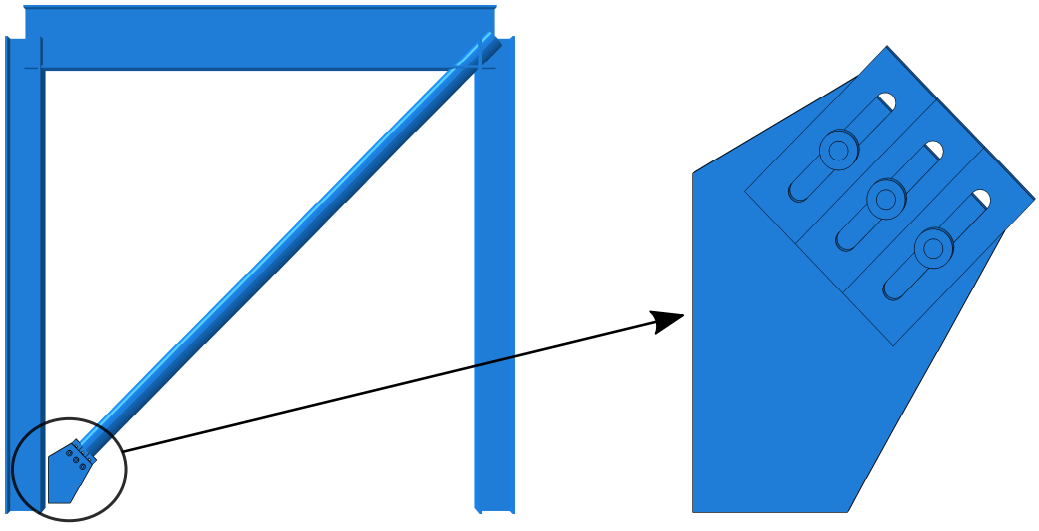

(a) Frame model (b) Enlarged view of the SBC

Figure 4.25: Frame model with the SBC enlarged

The preferred SBC slotted-plate setup as explained in Section 4.1 was employed. The gussets and slotted-plate were not designed to carry a specific ultimate force since bolt-impact would not

occur. Details were therefore developed to simply withstand the slip-force of the connection. The three bolts were pre-loaded to 32.5 kN and the friction coefficient was assumed to be 0.36 resulting in an expected slip-force of 70 kN. The 32.5 kN bolt pre-load was used by Loo et al. (2014) in their experimental tests. The friction coefficient of 0.36 corresponds to the average friction coefficient of the Bisalloy-400 ARS in the experimental tests of Loo et al. (2014). Figure 4.25 (b) shows the SBC with the front gusset plate omitted for illustration purposes.

Similar to the first model explained in Section 3, a constraint was used to couple the top surface of the slotted-plate to the end of the brace member, which is shown in Figure 4.26. All the degrees of freedom were coupled resulting in a fixed interface between the bracing member and the slotted-plate. In this case the slotted-plate was assumed to be an extended spade-plate welded to the CHS.

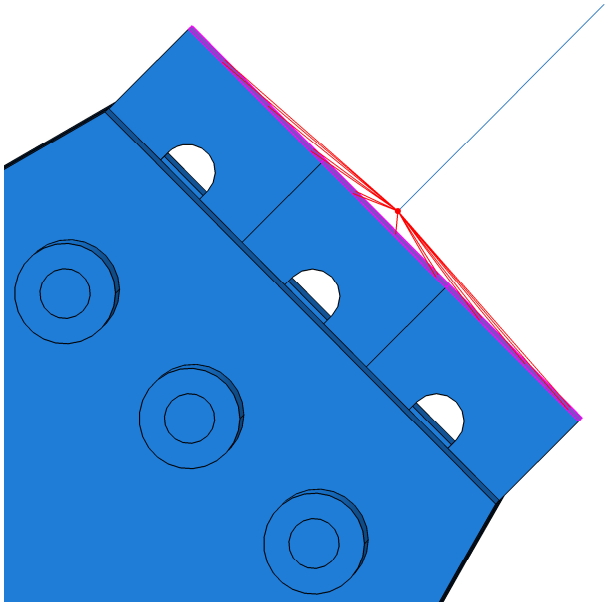

Figure 4.26: Coupling constraint between the slotted-plate and the brace member end

For the boundary conditions of the frame, pinned footings were assumed for the column bases in line with general practice for simple construction. Out-of-plane and torsional rotation of the column bases were restrained. The beam ends were released on either side at the beam-column connections. This corresponds to normal procedure for analysis of beam-column connections assumed to be simply connected with shear-tabs. Two approaches are available to obtain pinned beam-ends; the first is creating separate parts in Abaqus/CAE and using constraints to join the nodes, while the second is using the *RELEASE keyword in the input file. Using constraints, the rotational degrees of freedom can be prevented from being carried over at the nodes that are connected. This method is tedious and generally causes analysis errors when more than two nodes are joined and was therefore not used. The *RELEASE keyword releases rotational degrees of freedom at the positions in the mesh element specified (SIMULIA, 2012d). The *RELEASE keyword is not supported in the Abaqus/CAE interface and must be hard-coded into the input text file that is used for the analysis (SIMULIA, 2012c). This is conducted in the part definition section of the code in the following manner:

*RELEASE
41, S1, M1

Where "41" refers to the element number, "S1" is the element end identifier and "M1" is the release combination code (SIMULIA, 2012c). In this case the "M1" code releases rotations around the "n_1" local beam element axis which is shown in Figure 4.27 (a). Figure 4.27 (b) shows a comparison between the behaviour of a simple frame with and without the use of the *RELEASE keyword.

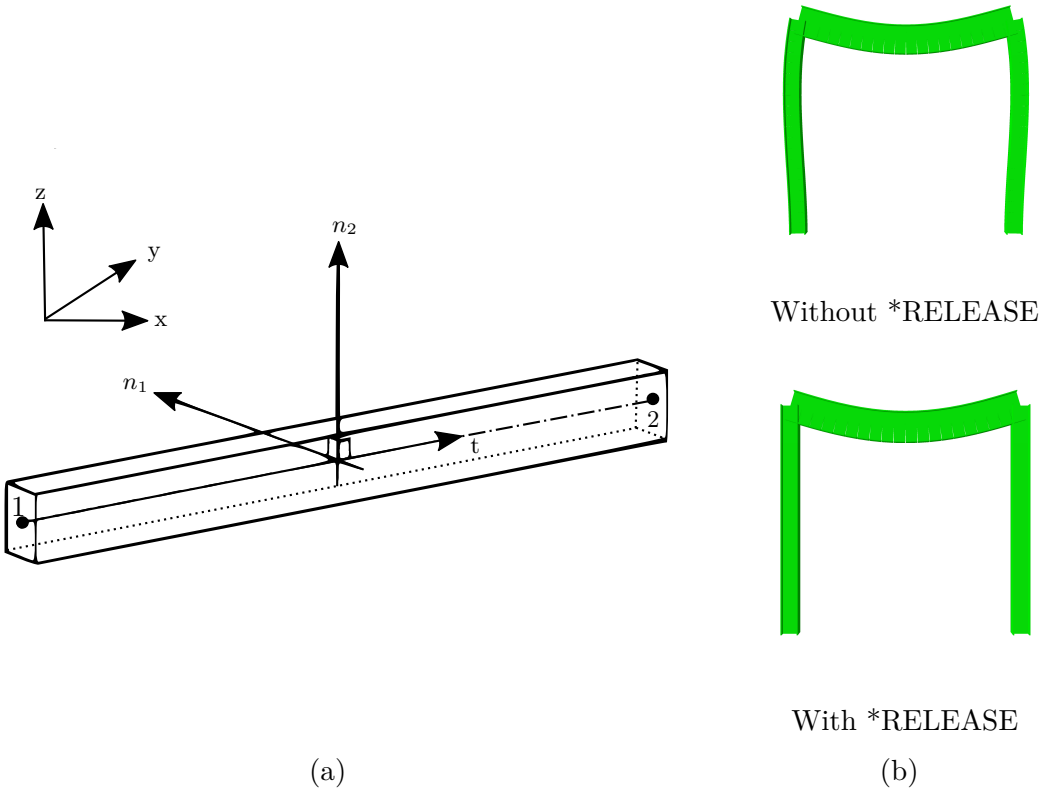

Figure 4.27: Local beam element axis and comparison of using the *RELEASE keyword for n_1 axis

Two conditions were considered for the connection between the brace and the column. Firstly; the rotational degrees of freedom were released and secondly; the connection was fixed with full moment transfer. This was performed because it was believed that if rotation could take place freely at the top of the brace, corresponding to the first condition, sliding would be mainly collinear in the SBC. With the second condition, rotation would have to take place at the bottom of the brace and consequently there would be some degree of non-collinear sliding.

Due to the complexities associated with connecting dissimilar element types in FE modelling, no constraint was added between the beam element of the column base and the 3D solid elements of the gussets. Instead, the gusset plates and column bases had separate boundary conditions. While it is conservative to assume pinned footings for columns in global analysis, the rotations associated with this boundary condition were thought to be unsuitable for the actual behaviour of the gusset plates. The welds connecting the gusset plates to the column base and accompanying

base plate would cause the gussets to be relatively rigid with small rotations in the column base not causing significant rotations in the gussets. The gusset plates were therefore assumed to be fully welded to the column base and modelled as a fixed connection in Figure 4.28 (a). Nevertheless, a condition was considered that accounted for this assumed rotation of the column base, which is shown in Figure 4.28 (b). Here the out-of-plane translational fixity is unchanged, while the vertical and horizontal fixities of the gussets are only retained on the corresponding vertical and horizontal parts of the gusset plates. This results in the ability of the gussets to rotate in the same manner as the pinned footing.

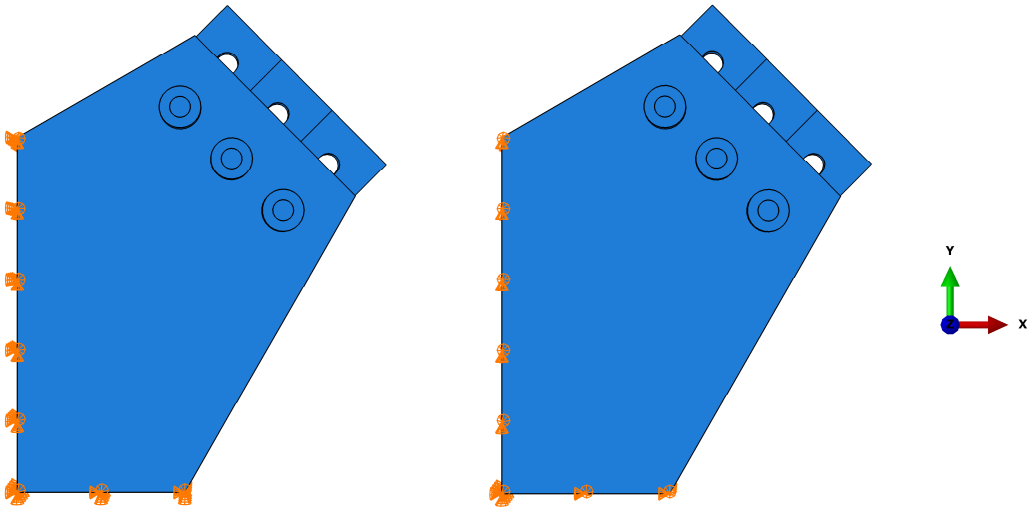

(a) (b)

Figure 4.28: Boundary conditions considered for the gusset plates: In (a) the vertical and horizontal edges of the gusset plates are restrained in all translational directions. In (b) the vertical and horizontal edges of the gussets can translate in the x- and y-directions respectively.

4.3.3 Analysis

The analysis was displacement-controlled, with the displacement applied to the right top chord of the frame. The displacement schedule used is shown in Figure 4.29. The 90 mm amplitude was assumed from the 2.5% of storey height limitation for inter-storey drift from SANS 10160-4 (SABS, 2011a).

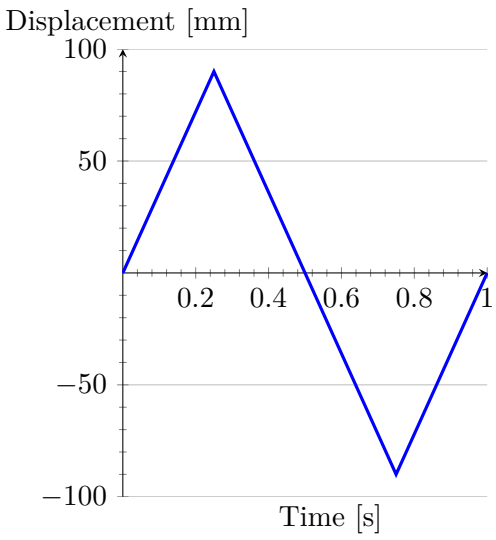

Figure 4.29: Displacement schedule used for non-collinear sliding analysis

4.3.4 Results and Discussion

As discussed in Section 4.3.2, two cases were considered for brace-column fixity; pinned and fully fixed. Figure 4.30 shows the results for bending moments in units of Nm for the two cases. Please note that the SBC was omitted from view and that horizontal displacements have been exaggerated. For the pinned brace-column frame in Figure 4.30 (a), practically no moments are present, while for the fixed brace-column in Figure 4.30 (b), it is clear that there is moment transfer between the brace and the column. This indicates that the *RELEASE keyword successfully releases the prescribed rotational degrees of freedom.

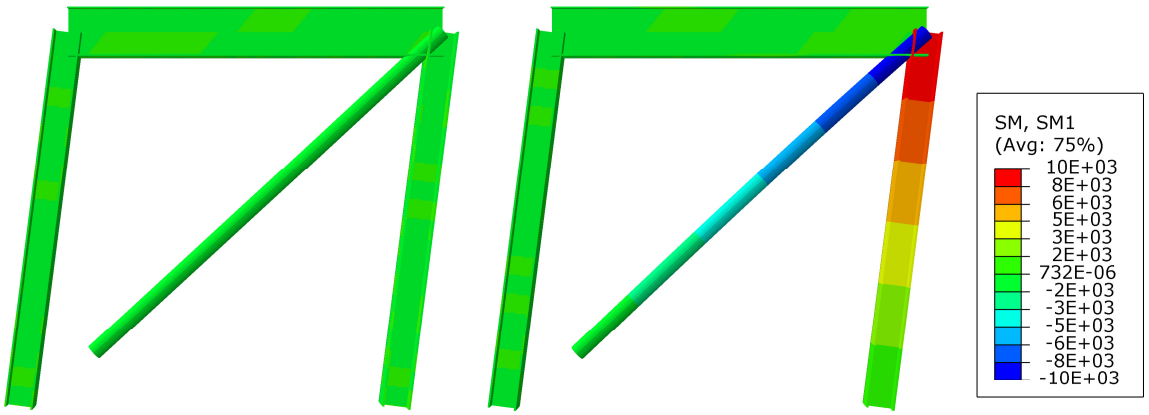

(a) Pinned (with *RELEASE) (b) Fixed (without *RELEASE)

Figure 4.30: Comparison between moments with pinned and fixed brace-column connections

The ability of the top end of the brace to rotate freely for the pinned case results in perfect collinear sliding with a rectangular hysteresis loop as shown in Figure 4.31. At no point during

this analysis do the bolt-shanks make contact with the slot-sides. The slip-force from the analysis compares well to the expected slip force.

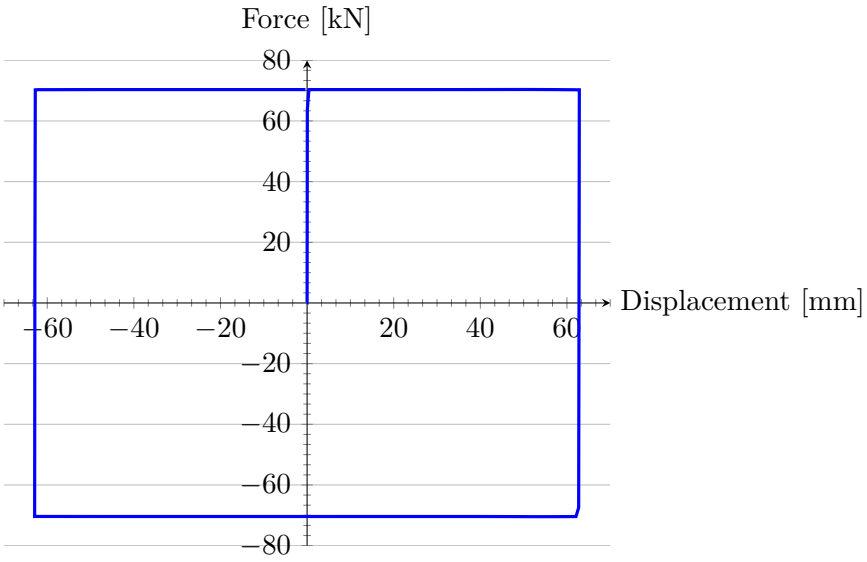

Figure 4.31: Hysteresis for pinned brace-column connection

For the case where moment-transfer occurs at the brace-column connection, no rotation takes place at this point. Subsequently, rotation occurs at the bottom end of the bracing member connected to the slotted-plate. This causes the bolts to make contact with the slot-sides, resulting in additional friction and a greater force through the SBC. The hysteresis for this case is shown in Figure 4.32 and the slight increase in force is evident at the points where the hysteresis diverges from the expected plateau corresponding to the slip-force.

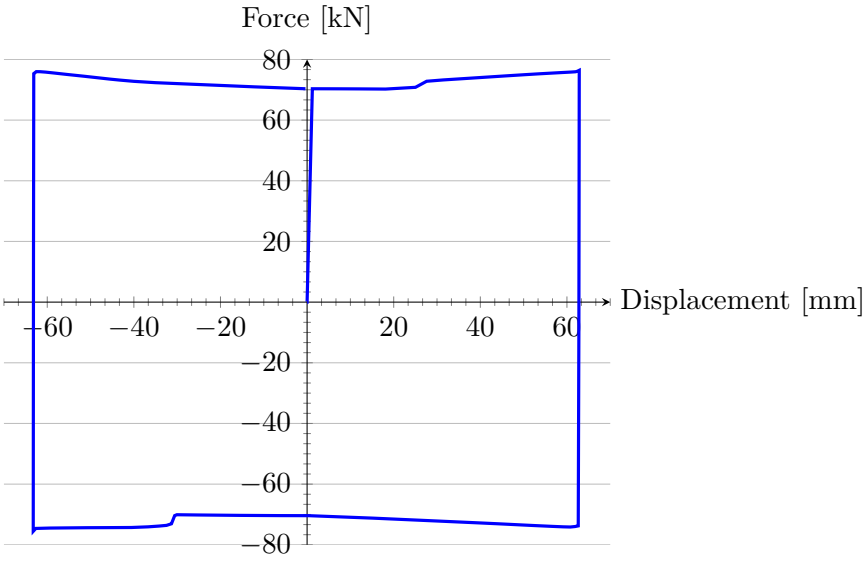

Figure 4.32: Hysteresis for fixed brace-column connection

Figure 4.33 shows the output for the Von Mises equivalent stress in Pascal. The bolt-shanks and slot-sides are shown at the time-step when the maximum force in the SBC is recorded. The

stress results show that the bolts and slotted-plate are far from their yield stresses which are listed in Table 4.2 on page 61. This indicates that the contact between the bolt-shanks and slot-sides is not problematic from a strength perspective.

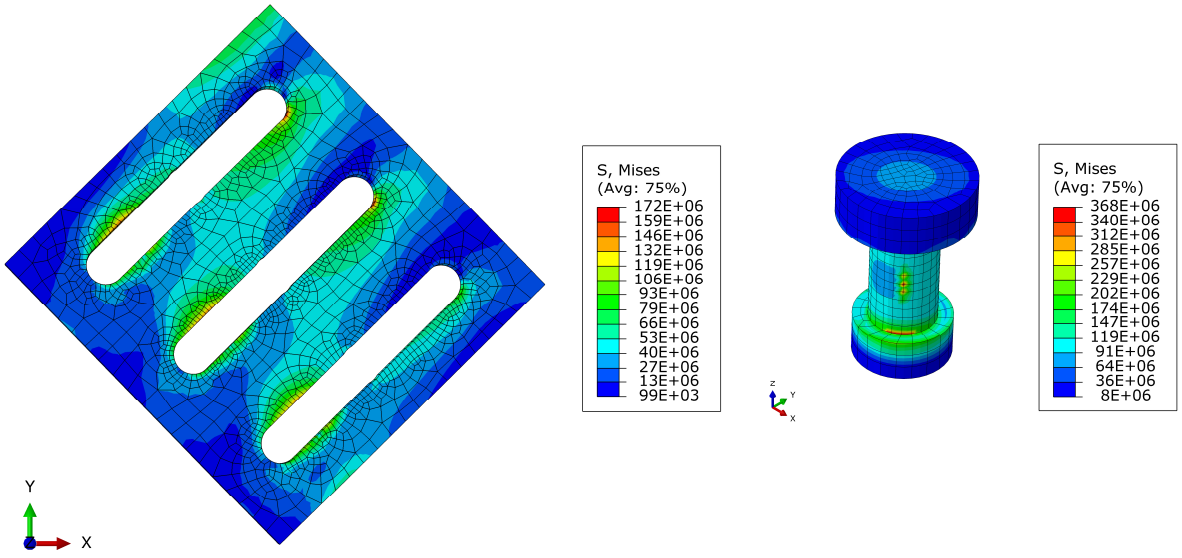

(a) Slotted-plate (b) Bolt

Figure 4.33: Stresses in SBC components during contact with non-collinear sliding

The effect of the rotational capability of the gusset plates as discussed in Section 4.3.2 affects the behaviour of the SBC insignificantly. Figure 4.34 shows the case where the gusset plates can rotate together with the pinned column base, the column section has been rendered for illustration. Figure 4.35 shows that while there is some difference in the hysteresis loop with the gusset rotation, it will not affect the ability of the connection to dissipate energy nor will it affect the strength of the SBC.

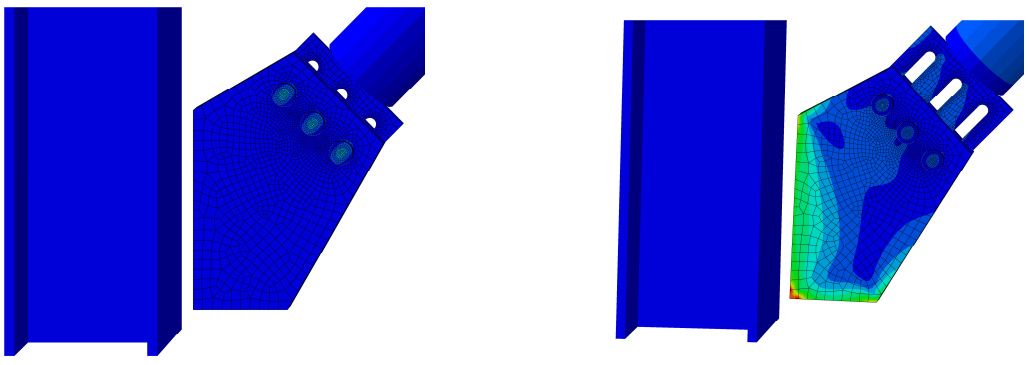

(a) Reference position (b) Maximum displacement

Figure 4.34: Rotational ability of gusset plate with pinned column base connection

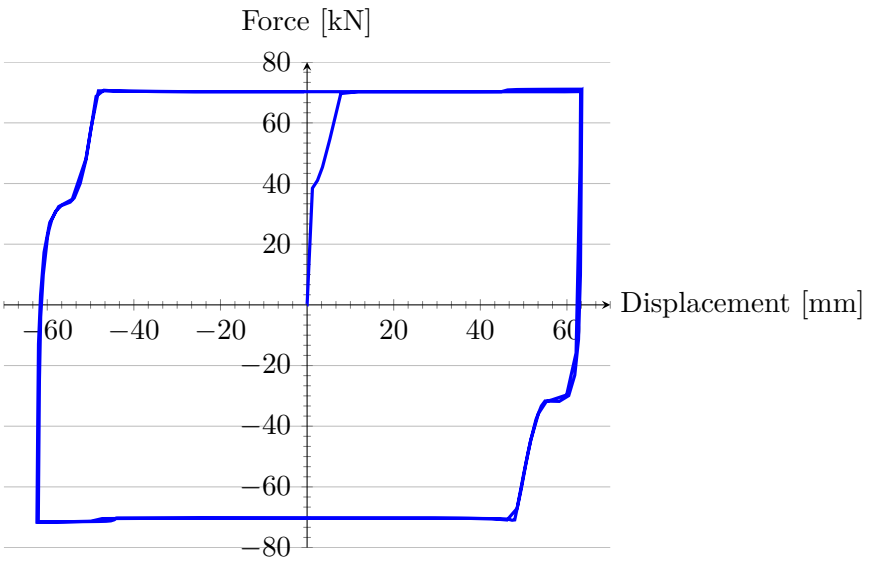

Figure 4.35: Hysteresis for gusset with rotational ability

The possible effect of having the bolt thread in the shear planes of the connection must be recognized. In this case the bolt thread could experience permanent deformation under normal sliding conditions against the slot-sides due to non-collinear sliding.

The results from the analysis indicate that while non-collinear sliding affects the behaviour of the SBC, there is no cause for concern. The magnitude of stress in the bolt-shanks and slot-sides during impact indicate that damage to the components of the connection should not be expected. Friction increases during non-collinear sliding, but the increase is of an insufficient magnitude to be detrimental to the energy dissipation capability of the SBC in the structural members connected to the SBC.

In addition to this, the results from the analysis correspond to findings of experimental tests conducted by master's students at the University of Canterbury, New Zealand. Tests were conducted at the same time this research was conducted. Structural frames with braces connected to SBCs were tested. During correspondence with Associate Professor Gregory MacRae (MacRae, 2015b), he stated that: "Even though there was some rubbing on the side of the bolts due to frame deformations, it did not seem to affect the strength significantly".

Chapter 5

Energy dissipation and global analysis

In this section, the emphasis shifts from the local behaviour towards the global influence of the SBC when incorporated in a bracing system. Non-linear time history analysis is necessary to investigate the beneficial effect of the SBC in a bracing system on a global structural level. The expensive computational cost of using 3D solid elements to model the SBC rendered this approach insufficient for global analysis. Lengthy running time of 3D solid elements, even during simpler analysis as in Section 4.3, necessitated simplification. A simplified modelling approach using non-linear springs was developed that ensured quicker global analysis which is discussed in Section 5.1. This was implemented in a model of a multi-storey structure subjected to earthquake ground motion and is discussed in Section 5.2.

5.1 Comparison of SBC modelling approaches

Non-linear springs were adopted as a simplification method for the combination of 3D solid elements and beam elements for the SBC and brace respectively. A comparison was required between the two approaches to ensure suitability of the simplification for global analysis. A single braced bay of a structure was considered. The bay was first modelled with 3D solid elements and beam elements, following this, a non-linear spring representing the SBC and bracing member was used. In this manner it was shown that the two approaches resulted in equivalent mechanical behaviour. Additionally, it was ensured that the dissipative qualities of the two approaches were similar, albeit in different forms of energy.

5.1.1 Combined behaviour of SBCs and brace members

Using the insight obtained from Chapters 2 and 4, the tensile and compressive behaviour of the SBC used with braces could be characterised as:

Tensile behaviour commences with the initial stiffness of the connection before slip. In this region, displacements arise from elastic strain in the brace and the slotted-plate of the SBC. Tension increases until the slip-force is reached. Slip occurs and the force remains constant while displacements increase. This continues until the slip-length is surpassed and bolt-impact occurs. The stiffness of the connection increases rapidly as bolts make contact with the slot-ends. If the loading is not reversed, tensile forces may increase to a level where failure occurs. The failure mode is governed by the design decisions which affect the detailing of the connection. It is important to design for a target failure mode that will ensure ductility, which is discussed in Section 5.2. A number of tensile failure modes are listed in Table 5.1.

Compressive behaviour is equivalent to that of tension, except that the failure mode will differ and failure will presumably occur at a lower force. Compressive failure may occur in the brace or the SBC and is governed by the type of section used for bracing and the detailing of the connection. A number of compressive failure modes are listed in Table 5.1. The tensile and compressive characteristics were used to define the non-linear spring behaviour which is explained in Section 5.1.2.

Table 5.1: Certain failure modes of the SBC in bracing

Tensile failure mode	Failure region
Failure away from connection	Brace
Bearing deformation	Slotted-plate
Block shear	Slotted-plate
Weld fracture	Gusset plates or brace
Bolt shear	Bolts
Compressive failure mode	**Failure region**
Buckling or local buckling	Brace
Side-sway or sway-buckling	Gussets or slotted-plate
Bearing deformation	Slotted-plate
Bolt shear	Bolts

5.1.2 Non-linear spring definition

The non-linear force-displacement behaviour of the SBC and accompanying brace member motivated the use of non-linear springs in Abaqus. Non-linear springs are non-standard elements and are therefore not supported in the Abaqus/CAE interface. The *SPRING, NONLINEAR keyword was used in the input file of the model in this case. Non-linear spring behaviour is defined by providing pairs of points to establish a force-displacement relationship (SIMULIA, 2012c). Figure 5.1 graphically shows such a relationship for a non-linear spring. Force-displacement pairs F_1-u_1 to F_4-u_4 are defined in ascending order by the user. Outside of the defined range, Abaqus assumes a constant force which results in zero stiffness, which is shown by the horizontal lines in Figure 5.1. Using the *SPRING, NONLINEAR keyword, the force-displacement behaviour of the SBC and brace described in Section 5.1.1 was defined. The assumptions made with regard to the force-displacement values that were used is discussed in Section 5.1.4

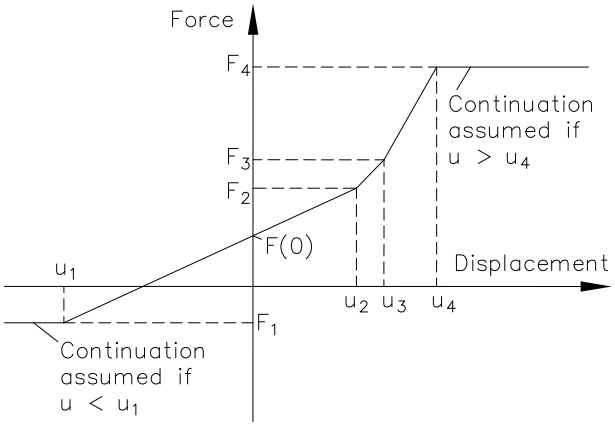

Figure 5.1: Non-linear spring definition in Abaqus (adapted from SIMULIA, 2012c)

5.1.3 Abaqus energy outputs

Since SBCs act as energy dissipation devices, the total energy output quantities from Abaqus were useful for the interpretation of results. The analysis performed in this section meant that the specific energy output variables listed in Table 5.2 were relevant. The absolute energy formulation for structures subjected to seismicity that was discussed in Section 2 is recalled here. Equation 2.1 on page 13 describes the way in which earthquake input energy is converted in the structure. Table 5.2 shows that the variables from Abaqus corresponds to the variables in the absolute energy formulation. The results from certain variables of the analysis were used to ensure that the energy dissipated through friction in one bay was equal to the strain energy of the other bay. This was the basis on which the non-linear spring model was confirmed.

Table 5.2: Variable comparison between Abaqus and the Absolute Energy Formulation

Abaqus (SIMULIA, 2012a)		
ALLFD	-	Total energy dissipated through frictional effects
ALLSE	-	Recoverable strain energy
ALLKE	-	Kinetic energy
ALLVD	-	Energy dissipated by viscous effects
ALLWK	-	External work
Absolute energy formulation		
E_μ	-	Energy dissipation through hysteretic action
E_S	-	Elastic strain energy
E_K	-	Absolute kinetic energy
E_ζ	-	Energy dissipation through viscous damping
E_I	-	Absolute earthquake input energy

5.1.4 Models

The single braced bay of a diagonally-braced frame that was discussed in Section 4.3.2 was used for the model incorporating the 3D solid elements. The connections in the frame were pinned

and the gusset plates were assumed to be fully fixed. The bolt pre-load was increased to 65 kN which resulted in a slip-force of 140 kN. Please refer to Section 4.3.2 for a detailed explanation of this model.

The bay with the non-linear spring retained only the beam and columns of the previous model. The SBC and brace were substituted by a non-linear spring. Figure 5.2 shows the rendered beam sections and a visualisation of the spring.

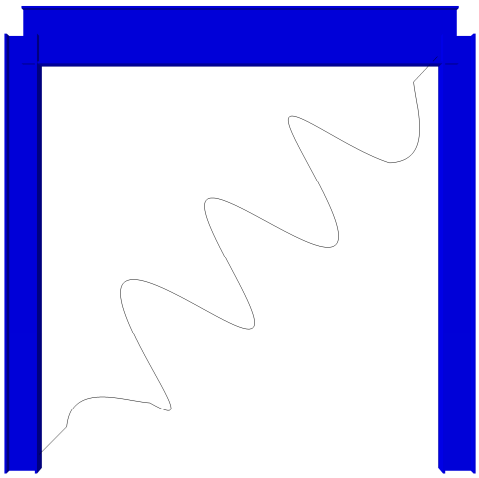

Figure 5.2: Braced bay with beam, columns and non-linear spring shown

The force-displacement relationship of the non-linear spring in the model is shown in Figure 5.3. The plateau after the initial stiffness corresponds to the slip-force of 140 kN. The slot-length is 65 mm on both sides, with the bolts initially positioned in the middle of the slot. In this case the tensile and compressive capacity was limited by the resistance of the bolts in shear and the critical buckling load of the brace, respectively. Please note that this value of 525 kN for three M20 Class 8.8 bolts in double shear is a resistance value obtained from the Red Book (SAISC, 2013). Material variability and partial factors mean that the capacity is often significantly higher than this resistance. This is referred to as overstrength and is an important factor in seismic capacity design. Overstrength that has not been taken into consideration may cause other failure modes to govern. More discussion on this matter will follow in Section 5.2. The resistance value was accepted for this case.

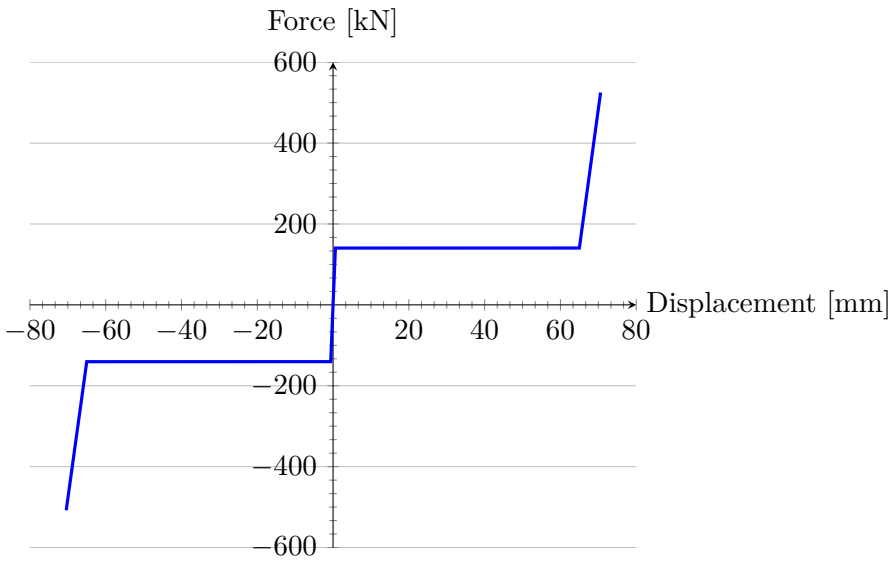

Figure 5.3: Force-displacement relationship used for non-linear spring definition

The force-displacement relationship of the non-linear spring resulted in equivalent behaviour to the 3D solid element connection and brace member under applied displacements. Since the use of non-linear springs was intended to replace the 3D solid elements in the global analysis, it was imperative that the energy dissipated under dynamic conditions by the two approaches was equivalent. An implicit dynamic analysis was therefore performed to compare the two frames. Structural damping equal to 5% of critical damping was assumed for the models (Craig et al., 2006). Two inertia point masses were also defined at the positions shown in Figure 5.4. The masses represent the seismic mass of the adjacent frames and were 20.1×10^3 kg and 42.8×10^3 kg, respectively. The masses were introduced because the lateral movements of the adjacent unbraced frames are restrained by the lateral bracing system. Further explanation of the model on which these values are based is provided in Section 5.2.

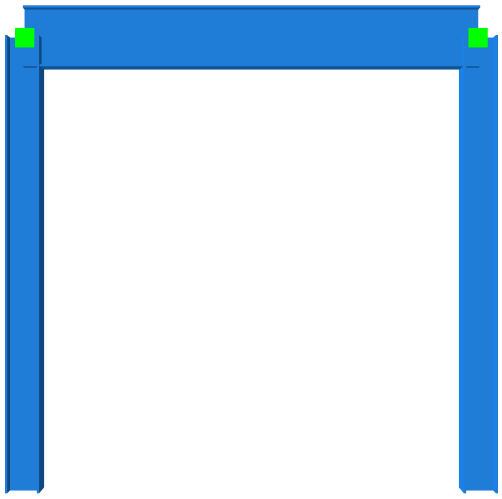

Figure 5.4: Positions of the point masses in the frame

5.1.5 Analysis

The displacement control used in the analysis is shown in Figure 5.5. It consisted of three sinusoidal cycles ramping up in amplitude towards the 90 mm displacement as used in Section 4.3.3. The three frequencies were obtained from the tests by Loo et al. (2014), which were based on the original frequencies of Grigorian et al. (1993) in their study on the use of SBCs in braced frames. The frequencies decreased from 1 Hz to 0.5 Hz to 0.25 Hz in the successive cycles. The dynamic analysis provided energy results which were used to compare the two modelling approaches.

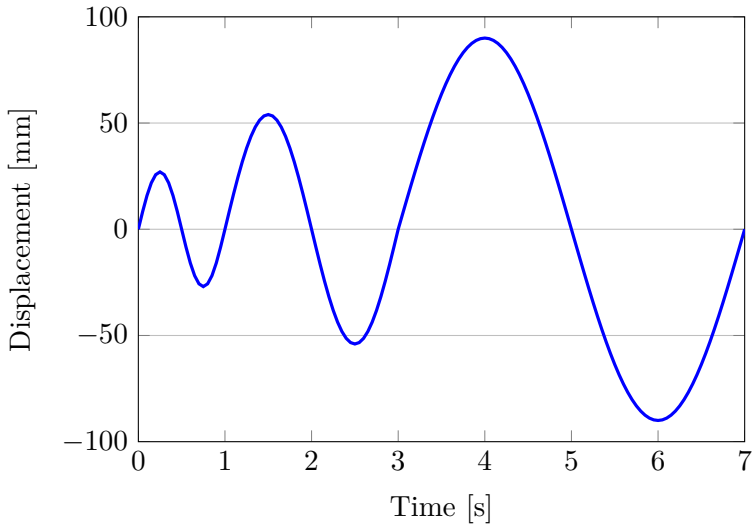

Figure 5.5: Displacement schedule for dynamic analysis

5.1.6 Results and discussion

The ALLFD output variable from Abaqus yields the total energy dissipated through frictional effects from time zero to a specific point in the analysis. The way in which Abaqus calculates this, is by continuously summing the frictional dissipation in each increment throughout the analysis. The frictional dissipation therefore increases irrespective of directional changes. The ALLSE output variable signifies the recoverable strain energy. With a change in direction at the maximum displacement of a particular cycle, the ALLSE diminishes until it reaches zero when the non-linear spring returns to its undeformed length. This meant that ALLFD from the 3D solid element model and ALLSE from the non-linear spring model could not be compared outright. The energy dissipated by friction therefore needed to be thought of as being “stored” when travelling towards maximum displacement and “released” again when returning in the opposite direction. This allowed for comparison between the two measures. It was achieved by using the energy total provided by Abaqus up until a change in direction after which the frictional dissipation in the subsequent intervals was subtracted from the maximum at the point of maximum displacement. The results, shown in Figure 5.6, demonstrate that the energy dissipated through friction corresponds well to the energy dissipated as strain in the non-linear spring. This confirms that the non-linear springs models the dissipative behaviour of the 3D solid elements and brace member suitably.

In addition, the analysis running time reduces from 2 hours to less than 10 minutes when transitioning from the solid element model to the non-linear spring element model. The non-linear springs were therefore accepted as being sufficiently accurate for use in the global analysis.

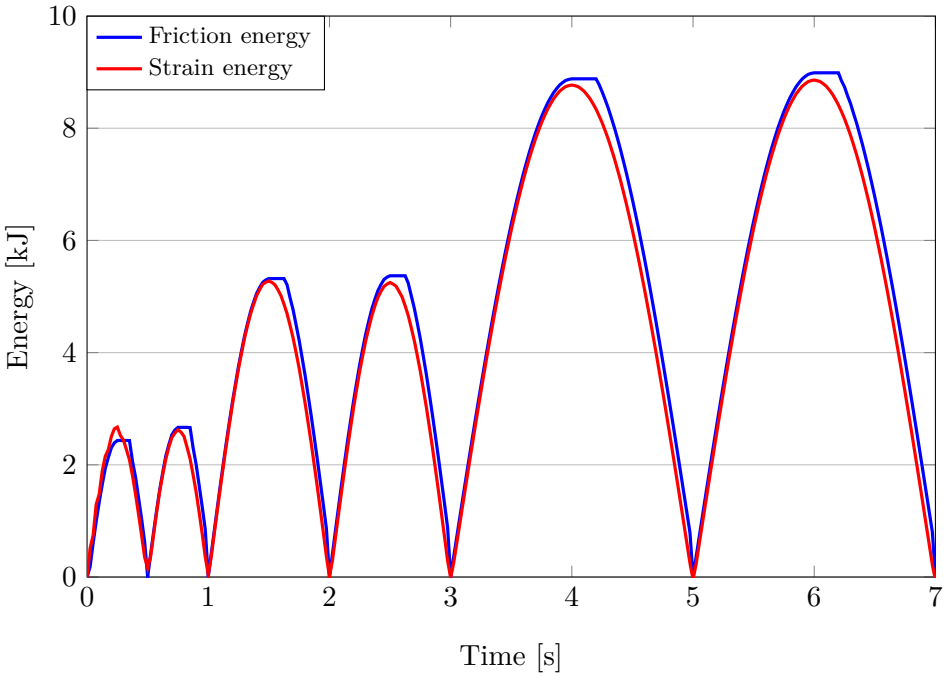

Figure 5.6: Energy dissipation results comparison from dynamic analyses

5.2 Global analysis

A non-linear, dynamic analysis was performed on a multi-storey building model where SBCs were used to connect the bracing elements. This was conducted by modelling the lateral bracing system as non-linear springs and investigating the response to seismic ground accelerations. Recorded earthquake acceleration-time histories were used to model ground motion in the analysis.

Non-linear dynamic analysis is a tool that can be used to investigate the actual behaviour of structures subjected to seismic loading. If used correctly, non-linear analysis can be used to determine realistic behaviour of structures subjected to ground accelerations (Deierlein et al., 2010). In this section, non-linear analysis was necessary to investigate the effect of the non-linear, force-dependent behaviour of the SBCs incorporated in the braces.

The results from the analysis were used to illustrate the beneficial effect that the introduction of the SBCs have on the response of the structure. The SBCs provide increased energy dissipation capability and more structural flexibility compared to conventional bracing connections. This increases the likelihood that braces would remain undamaged during an earthquake.

5.2.1 Design

As mentioned in Chapter 1, a published design procedure for lateral braces with SBCs is not available at present. The two most recognised approaches from the American steel code, AISC 341-10, used for seismic design of braced steel frames are: *Ordinary Concentrically Braced Frames* (OCBF) and *Special Concentrically Braced Frames* (SCBF)(AISC, 2010).

The OCBF is the approach adopted in Annex D of SANS 10160-4 (SABS, 2011b). OCBF uses a behaviour factor of three in the design and does not require any specific detailing for ductility. The behaviour factor is used to determine the design response spectrum for seismic loading. This is performed by dividing the elastic response spectrum by the behaviour factor which accounts for energy dissipation in the structure (Borzi et al., 2000). Therefore, the higher the behaviour factor, the more energy dissipation is believed to take place in the structure and the lower the forces from the equivalent lateral force procedure are. Ductility is the inelastic deformation capacity of a structure (Engelhardt, 2009). Annex D of SANS 10160-4 states that OCBFs "make use of low levels of energy dissipation which result from the inherent ductility of steel structures". This "inherent ductility" can be attributed to the reserve capacity that OCBFs possess (Fahnestock et al., 2014). Reserve capacity is provided amongst others by: flexural capacity of gravity connections that are assumed to be pinned, fixity of column bases and post-buckling strength of braces. These factors mean that OCBFs often have reserve capacities of 2.5 to 3 times their design strength (Clifton, 2015).

The SCBF design approach, which is primarily used in areas of high seismicity, utilises higher behaviour factors. This results in lower forces from the equivalent lateral force procedure, but also leads to higher inelastic drift demands. SCBF must therefore be detailed specifically for ductility, which results in more involved detailing practices.

For a braced frame incorporating SBCs, the OCBF design approach would result in energy dissipation in the connections resulting in inelastic deformations of the connections. This is unsuitable since damage to the SBC would reduce frictional energy dissipation in subsequent cycles of loading. In addition, the behaviour factor of three does not reflect the substantial energy dissipation capabilities of the SBC.

It is clear that the SCBF approach or a similar alternative would need to be employed for the design of braced frames with SBCs. The SCBF approach generally identifies the brace members as the dissipative zones. The braces buckle and yield while lateral resistance is maintained (Sabelli et al., 2013). Connections to the braces are designed to the expected capacity of brace members. This principle is referred to as "capacity design" and the corresponding detailing requirements are deemed to be satisfied.

The structure that was designed and considered for the analysis was a four-storey, diagonally braced steel frame office building. A schematic view of the planar frame that was considered is shown in Figure 5.7. More details on the structural arrangement can be found in Appendix D. Seismic design was negated for the model. This was done because of the absence of a design procedure for SBCs in brace members. Additionally, the requirements of AISC 341-10 for ductile

detailing of SCBFs require experience with seismic detailing which was beyond the scope of this study. Therefore, wind loading was used to size the braces and the slip-load was accepted as being above the wind load. Details regarding the design of the diagonally-braced frame are provided in Appendix E.

The building is not based on the design of an existing office complex nor is it intended to represent a "typical" mid-rise office building. The building is intended to illustrate the beneficial role of SBC-braces irrespective of building typology or structural layout in a relatively simple manner. The building that was designed is therefore of lesser importance and emphasis is placed on the results of the analysis.

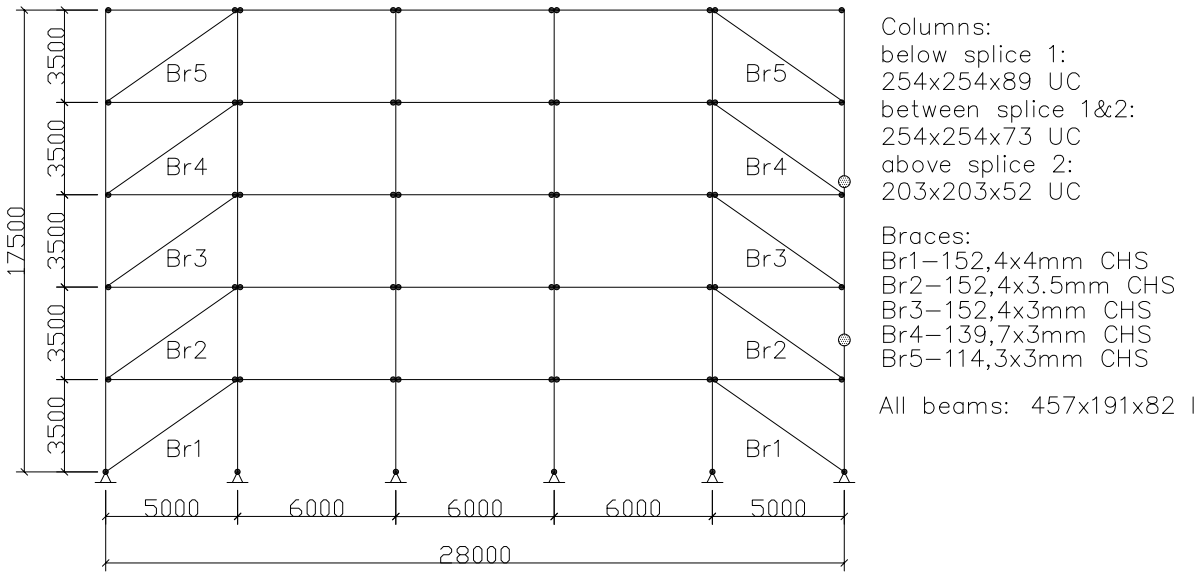

Figure 5.7: Schematic view of planar frame used for global analysis

5.2.2 Model

Figure 5.8 shows the model used for the dynamic analysis with the rendered sections of the beam elements for illustrative purposes. This model represents a planar braced frame, as located around the perimeter of the building. All beam-column connections were modelled as pinned connections. The column bases were fixed in translation only. Structural damping equal to 5% of critical damping was accepted for the model (Deierlein et al., 2010).

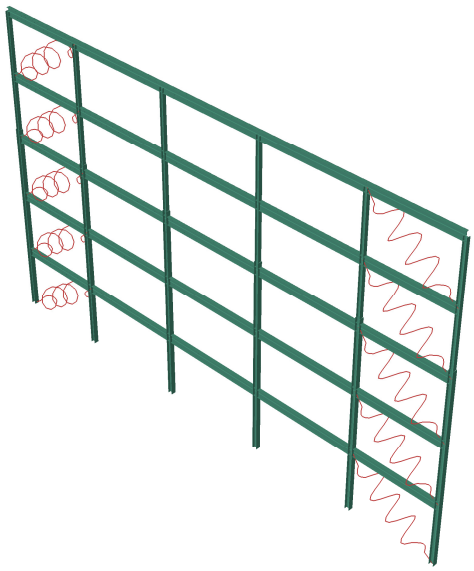

Figure 5.8: Abaqus model of the diagonally-braced frame for analysis

The non-linear springs represent the diagonal braces and their associated SBCs. It was assumed that the SBCs and other bracing connections would allow for the full development of the inelastic tensile and compressive strength of the braces. The non-linear springs were assigned the buckling and ultimate tensile capacities of the braces in compression and tension, respectively. The values indicating the force behaviour of the various non-linear springs are listed in Table 5.3.

Table 5.3: Ultimate force values assigned to the non-linear springs

Position and section	Slip-force (kN)	Buckling load (kN)	Tensile capacity (kN)
Br1 - 152.4x4mm CHS	187	272	1042
Br2 - 152.4x3.5mm CHS	168	241	918
Br3 - 152.4x3mm CHS	152	208	790
Br4 - 139.7x3mm CHS	109	160	722
Br5 - 114.3x3mm CHS	65	86	588

In order to illustrate the benefits that the inclusion of the SBCs have on the bracing members, five different conditions were modelled for the analysis. These conditions are listed in Table 5.4. The conditions range from “no-slip”, which simulates the slip possible with a normal construction tolerance on bolt holes, to 75 mm of slip-length in both directions, or 150 mm absolute slip.

Table 5.4: Slip-lengths investigated in the analysis

Condition	Absolute Slip Length
No-Slip	2 mm
1	10 mm
2	50 mm
3	100 mm
4	150 mm

Two braced perimeter frames are present in each direction of the structure. This means that half of the seismic mass of the structure in a particular direction must be resisted by one of the braced frames. As in Section 5.1.4, point masses were used to represent the seismic mass of the adjacent frames at the various nodes of the model. The calculations for the seismic masses and their nodal positions are provided in Appendix F.

The model and accompanying non-linear analysis is not aimed to be a full seismic analysis of a multi-storey building. The model should therefore not be interpreted as a model on the basis of which seismic design can be performed.

5.2.3 Analysis

An implicit dynamic analysis of the model was performed. The translational degree of freedom for the column bases in the lateral direction was released and ground accelerations were applied instead. The earthquake time histories that were used are listed in Table 5.5. The earthquakes had PGAs ranging from 0.05 g to 0.2 g. Relatively small PGAs were used because seismic design was disregarded which left the braces particularly vulnerable. The acceleration-time and displacement-time records of the earthquakes are provided in Appendix G.

Table 5.5: Earthquake records considered for the dynamic analysis

Name	Year	Location	Station no.	PGA
Anza	1980	USA	5049	0.05 g
Imperial Valley	1979	USA	286	0.1 g
Coyote Lake	1979	USA	57383	0.15 g
Loma Prieta	1989	USA	58222	0.2 g

For implicit dynamic analysis, the maximum allowable time increment size for the integration scheme must be selected to ensure accurate results (SIMULIA, 2012a). Using maximum increments less than a tenth of the period of the typical modes of response of the structure is recommended for implicit dynamic analysis (SIMULIA, 2012a). This is shown by Equation 5.1 where Δt is the increment size and T is the period. Consequently, a frequency analysis was performed. The fundamental sway mode of the structure had a frequency of 0.67 Hz and a period of 1.5 s. This ensured that the maximum time increments of 0.025 s that were prescribed for the analysis satisfied the criterion.

$$\Delta t < T/10 \tag{5.1}$$

5.2.4 Results and Discussion

The results from the analyses over the range of sliding lengths are discussed for each earthquake considered. The force response of the diagonal braces in the left side bays of the frame was

investigated. The lateral drift response and base shear forces were also examined.

Anza (0.05 g)

The structure responded elastically to the Anza earthquake. Slip was limited to the top level braces. These braces experienced only slight sliding behaviour and did not come close to reaching their buckling load in compression. The drift response and base shear results also suggest that for this particular earthquake, the introduction of SBCs would not have any beneficial effect on the response of the structure. Plots of relative displacements at the apex can be found in Appendix H.

Imperial Valley (0.1 g)

For this earthquake record, together with the "no-sliding" condition, the top level brace exceeded the buckling load a number of times throughout the analysis. Please note that it is appreciated that if a brace had buckled, its compressive capacity would be reduced in subsequent cycles to its post-buckling strength. For the relatively crude structural model used here however, this was not accounted for. Advanced non-linear models may allow for this through element removal or alternative advanced techniques during analysis. Nonetheless, when discussing the results, the number of times that the critical buckling load is reached will be mentioned throughout. Table 5.6 shows that as the sliding length increases, the number of times buckling load is reached in the top level of braces reduces to zero at a sliding length of 50 mm.

Table 5.6: Number of times buckling load is reached in top level braces

Sliding condition	No.
No-slip	7
10 mm	6
50 mm	0

The base shear force results exhibit negligible positive effects when transitioning from the "no-slip" braces to sliding lengths longer than 10 mm. The short 10 mm sliding length resulted in higher base shear forces than the "no-slip" condition. This indicates that the use of inappropriate slip-lengths could adversely affect certain structural members.

Coyote Lake (0.15 g)

Table 5.7 shows that the high stiffness of the structure with the "no-sliding" and 10 mm absolute sliding causes the buckling load in the braces at all levels to be reached numerous times. With an increase in sliding length, the damage decreases. Table 5.7 shows that the buckling load is reached once in the top and bottom level braces for the 50 mm absolute sliding condition, while for 100 mm only the top level braces reach buckling load three times. This occurs because of the effect of the sliding-length on the structural response. The frames with the 50 mm and

100 mm sliding lengths are therefore influenced differently by the ground acceleration at particular stages in the earthquake ground motion history. At 150 mm absolute sliding, all the braces respond elastically. In this structure, which is under-designed for a 0.15 g earthquake, the damage reduction capability of the SBC is clear.

Table 5.7: Number of times buckling load is reached in braces for the Coyote Lake earthquake

Sliding condition	Top	Level 3	Level 2	Level 1	Bottom
No-slip	36	22	16	9	11
10 mm	23	14	7	7	9
50 mm	1	0	0	0	1
100 mm	3	0	0	0	0
150 mm	0	0	0	0	0

The lateral drift results confirm the "softening" of the structure by the inclusion of the SBCs. Figure 5.9 shows the relative displacement at the apex of the structure for "no-slip", 50 mm and 100 mm absolute sliding lengths. The number of displacement cycles through which the apex of the structure travels decreases with increased slip-length. Figure 5.9 shows that the motion becomes steadier with increased sliding length.

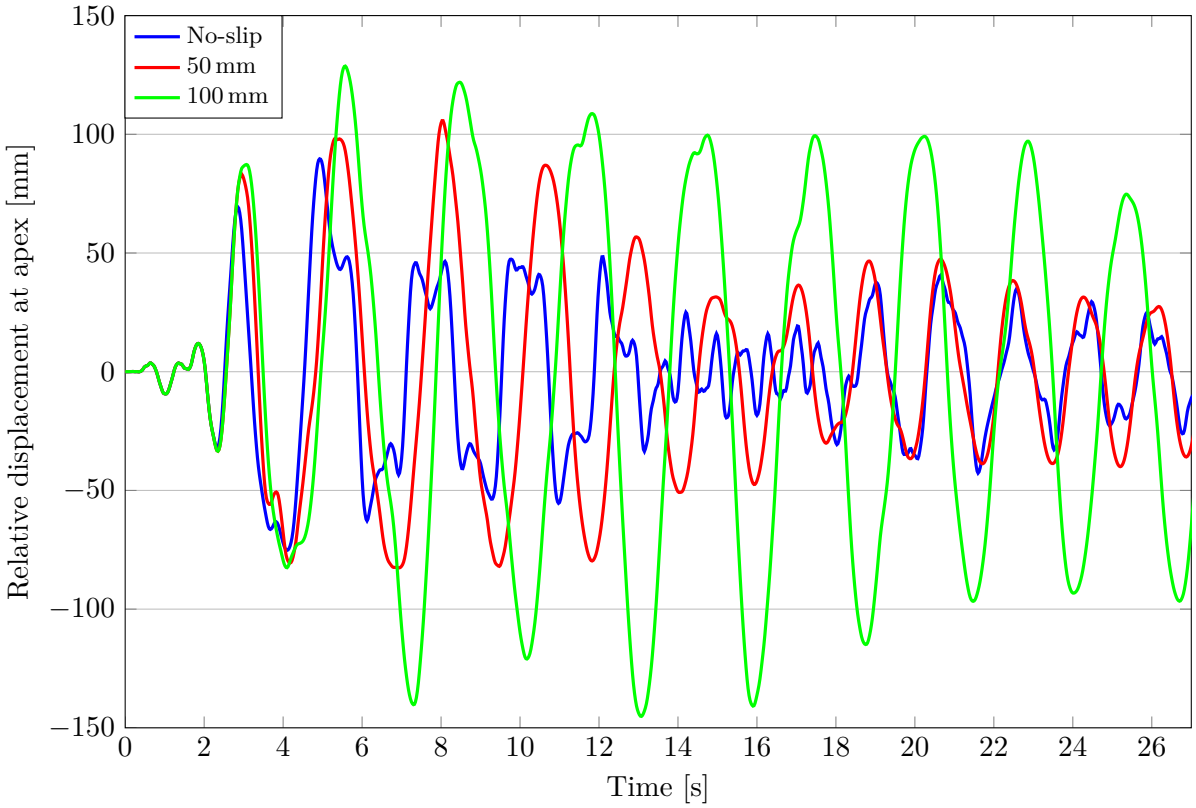

Figure 5.9: Relative displacements at apex for the Coyote Lake earthquake

The base shear results for Coyote Lake are listed in Table 5.8. As the sliding length increases, the stiff response of the structure decreases and it "attracts" less base shear than the "no-slip"

condition. Small increases in base shear are present from "no-slip" to certain sliding lengths. These increases are due to the differences in the structural response of the frame to the earthquake ground accelerations depending on the sliding condition. The difference in response means that depending on the sliding condition, the oscillations of the frame may be in or out of phase with the ground motion, which affects the peak base shear. This is demonstrated in Figure 5.9 where the peak relative displacements with differing sliding conditions do not occur in the same positions. For slip-lengths longer than 50 mm, there is a reduction in base shear compared to the no-slip condition.

Table 5.8: Base shear force results for the Coyote Lake earthquake

Sliding condition	Maximum (kN)	% Reduction	Minimum (kN)	% Reduction
No-slip	473	-	-466	-
10 mm	455	3.8	-489	-4.9
50 mm	484	-2.3	-419	10.1
100 mm	434	8.2	-426	8.6
150 mm	429	9.3	-440	5.6

Loma Prieta (0.2 g)

The results from the Loma Prieta ground motion confirm that the structure is not designed for a PGA 0.2 g earthquake. Table 5.9 shows the number of times the brace buckling load was reached during the ground accelerations. Structural collapse is likely even with sliding lengths of up to 100 mm. It can be argued that with 150 mm sliding length, the building might not have collapsed, albeit with significant structural damage. The results once again indicate a relationship between the decrease in the number of times the buckling load is reached and the magnitude of sliding that is permitted in the SBCs.

Table 5.9: Number of times buckling load is reached in braces for the Loma Prieta earthquake

Sliding condition	Top	Level 3	Level 2	Level 1	Bottom
No-slip	46	33	25	29	14
10 mm	41	29	27	22	18
50 mm	13	3	9	11	5
100 mm	9	5	4	2	2
150 mm	3	2	1	0	1

The relative displacement at the apex of the structure for the no-slip, 50 mm and 150 mm absolute sliding conditions is shown in Figure 5.10. Although it is unlikely that the structure could withstand the earthquake, the increased sliding length still exhibits the softening effect that decreases the number of cycles that the apex travels through. The maximum relative displacement of the apex during the "no-sliding" condition is reached through inelastic deformation of the

braces while the maximum relative displacement for 150 mm absolute sliding is reached primarily through sliding in the SBCs.

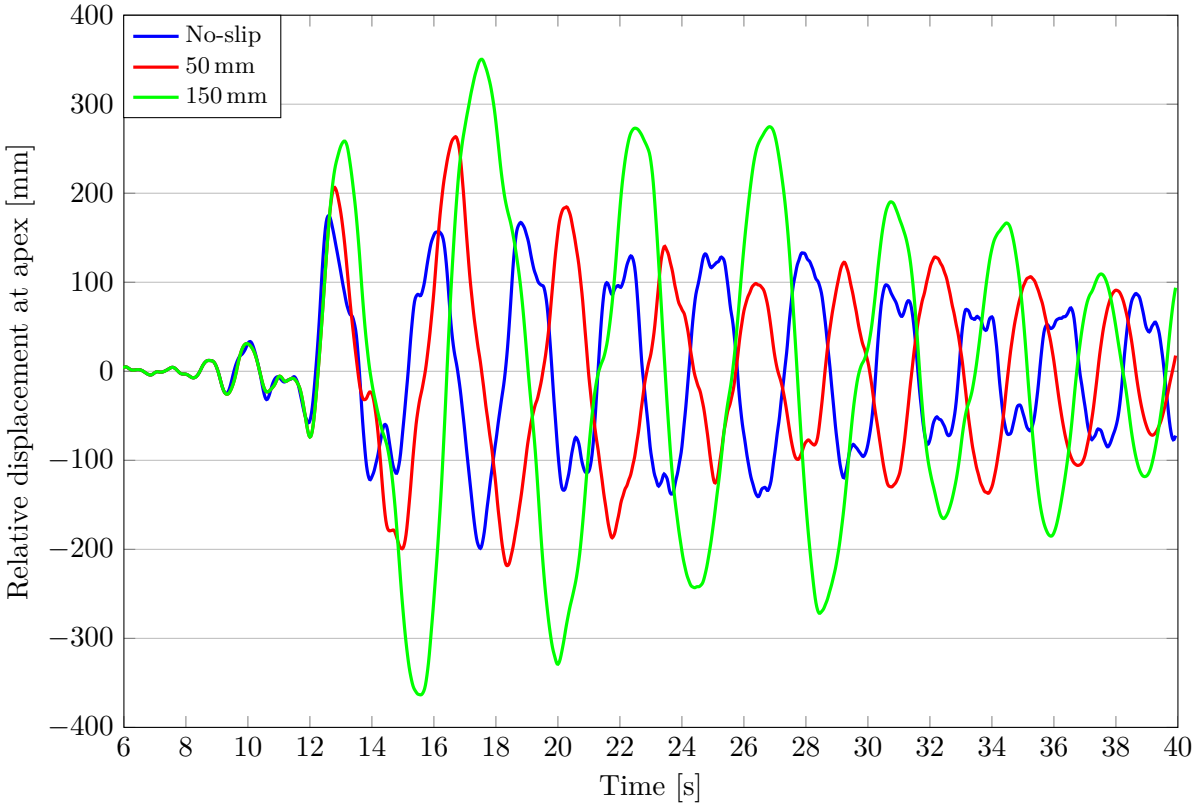

Figure 5.10: Relative displacements at apex for the Loma Prieta earthquake

The base shear results for Loma Prieta are listed in Table 5.10. Table 5.10 shows that the reduction in base shear is greater than 20% when sliding lengths of 50 mm or longer are used. Once more, a slight increase in base shear is observed between 50 mm and 100 mm due to the difference in the seismic response of the frames with different sliding conditions. The base shear results however indicate a reduction in the base shear compared to the no-slip condition for all sliding conditions. Irrespective of the possible collapse of the structure for this earthquake, a decrease in base shear provides a more economic design.

Table 5.10: Base shear force results for the Loma Prieta earthquake

Sliding condition	Maximum (kN)	% Reduction	Minimum (kN)	% Reduction
No-slip	736	-	-800	-
10 mm	707	3.9	-762	4.8
50 mm	563	23.5	-574	28.3
100 mm	585	20.5	-589	26.4
150 mm	587	20.2	-586	26.8

The results from the analysis indicate that the introduction of the SBCs in the braces are beneficial in terms of brace preservation, lateral drift and base shear forces. Where a demand for greater slip-lengths was present, the SBCs performed well at preserving brace members by

softening the response of the structure. In an approximate sense, a particular earthquake will demand a relatively fixed amount of drift from a structure, regardless of its stiffness (Engelhardt, 2009). Consequently, in stiffer structures the earthquake will achieve this enhanced drift through inelastic deformation of the braces or connections. The softening of the braced frame by the SBCs means that enhanced drift capacity can be provided by slip in the SBC, which preserves the braces. The results were similar to what Butterworth (2000) described as the slot-length controlling the ductility of the structure.

The base shear forces from the analyses for the three earthquakes with PGA of 0.1 g to 0.2 g are listed in Table 5.11. These base shear forces were averaged over the sliding lengths 10 mm to 150 mm for each earthquake. The design base shear force per braced frame calculated from SANS 10160-4 for behaviour factors of three and greater are shown in Table 5.12. Note that the calculations were performed considering a PGA of 0.1 g. This illustrates that the base shears from the equivalent lateral force procedure are in the same order as those from the dynamic analysis results. If the appropriate ductile detailing procedures are developed and followed, and the necessary advances are made in the understanding of long-term SBC behaviour, SBCs can be immensely beneficial in braced frames subjected to seismicity.

Table 5.11: Abaqus results for the base shear with earthquakes considered

Earthquake	Base shear
Imperial valley (0.1g)	357 kN
Coyote Lake (0.15g)	447 kN
Loma Prieta (0.2g)	619 kN

Table 5.12: Base shears according to SANS 10160-4 for 0.1 g

Behaviour factor	Base shear
3	876
4	657
5	525

The use of non-linear springs resulted in analysis times of under one hour. If failure of the brace and SBC can be assumed to be governed by the capacity of the brace member, this modelling approach is suitable. The non-linear spring can be used successfully in advanced models for non-linear time history analysis with recorded ground motion histories.

Chapter 6

Conclusion

Seismic design code provisions have prevented the collapse of steel structures during past earthquakes. Collapse prevention has however come at the expense of extensive structural damage, as viewed in the 1994 Northridge earthquake (Tremblay et al., 1995). The predominantly brittle failures of structural members and connections in steel framed buildings motivated extensive research into provisions that achieve a ductile seismic response.

The resulting code provisions for high seismic regions require structures to be capacity designed, which involves specific detailing for ductility. By specifying the position of ductile zones in the structure, designers aim to restrict the inelastic deformations to these zones and in this manner the brittle regions are assumed to remain free from damage. In Special Concentrically Braced Frames, the ductile zones are generally the braced bays where the braces buckle in compression and yield in tension.

Code provisions for moderate seismic regions, such as Annex D of SANS 10160-4, often do not require specific detailing for ductility. Annex D of SANS 10160-4 states that "low levels of energy dissipation" are provided by the "inherent ductility of steel structures". This "inherent ductility" in Ordinary Concentrically Braced Frames is associated with inelastic deformations of the connections and permanent damage to the braces following an earthquake.

This indicates that the current code provisions, both in high and moderate seismic regions, result in structural damage after an earthquake. This was viewed in the 2011 Christchurch New Zealand earthquake, where the level of damage was deemed unacceptable (MacRae, 2015a). There is a clear necessity for innovative design solutions that result in decreased structural damage due to earthquakes. Numerous devices have been developed that offer additional earthquake energy dissipation through viscous or hysteretic action. The implementation of energy dissipation devices for general applications has been inhibited by their complexity and cost (Grigorian et al., 1993). A simple and economic method of providing additional energy dissipation is through the friction between sliding plates in a Slotted Bolted Connection.

The implementation of Slotted Bolted Connections in the braces of Concentrically Braced Frames was proposed. A design procedure for Slotted Bolted Connection-braces has however not been

published. This is due to the limited research which has been conducted on the subject. The suitability of Slotted Bolted Connections for energy dissipation was the focus of previous research. The concerns included the maintenance of bolt pre-load and stable friction during sliding, as well as the simplification for enhanced constructibility. Literature indicated that an assessment of the way that the detailing and setup of the Slotted Bolted Connection affects its performance was required. The first objective of the study was to calibrate a Finite Element model of the Slotted Bolted Connection using existing experimental results. This Finite Element model was then used to investigate in particular; the effect of bolt-impact with the slot-ends on the performance, the differences between the Symmetric and the Asymmetric variants of the Slotted Bolted Connection and the interaction between the Slotted Bolted Connection and the brace in a braced bay. Following these investigations, a computationally efficient modelling technique was presented that accurately captured the energy dissipation characteristics of the Slotted Bolted Connection. A non-linear dynamic analysis of a multi-storey diagonally braced frame was performed to determine the effect of the Slotted Bolted Connection-braces on the structural response.

By investigating the various topics, the manner in which the detailing and setup of the Slotted Bolted Connection affects its performance as well as the effect of the Slotted Bolted Connection on a global structural level could be clarified. This will aid future research for the development of a design procedure for Slotted Bolted Connections in Concentrically Braced Frames.

The following paragraphs discuss the conclusion of the study. The implications of the findings on existing knowledge as well as on the application of Slotted Bolted Connections are discussed. Recommendations for future studies are provided with a brief description of each. Lastly, the study is concluded.

The results from the Finite Element model of the Slotted Bolted Connection in Chapter 3 compared favourably to the experimental results of Loo et al. (2014). The model was expanded to investigate the various topics. The bolt-impact analysis of Section 4.1 indicated that there was a significant increase in the stiffness of the connection when the bolt-shank made contact with the slot-end. The results from the analysis indicated that high stresses were present in the slotted-plate and the bolt-shank during bolt-impact which resulted in bearing deformation of the slotted-plate. Lukkunaprasit et al. (2004) noticed a decrease in the friction of the Slotted Bolted Connection during the successive cycles of bolt-impact in their experimental tests. The decrease in friction was due to the permanent deformation of the bolts which was arguably caused by using relatively light bolts compared to the thick plates of the Slotted Bolted Connection of Lukkunaprasit et al. (2004). The results from Section 4.1 however indicated that bearing deformations were largely concentrated in the slotted-plate and not the bolt. The investigation of Section 4.1 showed that a preferable layout of the Slotted Bolted Connection contains multiple bolts in a transverse line. This ensures that the combined strength of the bolts can resist the shear force and avoid unacceptable brittle shear-failure of the bolts during bolt-impact. In addition, when using multiple bolts in a transverse line, the preferred ductile failure mode of bearing deformation can take place at more areas in the Slotted Bolted Connection during severe bolt-impact.

In Section 4.2, the differences between the Symmetric and Asymmetric variants of the Slotted Bolted Connection were investigated. The results indicated minimal hysteretic differences during normal sliding for the two layouts. The bolt-shanks of the Asymmetric Slotted Bolted Connection makes contact with the outer- and cap-plate during normal sliding. Although the results showed increased stresses in the Asymmetric connection's bolts compared to the Symmetric connection, the stresses were not concerning from a strength perspective. When the effect of bolt-impact on the Symmetric and Asymmetric connections was examined, the two shear planes of the Symmetric connection were clearly preferable to the single shear plane of the Asymmetric connection. The results indicated high stresses throughout the bolt-shank of the Asymmetric connection in comparison to the bolt-shank of the Symmetric connection, which leads to a lower strength of the Asymmetric Slotted Bolted Connection. The research of Golondrino et al. (2014) focussed on the Asymmetric as opposed to the Symmetric Slotted Bolted Connection for use in braces. The results from Section 4.2 indicated that the performance of the Symmetric Slotted Bolted Connection was superior to that of the Asymmetric connection. The inclination of Golondrino et al. (2014) toward the Asymmetric connection may have been due to the availability of test information from earlier research performed on the Asymmetric connection in the Sliding Hinge Joint beam-column connection. While the results from Section 4.2 did not indicate problems during normal sliding for the Asymmetric connection, the stress variation in the bolt-shanks during successive cycles of sliding could affect the bolt pre-load. In addition, the eccentricity of the Asymmetric Slotted Bolted Connection could result in side-sway or sway-buckling of the gusset plate. The detailing and construction of the Asymmetric Slotted Bolted Connection is however simpler than the Symmetric connection due to the omission of one of the outer-plates and the use of a cap-plate instead.

The analysis of Section 4.3 investigated the possible interaction between the bolt-shanks and the sides of the slotted-hole during sliding of a Slotted Bolted Connection-brace. The investigation was motivated by the prevailing horizontal as opposed to vertical deflections of structures due to earthquakes. In experimental tests performed by Balendra et al. (2001), the short sliding-length meant that the effect of the interaction between the bolt-shanks and the slot-sides could not be established in their Slotted Bolted Connection-brace. The results of Section 4.3 indicated that the fixity condition at the brace-column connection away from the Slotted Bolted Connection governed the sliding behaviour. The sliding behaviour ranged from collinear sliding for a pinned condition, to non-collinear sliding with interaction between the bolts and the slot for a fixed condition. Although the interaction resulted in an increase of friction, it did not affect the performance of the Slotted Bolted Connection detrimentally. This was similar to what MacRae (2015b) found during ongoing tests of braced frames with Slotted Bolted Connections in New Zealand at the same time as this study.

The comparison between the energy outputs of the 3D solid elements and the non-linear springs in Section 5 ensured the suitability of the non-linear springs as a simplified modelling technique. In Section 5.2, a non-linear dynamic analysis of a multi-storey diagonally-braced frame was presented. The results from the analysis indicated that the Slotted Bolted Connections "soften" the seismic response of the building, which prevented damage in the braces and attracted less

base shear force during excitation. When the slot-length was sufficiently long for a particular ground motion record, the Slotted Bolted Connection-braces performed favourably to limit the damage to the braces. The results indicated that when the Slotted Bolted Connection-braces were used, the lateral drift demand of the earthquake could be satisfied by sliding in the connections as opposed to damage in the braces when conventional bolted connections are used.

Recommendations for future studies are:

- Bolt-impact testing: since insufficient experimental tests have been performed on the effect of bolt-impact on the Slotted Bolted Connection, more research is required. Future work should investigate whether the bolt-tension loss observed by Lukkunaprasit et al. (2004) is present in Slotted Bolted Connections that are suitably detailed for bolt-impact. An investigation must also be performed to determine the consequences of bolt-impact on the bolt pre-load and the spring washers.
- Long-term behaviour of the spring washers: it is necessary to ensure that the spring washers are able to retain their elasticity over long periods. This is required for the maintenance of bolt pre-load in the connections for lateral loads that do not initiate sliding as well as when seismic excitation necessitates the sliding of the Slotted Bolted Connections.
- Bolt pre-load: Loo et al. (2014) found that the use of a depth micrometer resulted in a significant increase in the accuracy of the bolt pre-load applied to the Slotted Bolted Connection. It is necessary to determine the preferred procedure for the bolt-tension application to ensure that the design friction is accurately achieved. Additionally, an investigation must be performed to determine the suitable level of stress in pre-loaded bolts that ensures sustained bolt pre-load.
- Full-scale testing: experimental testing of a bay with a Slotted Bolted Connection-brace must be performed to investigate the effect of the enhanced drift capability on the bolted beam-column connections. This study should consider the possible damage in the beam-column connections as well as the maximum viable slip-length for the braced bay.
- Non-linear seismic analysis: refined structural models should be used to investigate the effect of Slotted Bolted Connection-braces on the structural response in more depth. Such a model should also be used to determine the post-earthquake configuration of a structure with Slotted Bolted Connection-braces.

Slotted Bolted Connection-braces possess beneficial energy dissipation qualities and their use as an innovative low-damage seismic design solution to prevent brace damage in Concentrically Braced Frames is promising. The absence of a published design procedure and limited research performed to date meant that an assessment was required of the effect that the detailing and layout have on the performance of the Slotted Bolted Connection. The Slotted Bolted Connection should be suitably detailed for bolt-impact to ensure that the governing failure mode is ductile. In terms of layout and performance, the Symmetric Slotted Bolted Connection is preferable to the Asymmetric variant. The interaction between the bolt-shanks and slot-sides of the Slotted Bolted Connection in a braced bay do not affect its function detrimentally. The introduction of

Slotted Bolted Connection-braces has a "softening" effect on the seismic response of a structure that leads to diminished damage in the braces. These findings have clarified certain aspects that influence the performance of the Slotted Bolted Connection. This creates a basis for research to be performed towards the end objective of a design procedure for Slotted Bolted Connection-braces in Concentrically Braced Frames.

References

AISC (2010). *Seismic provisions for structural steel buildings (AISC 341-10) and commentary*. Chicago, IL: AISC.

ASME. *ASME DC*. URL: vibrationacoustics.asmedigitalcollection.asme.org.

Bachmann, Prof. Hugo (2003). *Seismic Conceptual Design of Buildings - Basic principles for engineers, architects, building owners, and authorities*. Ed. by Swiss Federal Office for Water and Geology.

Balendra, T., C.H. Yu, and F.L. Lee (2001). "An economical structural system for wind and earthquake loads". In: *Engineering Structures* 23, pp. 491–501.

Borzi, B. and A. Elnashai (2000). "Refined force reduction factors for seismic design". In: *Engineering Structures* 22, pp. 1244–1260.

Butterworth, John (2000). "Ductile concentrically braced frames using slotted bolted joints". In: *SESOC* 13.1, pp. 39–48.

Chen, W. and C. Scawthorn (2003). *Earthquake Engineering Handbook*. CRC Press.

Clifton, G.C. (2015). *Personal communication (email)*. 17th February.

Clifton, G.C., J.W. Butterworth, and J. Weber (1998). "Moment resisting steel framed seismic-resisting system with semi-rigid connections". In: *SESOC* 11.2.

Constantinou, M.C., T.T. Soong, and G.F. Dargush (1998). *Passive Energy Dissipation Systems for Structural Design and Retrofit*. Ed. by Jane Stoyle. Multridisciplinary Center for Earthquake Engineering Research.

Craig, R.R. and A.J. Kurdila (2006). *Fundamentals of Structural Dynamics*. 2nd ed. Wiley Press.

Datta, T.K. (2010). *Seismic Analysis of Structures*. Wiley.

Davet, G.P. (1997). *Using Belleville Springs To Maintain Bolt Preload*. Solon Manufacturing Company. 425 Center Street, Chardon, OH 44024.

Deierlein, G.G., A.M. Reinhorn, and M.R. Willford (2010). *Nonlinear Structural Analysis for Seismic Design*. Seismic Design Technical Brief 4. National Instituteof Standards and Technology.

DeMets, C., R.G. Gordon, and D.F. Argus (2010). "Geologically current plate motions". In: *Geophysics Journal International* 181, pp. 1–80.

DESY (2010). *Cross section of Earth's interior today*. Deutsches Elektronen-Synchrotron. URL: http://www.desy.de/information__services/press/press_releases/2013/pr_071113/index_eng.html.

Di Sarno, L. and A.S. Elnashai (2002). *Seismic Retrofiiting of Steel and Composite Building Structures*. Mid-America Earthquake Center.

Di Sarno, L. and A.S. Elnashai (2005). "Innovative Strategies for Seismic Retrofiiting of Steel and Composite Structures". In: *Progressive Structural Engineering Materials* 7, pp. 115–135.

Ellsworth, W.L. (1991). *The San Andreas Fault System, California*. URL: `http://www.johnmartin.com/earthquakes/eqsafs/safs_693.htm`.

Engelhardt, M. (2009). "An Introduction to Earthquake Engineering and Seismic Codes - Part 1: Ductility". In: *NASCC Steel Conference*.

ESDEP-WG17. *ESDEP WG17: Seismic Design*. URL: `http://www.fgg.uni-lj.si/~/pmoze/ESDEP/master/wg17/l0500.htm#SEC_3`.

Fahnestock, L.A. et al. (2014). "Reserve capacity and implications for seismic collapse prevention for low-ductility braced frames in moderate seismic regions". In: *NASCC Steel Conference*.

Geoscience, South African Council (2012). *Historical Earthquakes*. URL: `http://www.geoscience.org.za/index.php/component/content/article?id=1612:historical-earthquakes`.

Golondrino, J.C., R. Xie, G. MacRae, G. Chase G. anf Rodgers, and C. Clifton (2014). "Low damage braces using Asymmetrical Friction Connections (AFC)". In: *NZSEE Conference 2014*.

Grigorian, C. E., Yang T. S., and Popov E. P. (1993). "Slotted bolted connection energy dissipaters". In: *Earthquake Spectra* 9.3.

Hamburger, R.O., H. Krawinkler, J.O. Malley, and S.M. Adan (2009). *Seismic Design of Steel Special Moment Frames*. NEHRP Seismic Design Technical Brief 2. National Instituteof Standards and Technology.

Hartnady, C.J.H. (2003). *Cape Town Earthquakes: Review of the Historical Record*. Unpublished.

Hibbeler, R.C. (2008). *Mechanics of Materials*. 8th ed. Prentice Hall.

Holicky, M. (2009). *Reliability Analysis for Structural Design*. 1st. SUN Media Stellenbosch.

Khoo, H.H., G. Clifton, J. Butterworth, G. MacRae, and G. Ferguson (2012). "Influence of steel shim hardness on the Sliding Hinge Joiny performance". In: *Journal of Constructional Steel Research* 72, pp. 119–129.

Kijko, A., J.P. Retief, and G. Graham (2002). "Seismic Hazard and Risk Assessment for Tulbagh, South Africa: Part 1 - Assessment of Seismic Hazard". In: *Natural Hazards* 26, pp. 175–201.

Latour, M., V. Piluso, and G. Rizzano (2014). "Experimental analysis on friction materials for supplemental damping devices". In: *Construction and Building Materials* 65, pp. 159–176.

Law, S.S., Z.M. Wu, and S.L. Chan (2006). "Analytical model of a slotted bolted connection element and its behaviour under dynamic load". In: *Sound and Vibration* 292, pp. 777–787.

Lee, C., Y. Ju, C. Yoo, J. Ryu, and S. Kim (2013). "Frictional Behaviour of Low-Steel Composite Material on Milled Steel Surface". In: *International COnference on Fracture and Strength of Solids*.

Lee, S. et al. (2008). "Design of a Bracing-Friction Damper System for Seismic Retrofitting". In: *Smart Structures and Systems* 4.5, pp. 685–696.

Loo, W.Y., P. Quenneville, and N. Chouw (2014). "A new type of symmetric slip-friction connector". In: *Journal of Constructional Steel Research* 94, pp. 11–22.

Lukkunaprasit, P., A. Wanitkorkil, and A. Filiatrault (2004). "Performance Deterioration of Slotted-Bolted Connection Due to Bolt Impact and Remedy by Retrainers". In: *13th World Conference on Earthquake Engineering*.

MacRae, G. (2015a). "Better structures". In: *Structural Engineering Frontiers Conference*.

— (2015b). *Personal communication (email)*. 11th February.

McClamroch, N.H. and R.D. Hanson (1987). "Control Issues for Pseudo Dynamic Testing". In: *Structural Control*.

Miller, D.K. (1998). "Lessons learned from the Northridge earthquake". In: *Engineering Structures*.

Munich Re, NatCatSERVICE (2014). *Loss events worldwide 1980-2013*. URL: `http://www.munichre.com/site/corporate/get/documents_E-311190580/mr/assetpool.shared/Documents/5_Touch/_NatCatService/Significant-Natural-Catastrophes/2013/10-costliest-events-ordered-by-overall-losses-worldwide.pdf`.

Munich-Re (1999). *topics 2000 Natural Catastrophes - The Current Position*.

Paulay, T. and M.J.N. Priestley (1992). *Seismic Design of Reinforced Concrete and Masonry Buildings*. John Wiley & Sons.

Rabinowicz, E. (1995). *Friction and Wear of Materials*. John Wiley & Sons.

Roeder, C. W. and E. P. Popov (1977). "Inelastic behavior of eccentrically braced steel frames under cyclic loadings". In: *NASA STI/Recon Technical Report N* 78, p. 20375.

Sabelli, R., C. W. Roeder, and J.F. Hajjar (2013). *Seismic Design of Steel Special Concentrically Braced Frame Systems*. NEHRP Seismic Design Technical Brief 8. National Instituteof Standards and Technology.

SABS (2011a). *Part 4: Seismic actions and general requirements for buildings*. SANS 10160 4. SABS Standards Division.

— (2011b). *Seismic actions and general requirements for buidlings (SANS 10160-4)*. SABS.

SAISC (2013). *South African Steel Construction Handbook 2013*. 8th ed. Southern African Institute of Steel Construction.

SIMULIA (2012a). *Abaqus Analysis User's Manual*. Vol. 1. SIMULIA.

— (2012b). *Abaqus Analysis User's Manual*. Vol. 2. SIMULIA.

— (2012c). *Abaqus Analysis User's Manual*. Vol. 4. SIMULIA.

— (2012d). *Abaqus Analysis User's Manual*. Vol. 5. SIMULIA.

— (2012e). *Abaqus Theory Manual*. SIMULIA.

— (2012f). *Abaqus/CAE User's Manual*. SIMULIA.

Symans, M.D. et al. (2008). "Energy Dissipation Systems for Seismic Applications: Current Practice and Recent Developments". In: *Journal of Structural Engineering* 134, pp. 3–21.

Tremblay, R., P. Timler, M. Bruneau, and A. Filiatrault (1995). "Performance of Steel structures during the 1994 Northridge earthquake". In: *Canadian Journal of Civil Engineering*.

Uang, C. and V.V. Bertero (1990). "Evaluation of Seismic Energy in Structures". In: *Earthquake Engineering and Structural Dynamics* 19.1, pp. 77–90.

USGS (2013). *Global Earthquakes*. URL: `http://earthquake.usgs.gov/earthquakes/world/seismicity_maps/world.pdf`.

Wang, Z. (2009). *Seismic Hazard vs. Seismic Risk*. URL: `http://www.seismosoc.org/publications/SRL/SRL_80/srl_80-5_op.html`.

Yang, T.S. and Popov E. P. (1995). "Experimental and analytical studies of steel connections and energy dissipators". In: *Report No. UCB/EERC-95/13*. University of California, Berkeley.

Appendices

Appendix A

Detailed drawings of the SBC for model calibration

The detailed drawings of the parts of the SBC assembly used in Chapter 3 for the FE model calibration are provided below. The slotted-plate and outer-plate drawings are shown in Figures A1 and A2 while the bolt drawing is shown in Figure A3. The front views of the slotted- and outer-plates were drawn as shown in Abaqus and extruded 12 mm in their thickness direction. The bolt was initialised by sketching one half and revolving at about its symmetry-plane as indicated in Figure A3.

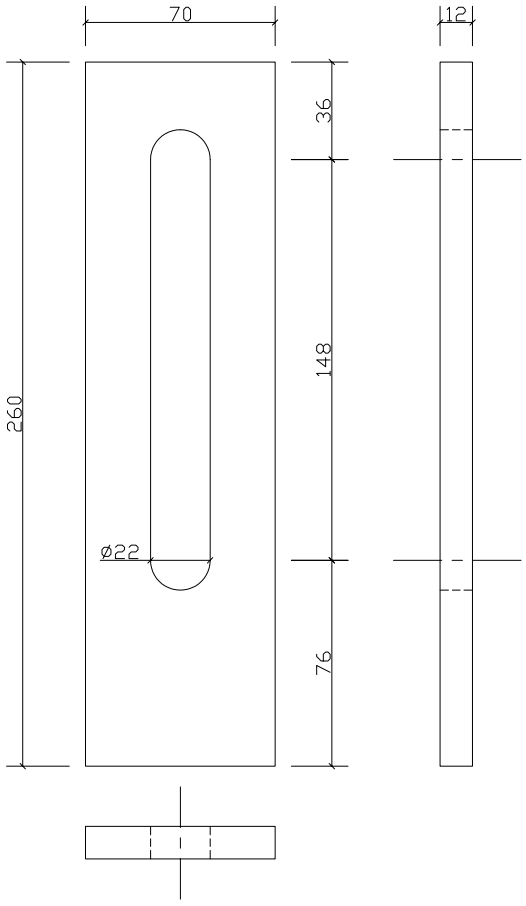

Figure A1: Slotted-plate

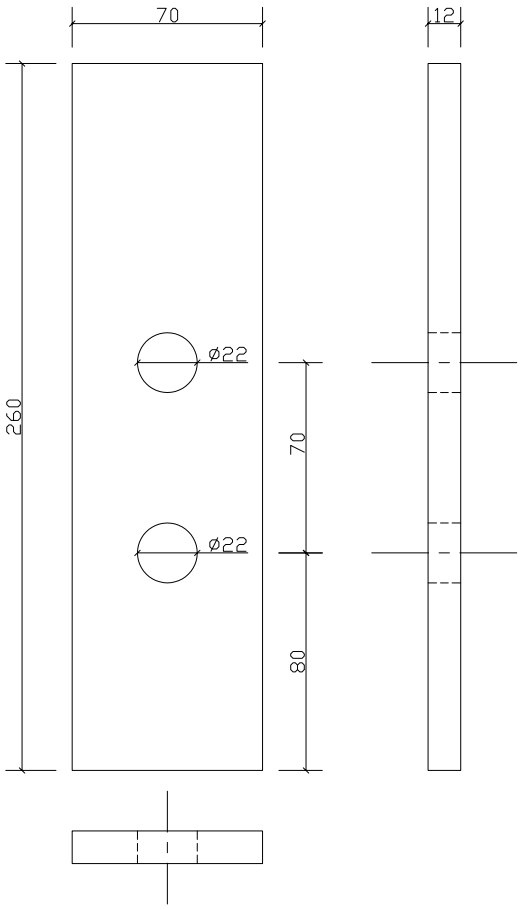

Figure A2: Outer-plate

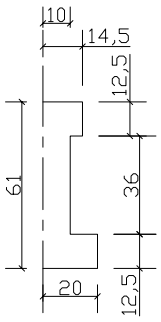

Figure A3: Bolt

Appendix B

Comparison between stress results for bolt-impact with meshes considered and symmetry models

The stress results of the bolt-impact analysis in Section 4.1 are provided for the various meshes as well as the symmetry models that were considered. Figures A4 and A5 show the stress results for the Hex-1 and Hex-2 meshes respectively, while Figures A6 and A7 show the stress results for the Tet-1 and Tet-2 meshes. Figures A8 and A9 show the stress results for the Sym-1 and Sym-2 symmetry models, respectively.

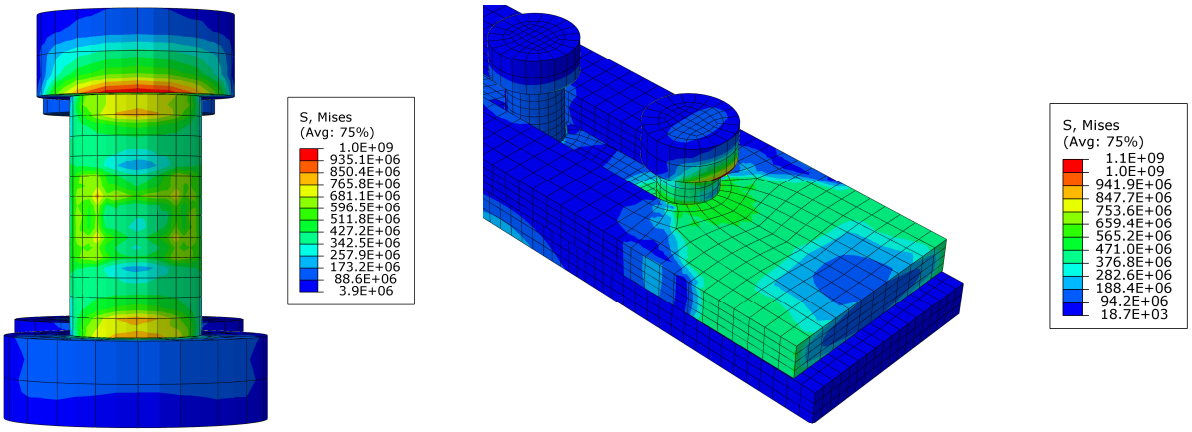

(a) (b)

Figure A4: Stresses in slotted-plate and bolt in contact for Hex-1 mesh

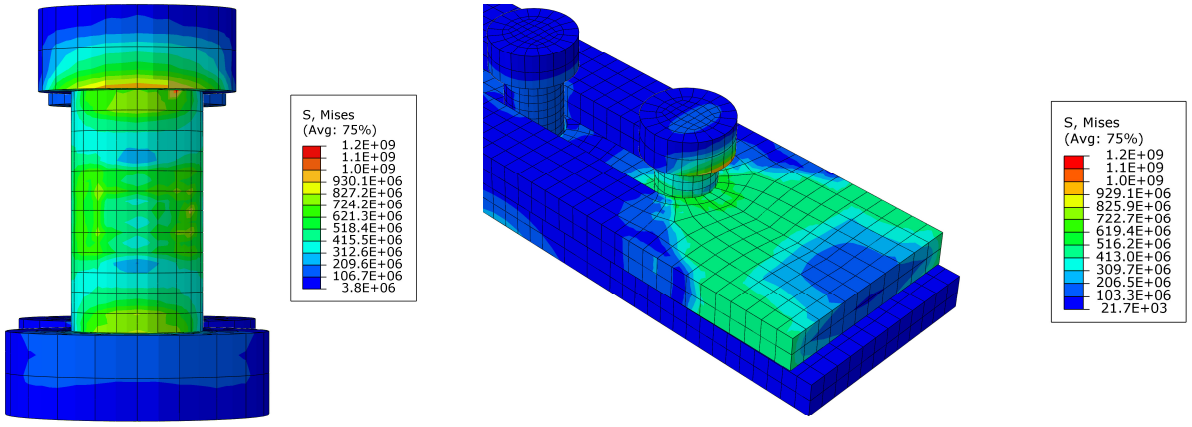

(a) (b)

Figure A5: Stresses in slotted-plate and bolt in contact for Hex-2 mesh

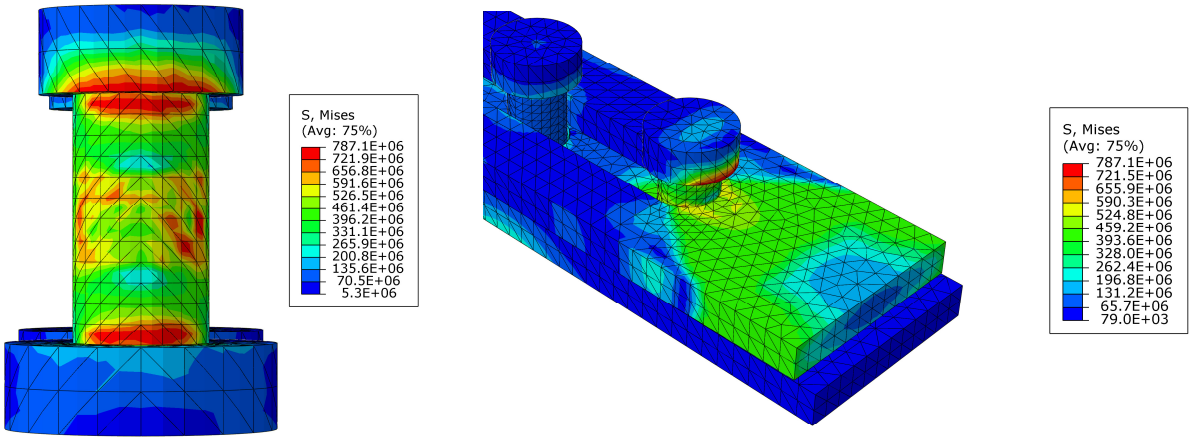

(a) (b)

Figure A6: Stresses in slotted-plate and bolt in contact for Tet-1 mesh

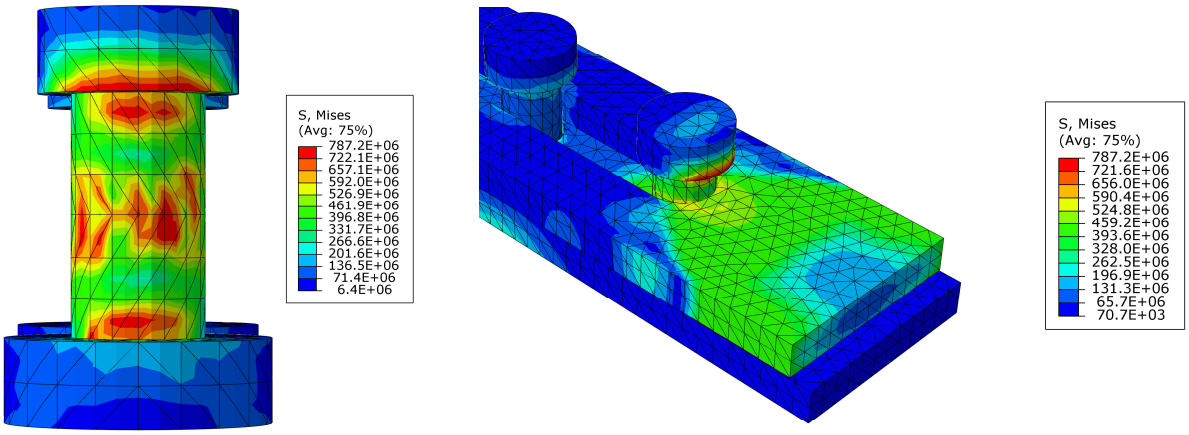

(a) (b)

Figure A7: Stresses in slotted-plate and bolt in contact for Tet-2 mesh

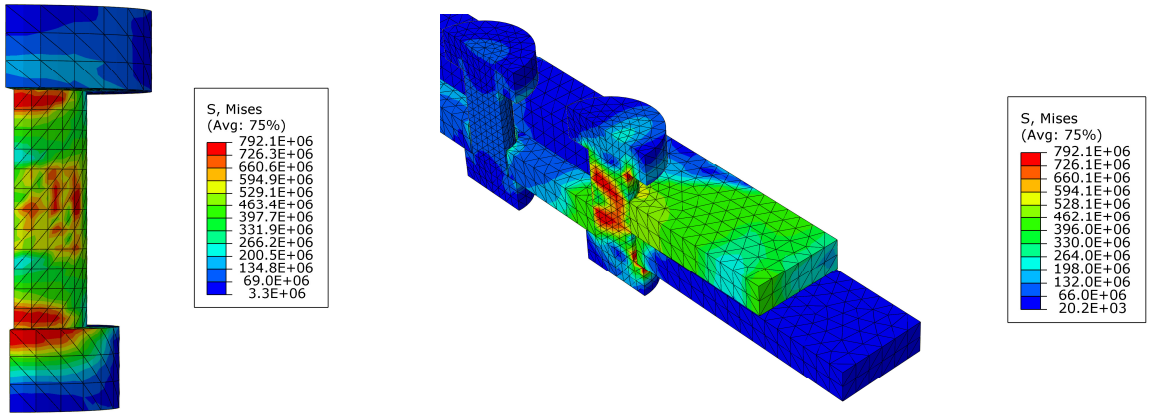

(a) (b)

Figure A8: Stresses in slotted-plate and bolt in contact for Sym-1 mesh

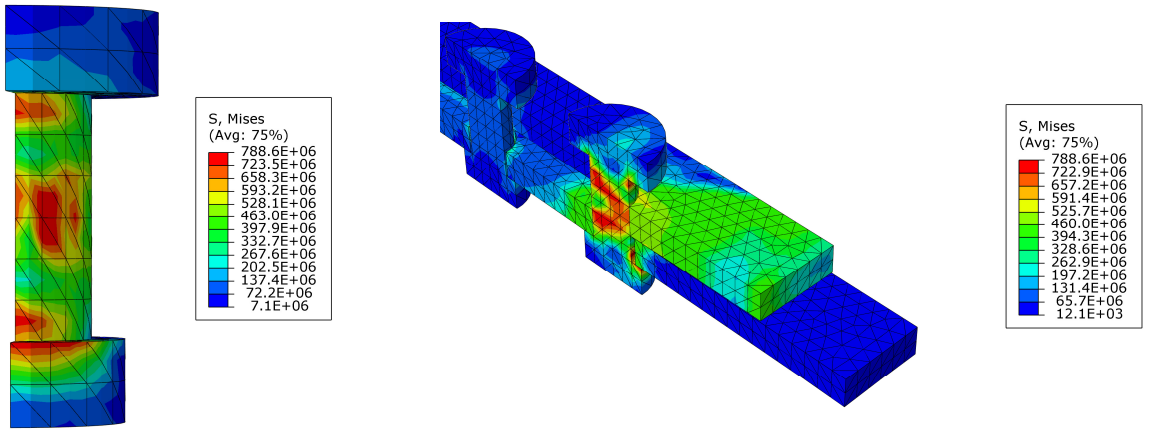

(a) (b)

Figure A9: Stresses in slotted-plate and bolt in contact for Sym-2 mesh

Appendix C

Detailed drawings of SBC-brace connection

The detailed drawings of the parts the the SBC assembly used in Section 4.3 for the model of the SBC-brace in a single braced bay are provided below. The slotted-plate that is a model of an extended spade-plate connected to a CHS is shown in Figure A10. The drawing of the M20 bolt model is shown in Figure A11. The bolt was initialised by sketching one half and revolving at about its symmetry-plane as indicated in Figure A11. The drawing of the gusset plates that function as the outer-plates of the SBC is shown in Figure A12.

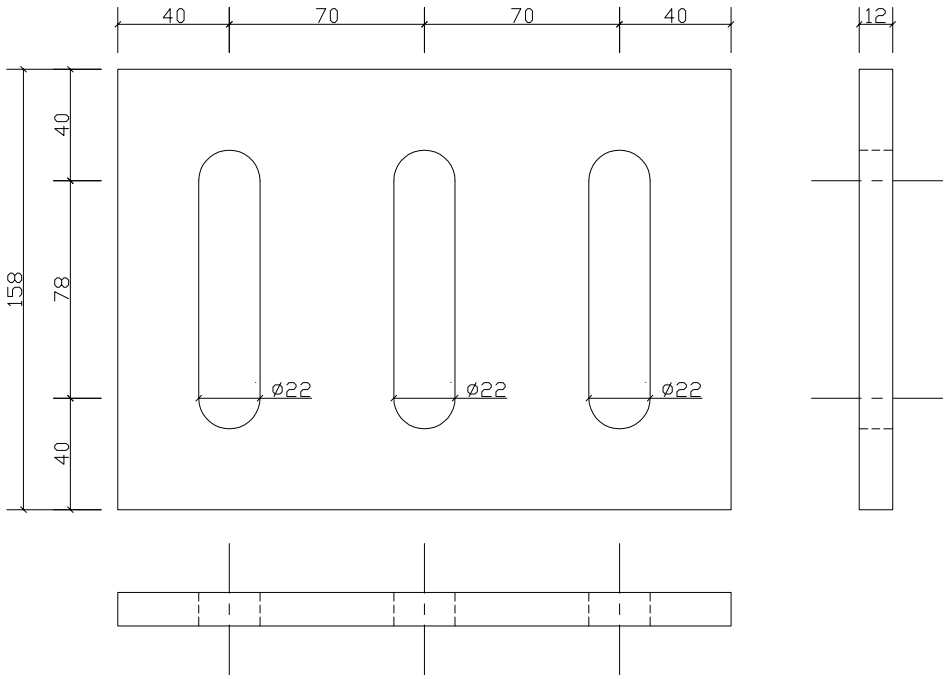

Figure A10: Spade-plate as the slotted-plate

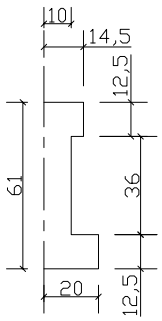

Figure A11: Bolt

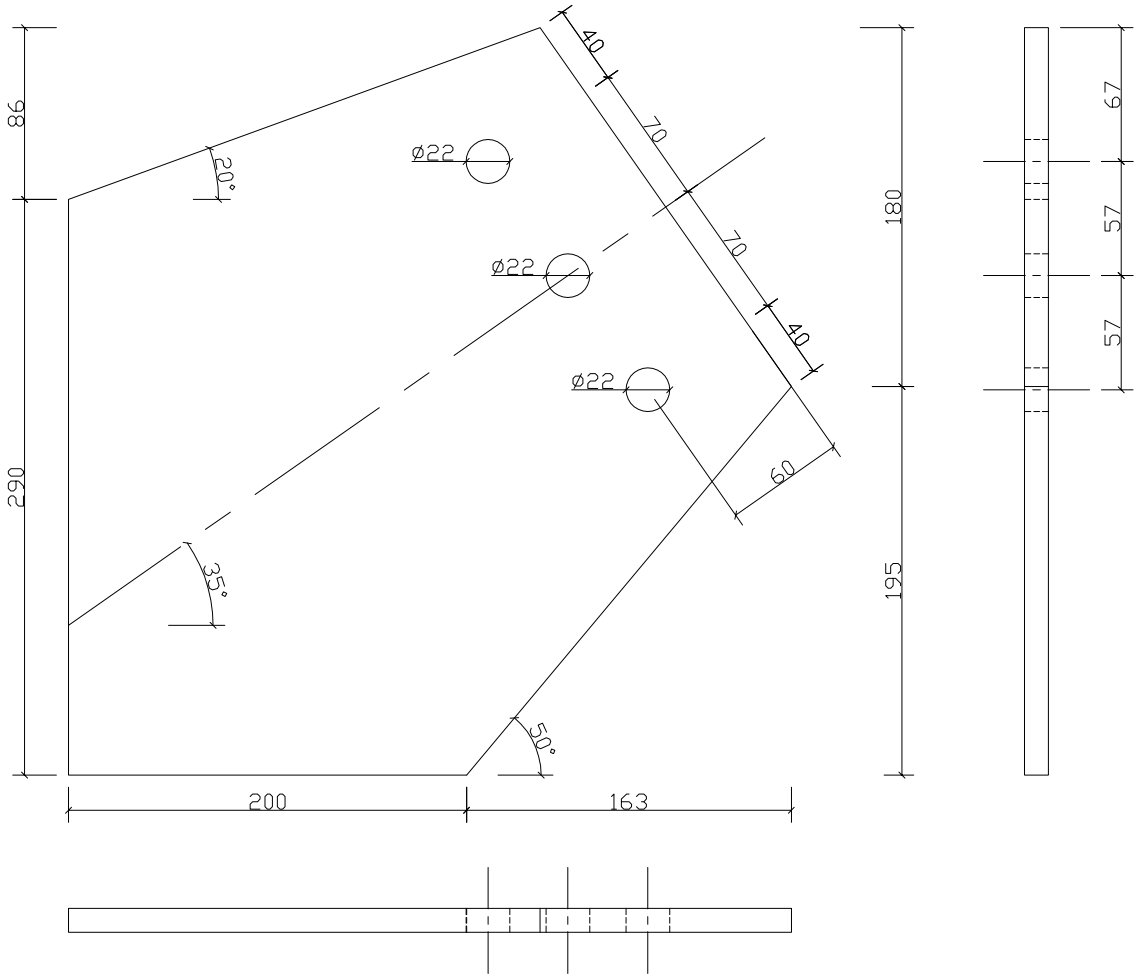

Figure A12: Gusset plates as the outer-plates

Appendix D

Structural arrangement of 4-storey diagonally-braced frame

The structural layout of the 4-storey diagonally-braced frame that was used for global analysis in Section 5.2 is provided in Figure A13. The frame is assumed to be simply constructed with dimensions as shown in Figure A13. Information on the sections and section sizes that were used is provided in Table A1. The plan layout is provided in Figure A14. The primary beams span in the North-South direction as well as around the perimeter. The secondary beams span in the East-West direction and are used for construction purposes only. The Bond-lok composite slab spans in the East-West direction onto the primary beams. There are two braced-bays on each face of the structure in each direction. The floor area is 784 m^2/storey.

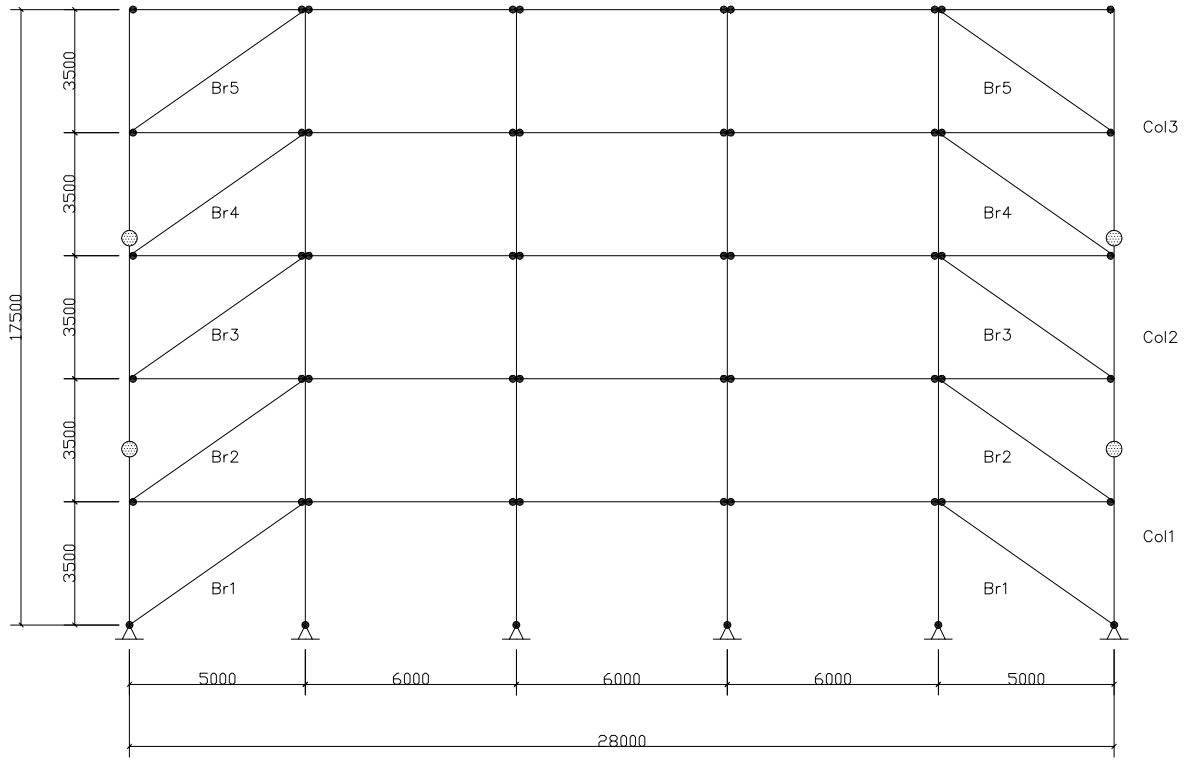

Figure A13: Layout of the diagonally-braced frame

Table A1: Section sizes for the diagonally-braced frame

Structural member	Position	Section designation
Beams	Primary	457x191x82 I-section
	Secondary	IPE200
Braces	Br1	152.4x4mm CHS
	Br2	152.4x3.5mm CHS
	Br3	152.4x3mm CHS
	Br4	139.7x3mm CHS
	Br5	114.3x3mm CHS
Columns	Col1	254x254x89 UC
	Col2	254x254x73 UC
	Col3	203x203x52 UC
Slab	All	Bond-lok 1.6 mm thick steel and 190 mm slab

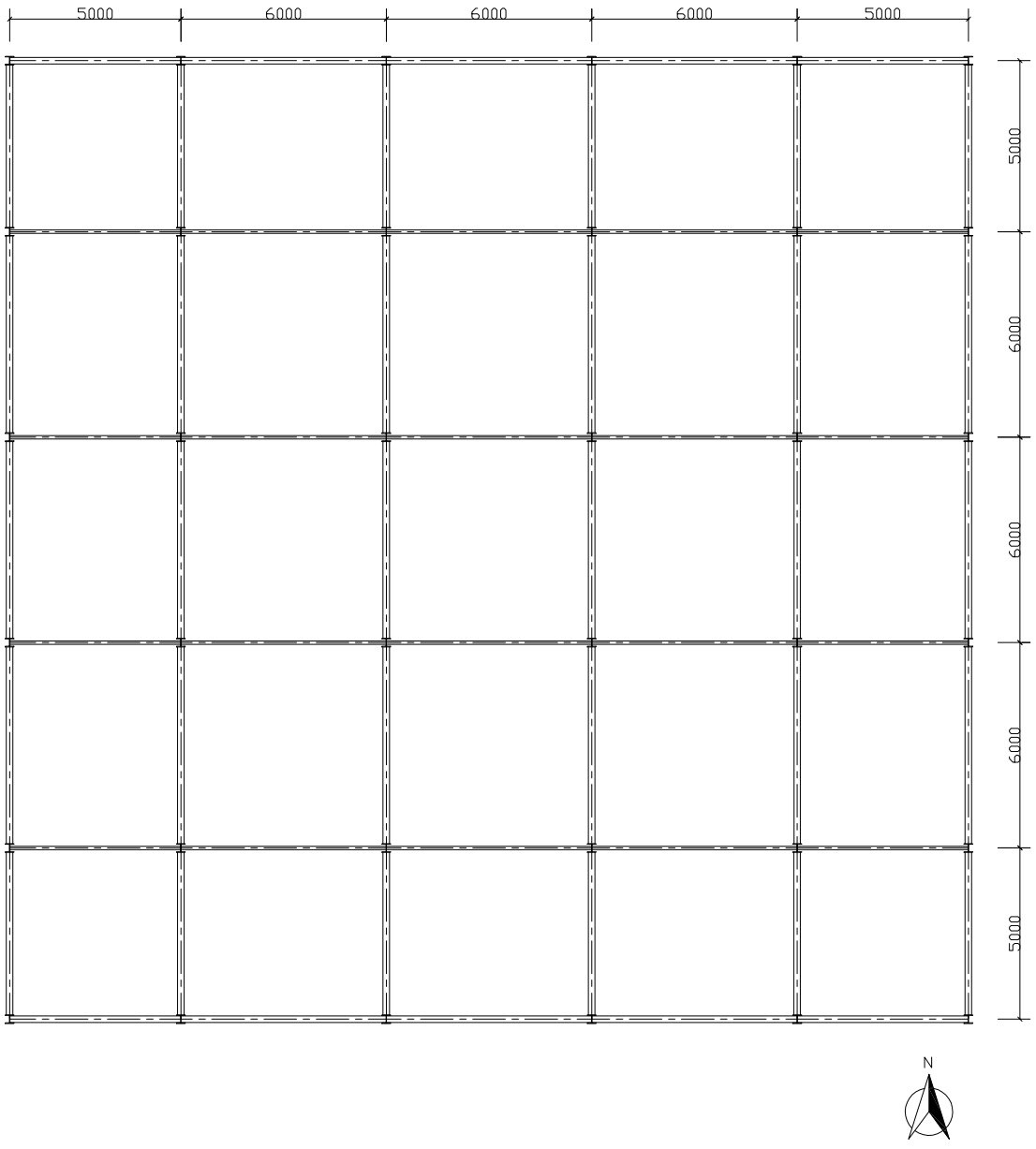

Figure A14: Plan layout of the diagonally-braced frame

Appendix E

Details regarding the design of the diagonally-braced frame

Details on the design of the gravity system, lateral load resisting system and the SBCs are provided.

Gravity system

The floor loads were calculated by considering the following dead and imposed loads:

Dead loads:

- Bond-lok composite slab with 1.6 mm thick steel and 190 mm thick slab, suitable for the 6 m span used. Unfactored dead load: 4.67 kN/m^2 (South African Steel Construction Handbook 2013)

Imposed loads:

- Office areas for general use. Unfactored imposed load: 2.5 kN/m^2 (SANS 10160-2)
- Accessible flat roof. Unfactored imposed load: 2 kN/m^2 (SANS 10160-2)

The following Load Cases were used to calculate the loads for the gravity system in Prokon. Only the beams and columns were present for this gravity model and the largest contributing length of 6 m was used to calculate the distributed loads that were applied to the beams.

- Load case 1: 1.2DL + 1.6LL all spans
- Load case 2: 1.2DL all spans + 1.6LL alternate spans
- Load case 3: 1.35DL + 1.0LL all spans

The Prokon analysis led to the following ultimate limit state Gravity Loads for the beams and columns:

- Beams - maximum moment: 259 kNm
- Columns ground level - maximum axial load: 1745 kN

- Columns level 1 - maximum axial load: 1390 kN
- Columns level 2 - maximum axial load: 1035 kN
- Columns level 3 - maximum axial load: 680 kN
- Columns level 4 - maximum axial load: 325 kN

The following Member Sizes were therefore selected for the gravity system:

- Beams - 457x191x82 I-section with $M_{rx} = 295$ kNm
- Column between ground level and splice 1 (5 m and $K = 1$) - 254x254x89 Universal Column with $C_r = 2080$ kNm
- Column between splice 1 and splice 2 (6 m and $K = 1$) - 254x254x73 Universal Column with $C_r = 1370$ kNm
- Column between splice 2 and roof level (6.5 m and $K = 1$) - 203x203x52 Universal Column with $C_r = 713$ kNm

Lateral loads

The Wind Loading was calculated using SANS 10160-3:

- Fundamental basic wind speed: $v_{b,0} = 28$ m/s
- Basic wind speed: $v_b = 28$ m/s
- Terrain category: C
- Reference height: 17.5 m
- Topography coefficient: $c_0(z) = 1$
- Roughness/height coefficient: $c_r(z) = 0.93$
- Peak wind speed: $v_p(z) = 36.4$ m/s
- Peak wind speed pressure: 363 kN (unfactored) $\times$ 1.3 = 471 kN (factored lateral wind load)

In addition to the wind loads, Notional Horizontal Loads were considered to account for out-of-straightness or eccentricities introduced during erection. Table A2 shows the calculation of the unfactored dead loads of the structure. The notional horizontal loads were then calculated:

- Total notional horizontal loads: 19 761 kN $\times$ 0.5% $\times$ 1.2 (Dead Load factor) = 119 kN

The lateral load to be resisted by one of the braced frames was therefore:

- Total lateral load = 471 kN + 119 kN = 590 kN
- Lateral load per lateral system: 590 kN $\div$ 2 (braced frames in each direction) = 295 kN

Table A2: Calculation of the unfactored dead load of the structure

Members	No. of	Length or area	Mass or weight/unit	Load
Columns	36	5 m	89 kg/m	157 kN
		6 m	73 kg/m	155 kN
		6.5 m	52 kg/m	119 kN
Primary beams	6x5 levels	28 m	82 kg/m	676 kN
	2x5 levels	28 m	82 kg/m	225 kN
Secondary beams	4x5 levels	28 m	22.4 kg/m	123 kN
Slabs	5 levels	784 m^2	4.67 kN/m^2	18 306 kN
			TOTAL	19 761 kN

Bracing system

The lateral loads due to the wind load and notional loads on the bracing system were distributed triangularly:

- Apex = 98 kN
- Level 4 = 79 kN
- Level 3 = 59 kN
- Level 2 = 39 kN
- Level 1 = 20 kN

A frame analysis was performed in Prokon with the calculated lateral loads applied. Please note that braces were present in tension as well as compression and not tension-only as is common practice for braced frames. The compression braces should not buckle before the slip-force in the SBCs are exceeded. Since seismic design of the SBC-braces has been negated, the slip-force of the SBCs are designed to be larger than the ultimate limit state wind and lateral loads. The compression braces should therefore clearly be present in the model at the ultimate limit state lateral load. The ultimate limit state (pre-slip) Axial Loads were calculated as listed in Table A3. The loads were used to size the braces as shown in Table A3 as well as to design the SBCs.

Table A3: Ultimate limit state lateral loads in the braces

Position	Tension	Compression	Brace selected	Euler buckling load
Bottom	185 kN	180 kN	152.4x4mm CHS	272 kN
Level 1	167 kN	165 kN	152.4x3.5mm CHS	241 kN
Level 2	144 kN	144 kN	152.4x3mm CHS	208 kN
Level 3	107 kN	108 kN	139.7x3mm CHS	160 kN
Top	59 kN	62 kN	114.3x3mm CHS	86 kN

SBC design

The SBCs were designed to slip at a force larger than the ultimate limit state lateral loads as listed in Table A3. It is necessary to recall the equations listed in Section 3.1:

$$\delta_{flat} = n_s \times \delta_{Belleville} \tag{A1}$$

$$T_b = n_p \times P_{flat} \times \frac{\delta}{\delta_{flat}} \tag{A2}$$

$$F_{slip} = 2 \times n_b \times T_b \times \mu \tag{A3}$$

Where:

- δ_{flat} - Flat deflection of spring washers
- n_s - Number of spring washers in series stack
- $\delta_{Belleville}$ - Flat deflection of a particular Belleville spring washer
- T_b - Bolt tension
- n_p - Number of spring washers in parallel stack
- P_{flat} - Load required to achieve flat deflection of a spring washer
- δ - Spring washer group deflection
- F_{slip} - Slip-force of the SBC
- n_b - Number of bolts
- μ - Coefficient of friction

In addition, it is necessary to reproduce the spring washer properties that were obtained from Loo et al. (2014) as listed in Table A4.

Table A4: Belleville spring washer properties from Loo et al. (2014)

Variant no.	D_i	D_o	Thickness	Height	$\delta_{Belleville}$	P_{flat}
1	20.6 mm	40 mm	2.3 mm	3.2 mm	0.787 mm	15 kN
2	20.6 mm	44.5 mm	3.5 mm	4.2 mm	0.762 mm	32.5 kN
3	20.6 mm	44.5 mm	3.4 mm	4.3 mm	0.914 mm	37.8 kN

With the equations and the properties, the various SBCs in the braces can be designed:

Bottom braces:

- $F_{slip} > 185\,\text{kN}$
- Choose 4 M20 bolts and 2 variant no.2 spring washers in parallel for a $P_{flat} = 65\,\text{kN}$
- $F_{slip} = 2 \times 4 \times 65 \times 0.36 = 187\,\text{kN}$

Level 1 braces:

- $F_{slip} > 167\,\text{kN}$
- Choose 4 M20 bolts and 2 variant no.2 spring washers in parallel, but deflect washers only to 90% of flat deflection for a $P_{flat} = 65\,\text{kN} \times 0.9$
- $F_{slip} = 2 \times 4 \times 65 \times 0.9 \times 0.36 = 168\,\text{kN}$

Level 2 braces:

- $F_{slip} > 144\,\text{kN}$
- Choose 3 M20 bolts and a variant no.2 and variant no.3 spring washer in parallel for a $P_{flat} = 32.5 + 37.8 = 70.3\,\text{kN}$
- $F_{slip} = 2 \times 3 \times 70.3 \times 0.36 = 152\,\text{kN}$

Level 3 braces:

- $F_{slip} > 108\,\text{kN}$
- Choose 2 M20 bolts and 2 variant no.3 spring washers in parallel for a $P_{flat} = 75.6\,\text{kN}$
- $F_{slip} = 2 \times 2 \times 75.6 \times 0.36 = 109\,\text{kN}$

Top braces:

- $F_{slip} > 62\,\text{kN}$
- Choose 3 M20 bolts and 2 variant no.1 spring washers in parallel for a $P_{flat} = 30\,\text{kN}$
- $F_{slip} = 2 \times 3 \times 30 \times 0.36 = 65\,\text{kN}$

Appendix F

Seismic mass calculations and nodal positions

The calculations and positions of the seismic masses for the structure in Section 5.2 are provided here. Figure A15 presents the area of the seismic mass of the structure that must be resisted by a particular braced frame due to the adjacent unbraced frames. Tables A5, A6 and A7 list the calculations for the seismic masses per floor of the slab, primary and secondary beams respectively. Tables A8 and A9 list the calculations for the seismic masses of floor levels 1 to 4 and the roof level respectively. Table A10 lists the total seismic masses that were applied to the corresponding concentric nodes in Figure A16.

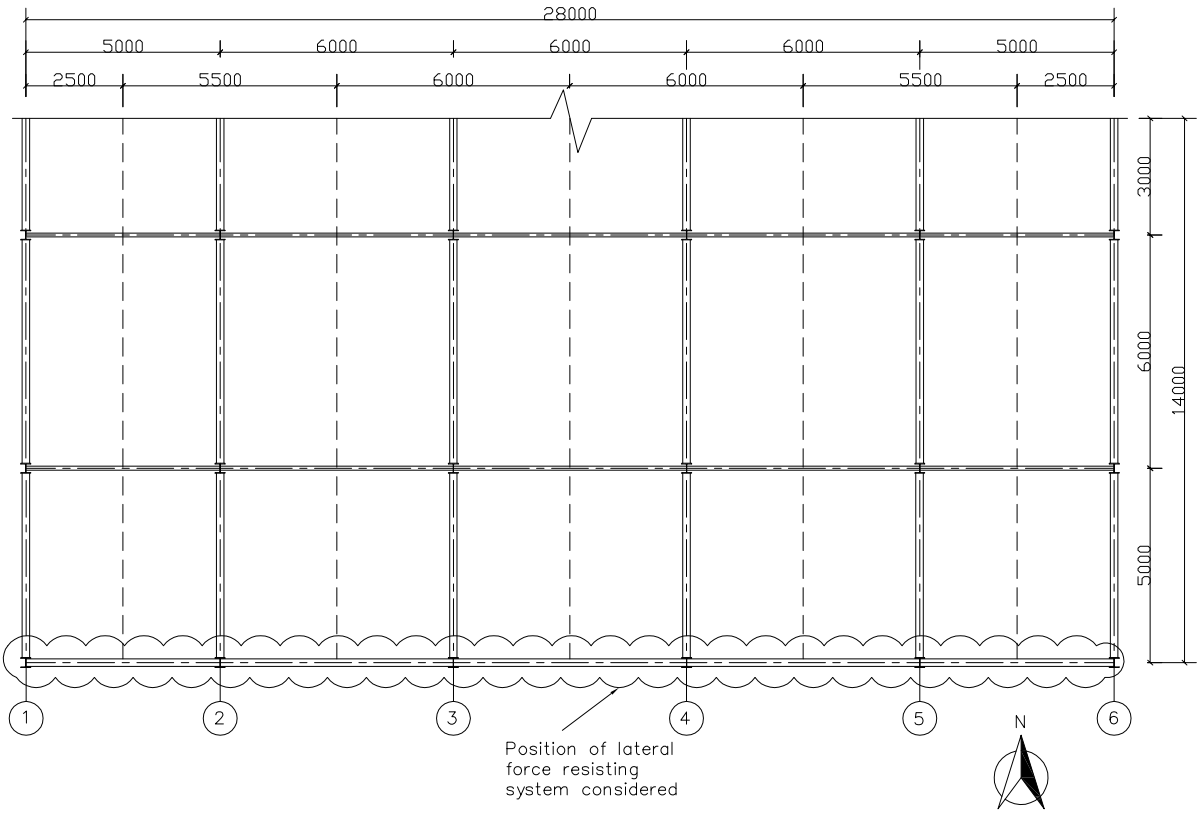

Figure A15: Position of the braced frame that resists the adjacent seismic masses

Table A5: Seismic masses per floor due to slab with unfactored dead load of $4.67\,\text{kN/m}^2$

Gridline	Calculation		Total (kg)
1	$14\,\text{m} \times 2.5\,\text{m} \times 4.67\,\text{kN/m}^2 \div 9.81$	=	16 700
2	$14\,\text{m} \times 5.5\,\text{m} \times 4.67\,\text{kN/m}^2 \div 9.81$	=	36 700
3	$14\,\text{m} \times 6\,\text{m} \times 4.67\,\text{kN/m}^2 \div 9.81$	=	40 000
4	$14\,\text{m} \times 6\,\text{m} \times 4.67\,\text{kN/m}^2 \div 9.81$	=	40 000
5	$14\,\text{m} \times 5.5\,\text{m} \times 4.67\,\text{kN/m}^2 \div 9.81$	=	36 700
6	$14\,\text{m} \times 2.5\,\text{m} \times 4.67\,\text{kN/m}^2 \div 9.81$	=	16 700

Table A6: Seismic masses per floor due to primary beams with a footweight of $82\,\text{kg/m}$

Gridline	Calculation		Total (kg)
1	$14\,\text{m} \times 82\,\text{kg/m}$	=	1 150
2	$14\,\text{m} \times 82\,\text{kg/m}$	=	1 150
3	$14\,\text{m} \times 82\,\text{kg/m}$	=	1 150
4	$14\,\text{m} \times 82\,\text{kg/m}$	=	1 150
5	$14\,\text{m} \times 82\,\text{kg/m}$	=	1 150
6	$14\,\text{m} \times 82\,\text{kg/m}$	=	1 150

Table A7: Seismic masses per floor due to secondary beams with a footweight of $22.4\,\text{kg/m}$

Gridline	Calculation		Total (kg)
1	$2 \times 2.5\,\text{m} \times 22.4\,\text{kg/m}$	=	112
2	$2 \times 5.5\,\text{m} \times 22.4\,\text{kg/m}$	=	246
3	$2 \times 6\,\text{m} \times 22.4\,\text{kg/m}$	=	269
4	$2 \times 6\,\text{m} \times 22.4\,\text{kg/m}$	=	269
5	$2 \times 5.5\,\text{m} \times 22.4\,\text{kg/m}$	=	246
6	$2 \times 2.5\,\text{m} \times 22.4\,\text{kg/m}$	=	112

Table A8: Seismic masses per floor for levels 1 to 4 due to imposed office loading with unfactored load of $2.5\,\text{kN/m}^2$ and combination factor of $\psi = 0.3$ from SANS 10160-1 Table 2

Gridline	Calculation		Total (kg)
1	$0.3 \times 14\,\text{m} \times 2.5\,\text{m} \times 2.5\,\text{kN/m}^2 \div 9.81$	=	2 676
2	$0.3 \times 14\,\text{m} \times 5.5\,\text{m} \times 2.5\,\text{kN/m}^2 \div 9.81$	=	5 887
3	$0.3 \times 14\,\text{m} \times 6\,\text{m} \times 2.5\,\text{kN/m}^2 \div 9.81$	=	6 422
4	$0.3 \times 14\,\text{m} \times 6\,\text{m} \times 2.5\,\text{kN/m}^2 \div 9.81$	=	6 422
5	$0.3 \times 14\,\text{m} \times 5.5\,\text{m} \times 2.5\,\text{kN/m}^2 \div 9.81$	=	5 887
6	$0.3 \times 14\,\text{m} \times 2.5\,\text{m} \times 2.5\,\text{kN/m}^2 \div 9.81$	=	2 676

Table A9: Seismic masses for roof level due to imposed loading with unfactored load of $2\,\mathrm{kN/m^2}$ and combination factor of $\psi = 0.3$ from SANS 10160-1 Table 2

Gridline	Calculation		Total (kg)
1	$0.3 \times 14\,\mathrm{m} \times 2.5\,\mathrm{m} \times 2\,\mathrm{kN/m^2} \div 9.81$	=	2 141
2	$0.3 \times 14\,\mathrm{m} \times 5.5\,\mathrm{m} \times 2\,\mathrm{kN/m^2} \div 9.81$	=	4 709
3	$0.3 \times 14\,\mathrm{m} \times 6\,\mathrm{m} \times 2\,\mathrm{kN/m^2} \div 9.81$	=	5 138
4	$0.3 \times 14\,\mathrm{m} \times 6\,\mathrm{m} \times 2\,\mathrm{kN/m^2} \div 9.81$	=	5 138
5	$0.3 \times 14\,\mathrm{m} \times 5.5\,\mathrm{m} \times 2\,\mathrm{kN/m^2} \div 9.81$	=	4 709
6	$0.3 \times 14\,\mathrm{m} \times 2.5\,\mathrm{m} \times 2\,\mathrm{kN/m^2} \div 9.81$	=	2 141

Table A10: Total seismic masses included at each node for a corresponding gridline and floor level

Gridline	Levels 1 to 4 (kg)	Roof level (kg)
1	20.6×10^3	20.1×10^3
2	44×10^3	42.8×10^3
3	47.8×10^3	46.6×10^3
4	47.8×10^3	46.6×10^3
5	44×10^3	42.8×10^3
6	20.6×10^3	20.1×10^3

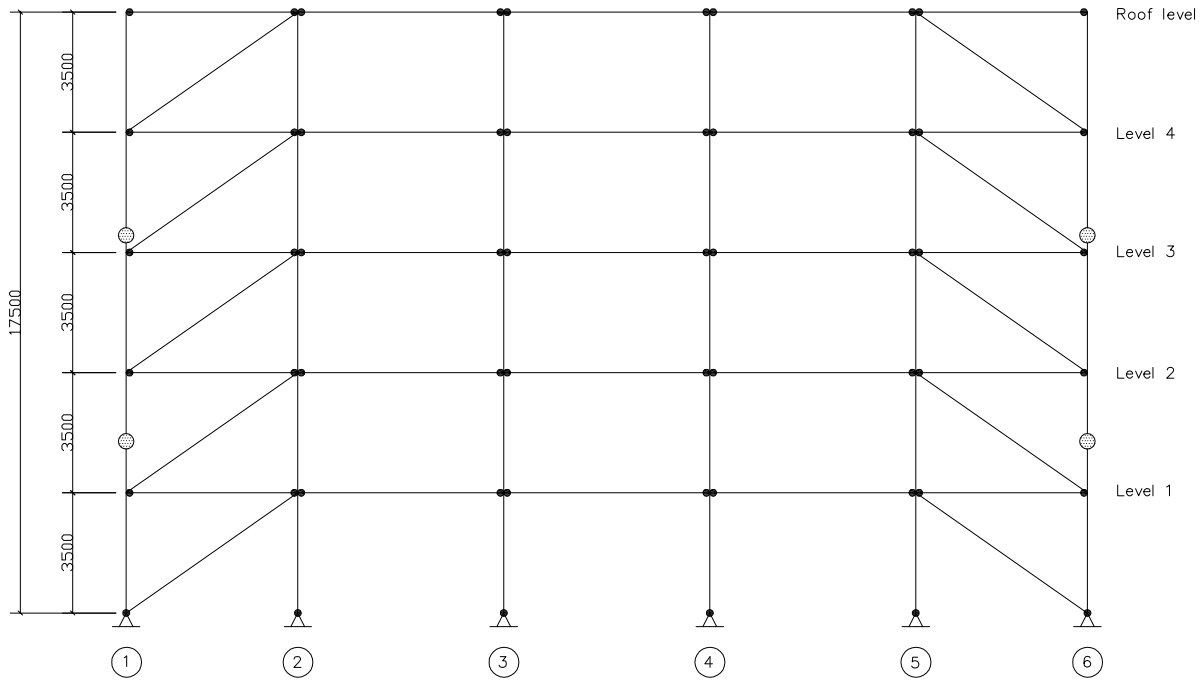

Figure A16: Diagonally-braced frame with positions of gridlines and floor levels indicated for seismic mass applications

Appendix G

Seismic records considered

The seismic records that were considered in Section 5.2 are provided. The acceleration-time and displacement-time histories of the earthquakes are provided. Anza (0.05 g) is presented in Figures A17 and A18. Imperial Valley (0.1 g) is presented in Figures A19 and A20. Coyote Lake (0.15 g) is presented in Figures A21 and A22. Loma Prieta (0.2 g) is presented in Figures A23 and A24. The seismic records were obtained from the Pacific Earthquake Engineering Research Center (PEER) Strong Motion database.

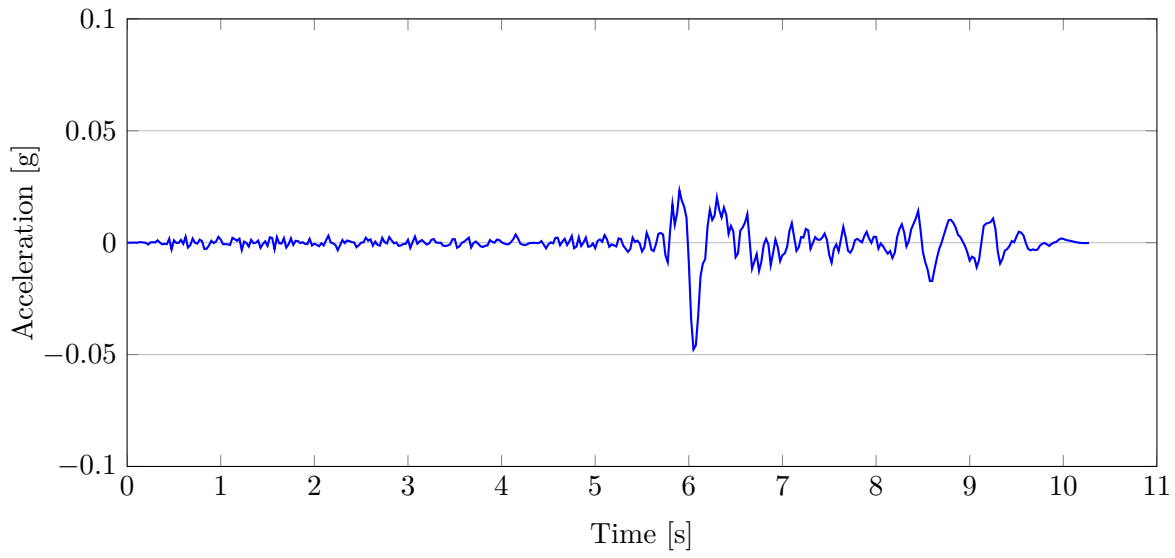

Figure A17: Acceleration-time history of Anza (0.05 g)

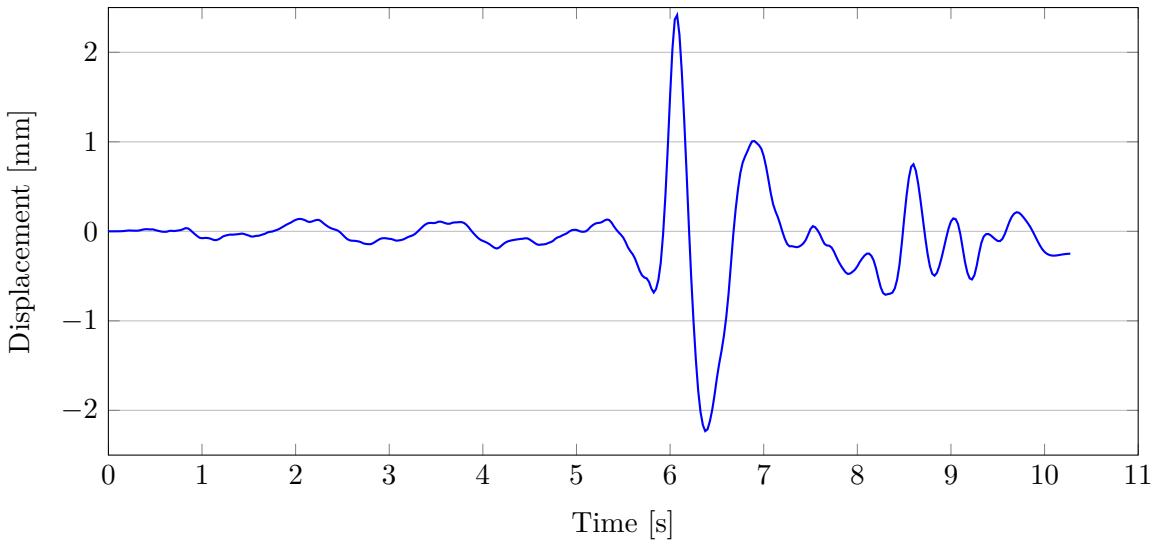

Figure A18: Displacement-time history of Anza (0.05 g)

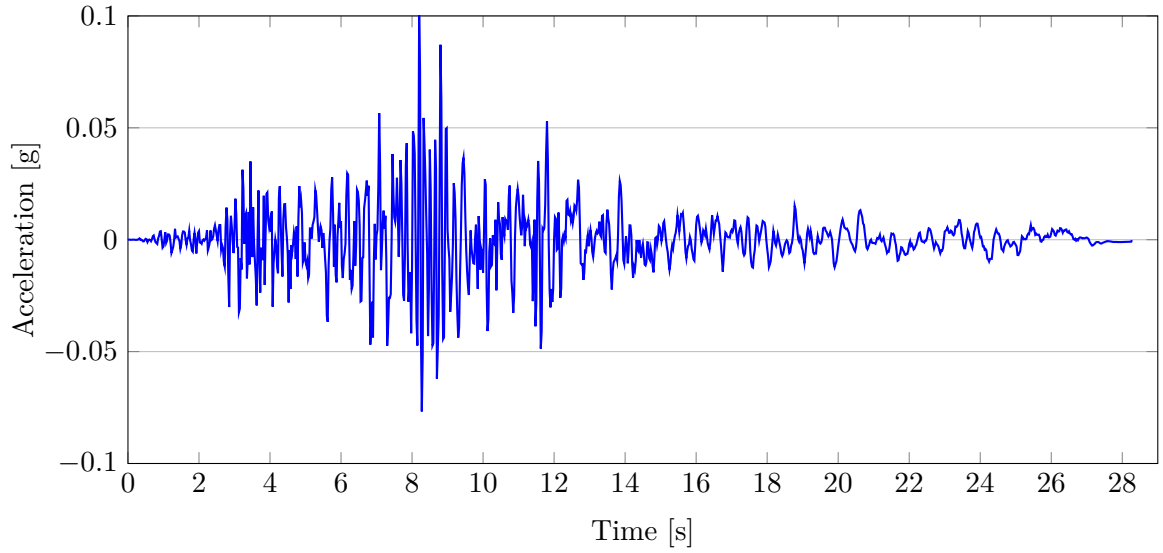

Figure A19: Acceleration-time history of Imperial Valley (0.1 g)

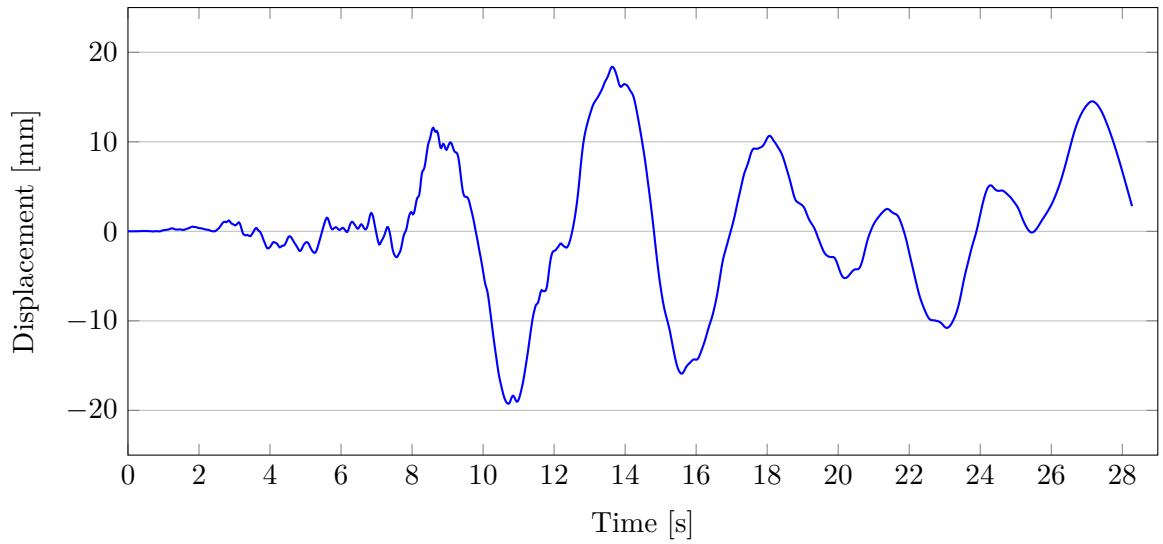

Figure A20: Displacement-time history of Imperial Valley (0.1 g)

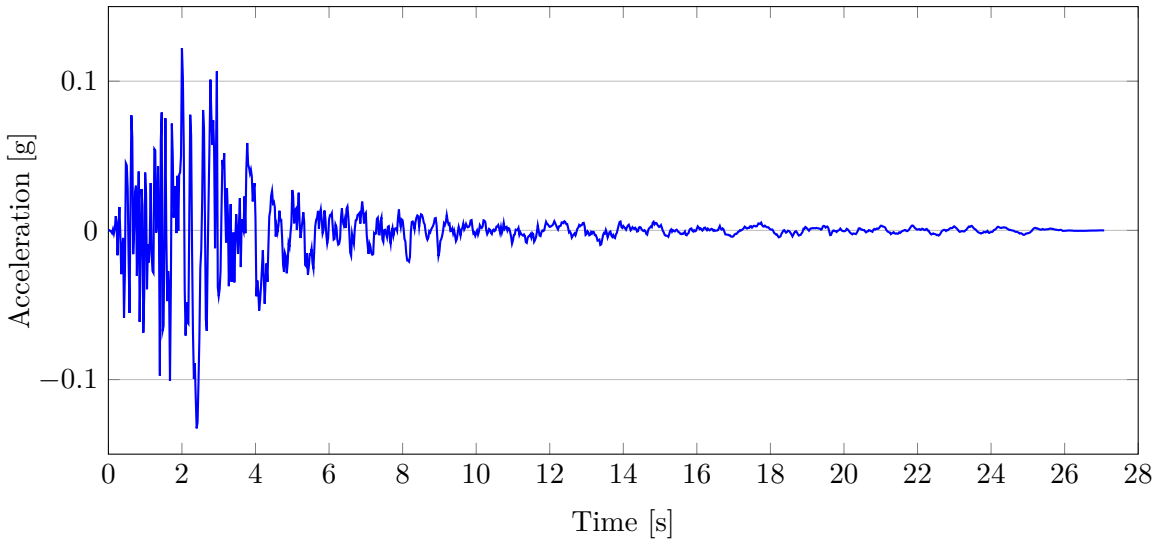

Figure A21: Acceleration-time history of Coyote Lake (0.15 g)

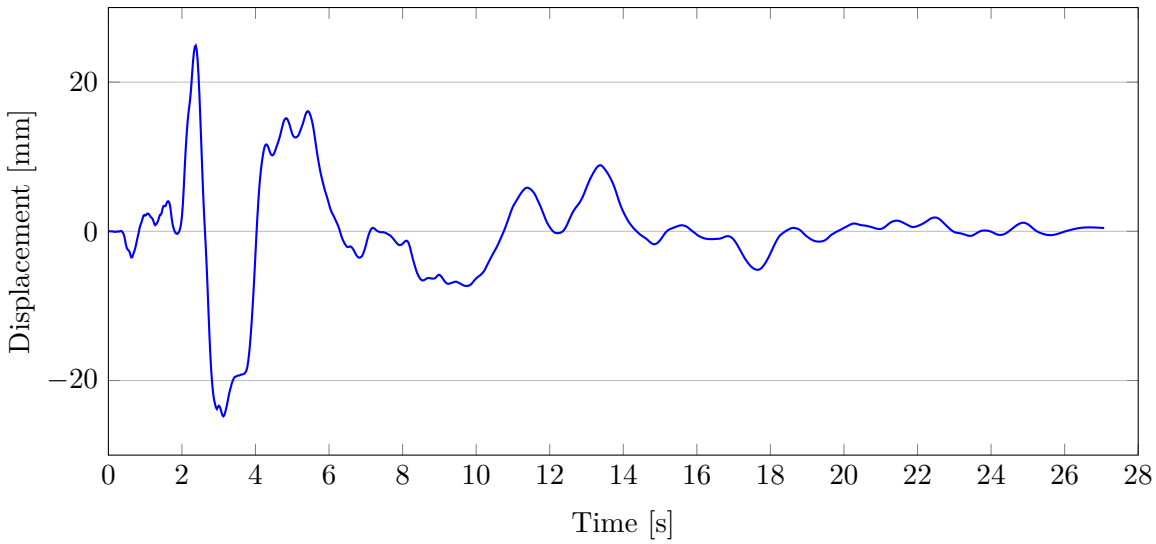

Figure A22: Displacement-time history of Coyote Lake (0.15 g)

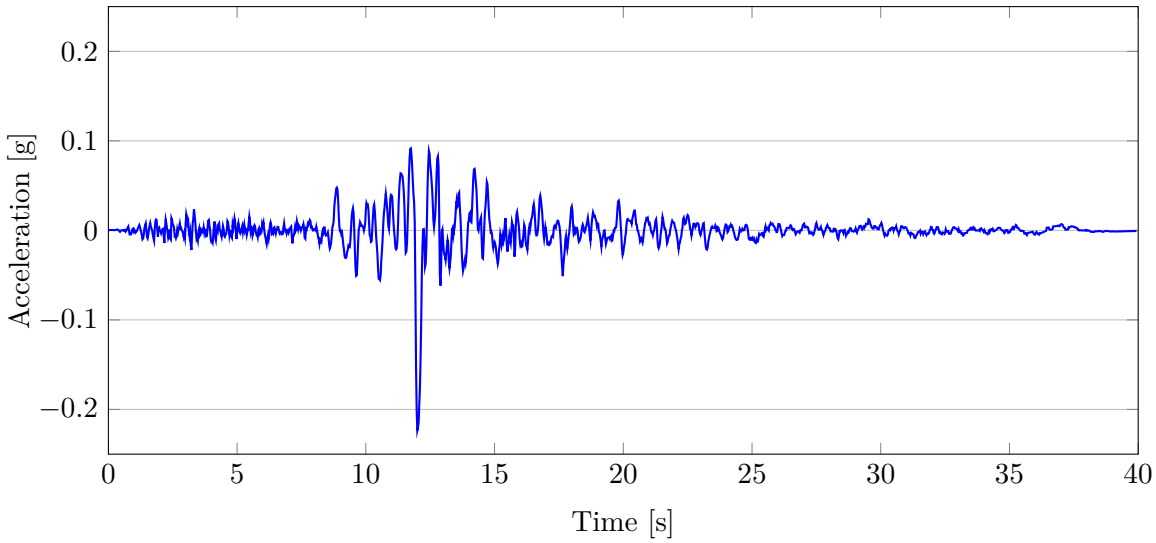

Figure A23: Acceleration-time history of Loma Prieta (0.2 g)

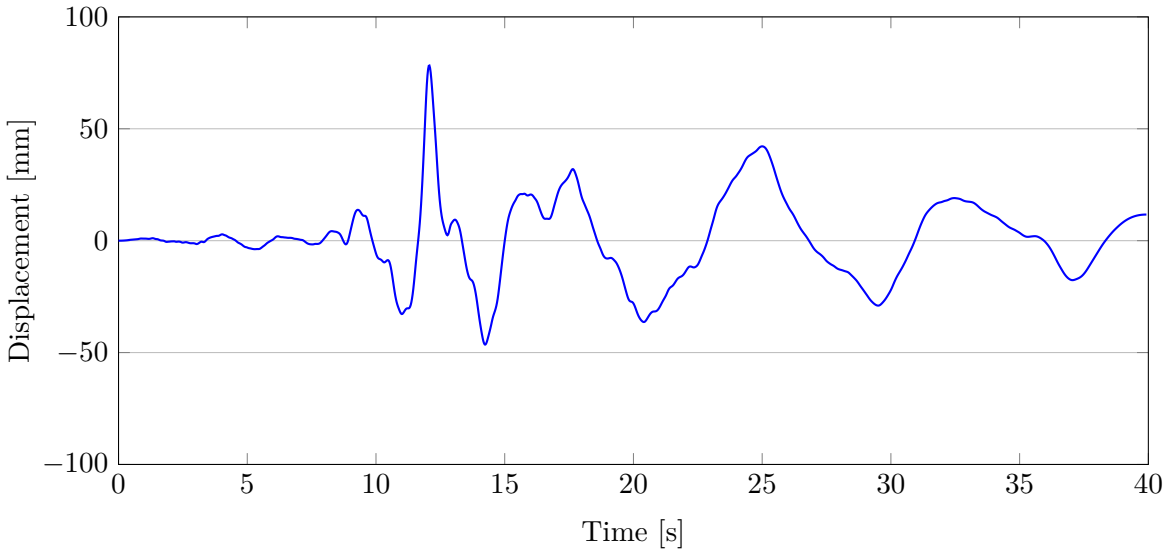

Figure A24: Displacement-time history of Loma Prieta (0.2 g)

Appendix H

Drift results at apex for earthquakes and sliding lengths considered

The relative drift results at the apex of the structure due to the ground accelerations from the analysis in Section 5.2 are provided here. The results are provided with reference to the various sliding conditions that were considered. Figure A25 shows the results from Anza (0.05 g) and there is essentially no variation between the various slip conditions. Figure A26 shows the results from Imperial Valley (0.1 g), note that the results start at 8 s, prior to this the relative displacements are equivalent for all sliding conditions. Figures A27 and A28 show the results that were not included in Section 5.2.4 from Coyote Lake (0.15 g) and Loma Prieta (0.2 g) respectively.

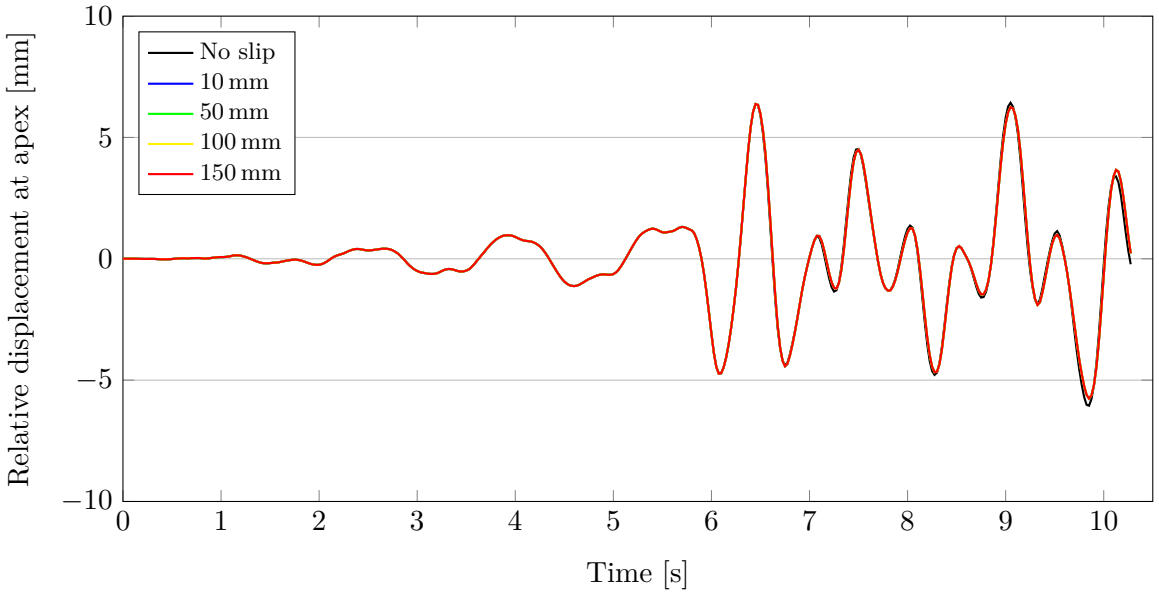

Figure A25: Relative displacements at the apex for Anza (0.05 g)

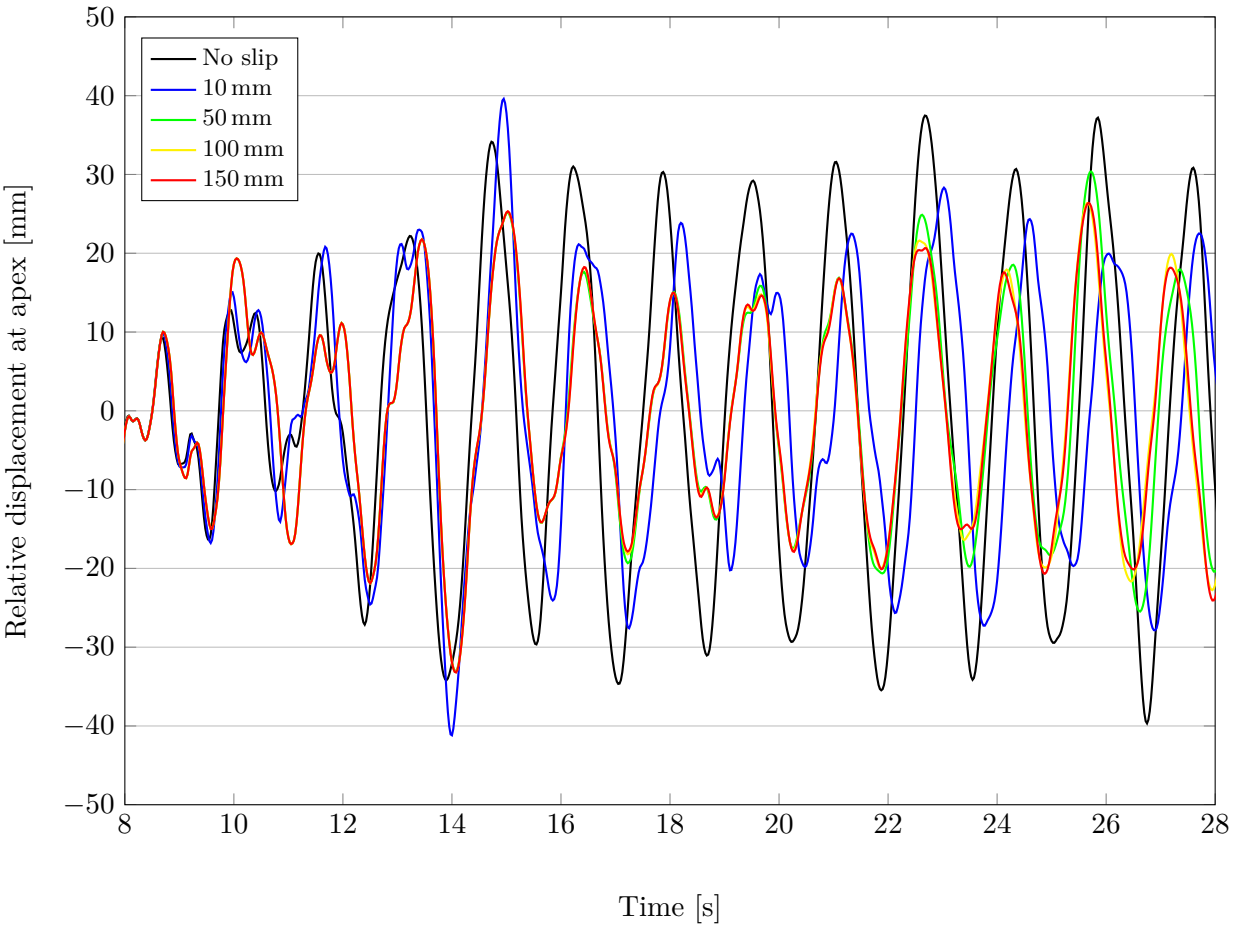

Figure A26: Relative displacements at the apex for Imperial Valley (0.1 g)

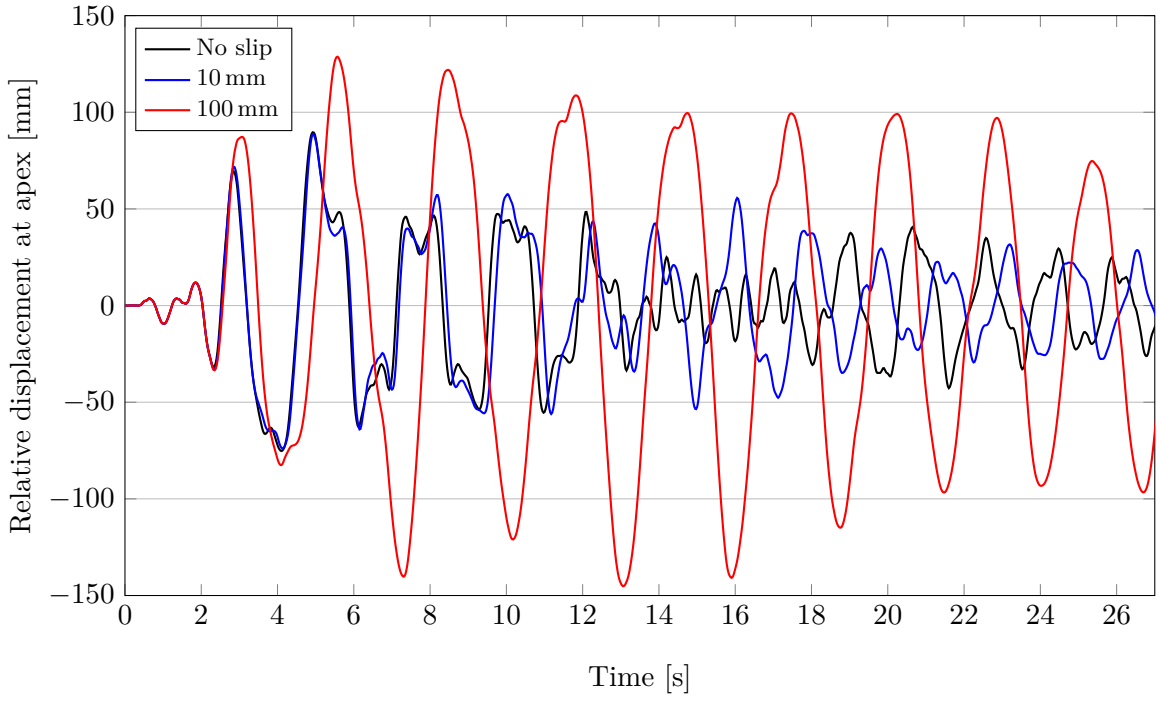

Figure A27: Relative displacements at the apex for Coyote Lake (0.15 g)

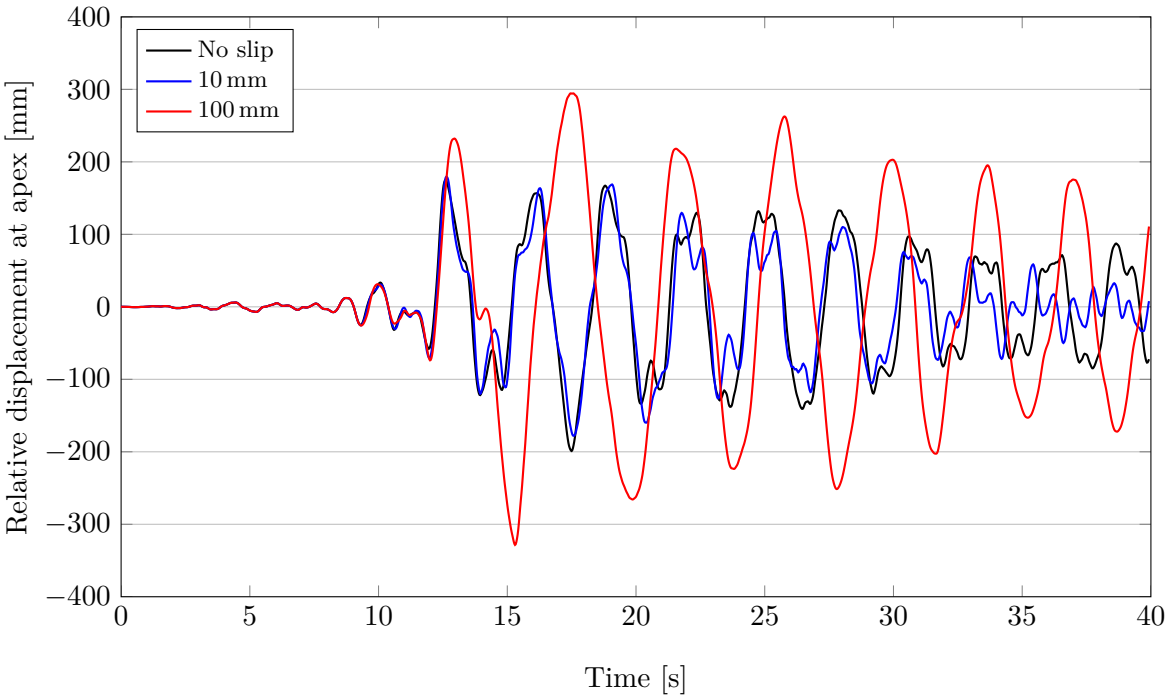

Figure A28: Relative displacements at the apex for Loma Prieta (0.2 g)